NUREG/CR-0588
PNL-2709
R-3

Interim Report

The Analysis of Fuel Relocation for the NRC/PNL Halden Assemblies IFA-431, IFA-432, and IFA-513

April 1980

Prepared for
the U.S. Nuclear Regulatory Commission

Pacific Northwest Laboratory
Operated for the U.S. Department of Energy
by Battelle Memorial Institute

Battelle

PNL-2709

PACIFIC NORTHWEST LABORATORY
operated by
BATTELLE
for the
UNITED STATES DEPARTMENT OF ENERGY
Under Contract DE-AC06-76RLO 1830

Available from
GPO Sales Program
Division of Technical Information and Document Control
U.S. Nuclear Regulatory Commission
Washington, D.C. 20555
and
National Technical Information Service
United States Department of Commerce
5285 Port Royal Road
Springfield, Virginia 22151

Price: Printed Copy $ ______*; Microfiche $3.00

*Pages	NTIS Selling Price
001-025	$4.00
026-050	$4.50
051-075	$5.25
076-100	$6.00
101-125	$6.50
126-150	$7.25
151-175	$8.00
176-200	$9.00
201-225	$9.25
226-250	$9.50
251-275	$10.75
276-300	$11.00

NUREG/CR-0588
PNL-2709
R-3

INTERIM REPORT

THE ANALYSIS OF FUEL RELOCATION FOR THE NRC/PNL HALDEN ASSEMBLIES IFA-431, IFA-432, AND IFA-513

R. E. Williford
C. L. Mohr
D. D. Lanning
M. E. Cunningham
W. N. Rausch
E. R. Bradley

April 1980

Prepared for
the Fuel Behavior Research Branch
Division of Reactor Safety Research
U.S. Nuclear Regulatory Commission
under a Related Services Agreement
with the U.S. Department of Energy
under Contract DE-AC06-76RLO 1830

Pacific Northwest Laboratory
Richland, Washington 99352

DOE Richland, WA

ABSTRACT

The effects of the thermally-induced cracking and subsequent relocation of UO_2 fuel pellets on the thermal and mechanical behavior of light-water reactor fuel rods during irradiation are quantified in this report.

Data from the Nuclear Regulatory Commission/Pacific Northwest Laboratory Halden experiments on instrumented fuel assemblies (IFA) IFA-431, IFA-432, and IFA-513 are analyzed. Beginning-of-life in-reactor measurements of fuel center temperatures, linear heat ratings, and cladding axial elongations are used in a new model to solve for the effective thermal conductivity and elastic moduli of the cracked fuel column. The primary assumptions of the new model are that 1) the cracked fuel is in a hydrostatic state of stress in the (r, θ) plane, and that 2) there is no axial slipping between fuel and cladding. Three basic parameters are used to describe the cracked fuel: 1) the crack pattern, 2) the crack roughness, and 3) the fuel surface (gap) roughness.

The effective thermal conductivity and el stic moduli for the cracked fuel were found to be significantly reduced from the values for solid UO_2 pellets. The calculated fuel-cladding gap remained relatively constant (closed) with respect to power level, indicat that the fuel fragments do not retreat from the cladding when the power/temperature is reduced. This implies that the cracked fuel column does not conform to the solid cylinder model that has traditionally been employed in fuel performance codes. Furthermore, analytical and experimental results indicate that the fuel rod mechanical response to power changes may be dominated by the effective radial elastic modulus of the cracked fuel at low powers and by the axial modulus at higher powers.

Recommendations are made pertaining to the work required to further refine the model.

CONTENTS

FIGURES

TABLES

1.0 SUMMARY

A series of experiments sponsored by the Fuel Behavior Research Branch of the Nuclear Regulatory Commission are being irradiated in the Halden Boiling Water Reactor to better define light-water reactor fuel behavior over the normal operating range of power reactor fuel rods. One fuel behavior variable of interest is the thermally induced cracking and subsequent relocation of UO_2 fuel pellets.

The effects of pellet cracking on the effective thermal conductivity and elastic moduli for the fragmented fuel were determined to be primarily dependent on the magnitude and spatial distribution of the free area in the (r, θ) plane of the fuel rod. The free area is defined as the area within the cladding inner surface that is not occupied by fuel fragments. The magnitude of the free area was determined by the initial gap size and the stress-free thermal expansion of the cracked fuel. The distribution of the free area between the fuel cracks and the gap was calculated using a new model. This model solves simultaneously for the crack and gap widths, assuming that a hydrostatic state of stress exists in the (r, θ) plane of the cracked fuel. Thus, equilibrium requires that the same radial stress exist at the cladding inner surface.

Three basic parameters were employed in the model: the crack pattern, the crack roughness, and the fuel surface (gap) roughness. The crack patterns observed from photo-macrographs of irradiated fuel provided values for the total crack lengths in the (r, θ) plane. The free area distribution between the cracks and gap determines the radial temperature distribution in the cracked fuel, which in turn determines values for the effective fuel thermal conductivity and gap conductance. Roughnesses were found by comparison of calculated conductivities and conductances to those deduced from an independent analysis of transient data. The crack/gap widths at equilibrium were calculated using a crack compliance formulation that relates the crack/gap width to the crack/gap roughness and the hydrostatic stress applied normal to the crack/gap. The crack width multiplied by the total crack length determined the total crack area in the fuel, and thus the free area distribution.

Fuel center temperature, linear heat rating, and cladding elongation data from the instrumented fuel assemblies (IFA) IFA-431, IFA-432, and IFA-513 experiments were analyzed. Beginning-of-life data was selected because the changes in the fuel structural state due to cracking were the greatest, and fission gas release was minimized.

The effective thermal conductivity of the cracked fuel column was found to be 10 to 30% less than that for solid UO_2 for a rod of typical boiling water reactor (BWR) design under normal operating conditions. It is important to note that the cracking of the fuel had resulted in approximately 80% relocation.

Because the stresses and strains were also calculated in the above described model, Hooke's Law could be used to evaluate the effective elastic moduli of the cracked fuel column. The radial elastic modulus of the cracked fuel column was calculated to be about 1/40 of that for solid UO_2 for a rod of typical BWR design under normal operating conditions. The reduction in the elastic modulus is the mechanical counterpart of the thermal conductivity reduction, and both always occur simultaneously.

The comparison of cracked fuel properties to those of solid UO_2 indicates that the cracked fuel column does not conform to the solid cylinder model that has traditionally been employed in fuel performance codes. Operating nuclear fuel is not a solid monolith. Furthermore, the cladding axial elongation was found to exhibit regimes of domination by the effective elastic moduli of the cracked fuel column. Radial domination at low powers, and a transition to axial domination at higher powers, was in general supported by calculations using in-reactor data, observations from post irradiation examination (PIE) data, and out-of-reactor experiments. This is expected to affect the calculation of the stored mechanical energy in the fuel rod, which in turn affects predictions of fuel-cladding mechanical interaction (FCMI) or pellet-cladding interaction-stress corrosion cracking (PCI-SCC) induced fuel rod failures.

2.0 INTRODUCTION

The Nuclear Regulatory Commission (NRC)/Pacific Northwest Laboratory (PNL) Halden instrumented fuel assemblies IFA-431, IFA-432, and IFA-513 are part of a series of experimental assemblies (Table 1) that are designed to better describe fuel behavior variables and quantify their uncertainties over the operating ranges of power reactor fuel rods. These assemblies have been undergoing irradiation at the Halden Boiling Water Reactor (HBWR) in Norway and are sponsored by the Fuel Behavior Research Branch of the NRC. The results and conclusions of these tests are used at PNL in the experimental support and

TABLE 1. Experimental Matrix

Assembly Rod	Power[(a)] (kW/m)	Fuel[(b)] Type	Diametral 50-75	Gap, 230	M x 10^{-6} 380	Initial Fill Gas: 100% He 0.1 MPa	Initial Fill Gas: 100% He >0.1 MPa	Initial Fill Gas: Xe 0.1 MPa	Detectors[(c)]: UTC	Detectors[(c)]: LTC	Detectors[(c)]: ES	PT	SPND
IFA-431	35/25												
1		95S		X		X			X	X	X	X	7
2		95S			X	X			X	X	X		
3		95S	X			X			X	X	X		
4		95S		X				100%	X	X	X		
5		92S		X		X			X	X	X	X	
6		92U		X		X			X	X	X	X	
IFA-432	50/35												
1		95S		X		X			X	X	X	X	7
2		95S			X	X			UT	X	X		
3		95S	X			X			X	X	X		
4		95S		X				100%	X	X	X		
5		92S		X		X			X	X	X	X	
6		92U		X		X			X	X	X	X	
IFA-513	40/28												
1		95S		X		X			X	X	X	X	9
2		95S		X			0.3MPa		X	X	X	X	
3		95S		X		X			X	X	X	X	
4		95S		X				8%	X	X	X	X	
5		95S		X		X			X	X	X	X	
6		95S		X				23%	X	X	X	X	
Fuel Relocation	14/10												
1		95S	X					100%	X	X	X	X	9
2		95S		X				100%	X	X	X	X	
3		95S		X				100%	X	X	X	X	
4		95S		X				100%	X	X	X	X	
5		95S		X				100%	X	X	X	X	
6		95S		X				100%	X	X	X	X	

(a) Linear power is given for upper and lower thermocouple positions respectively.
(b) Three fuel types are used, all enriched to 10% U-235
95S = 95% TD, Stable
92S = 92% TD, Stable
92U = 92% TD, Unstable
(c) UTC = Upper Thermocouple
LTC = Lower Thermocouple
ES = Elongation Sensor
PT = Pressure Transducer
SPND = Self-Powered Neutron Detector
UT = Ultrasonic Thermometer

development of single rod fuel codes. These codes[1,2,3] are used to audit vendor supplied calculations of steady state fuel behavior.

Many fuel performance codes model fuel rods by assuming the fuel geometry to be a solid right cylinder that is concentric with the cladding. This is an approximation of the actual state of the fuel, which has been observed in most cases to exhibit a multitude of cracks because of the thermal gradients experienced during irradiation. While the simplified geometry allows calculations to be performed economically, it may also have a significant impact on calculated fuel temperatures and cladding axial elongations, as described below.

Because the solid cylinder model envisions no fuel cracks, all the "free area" within the cladding is assigned to the fuel-cladding gap. The "free area" is the area within the cladding inner surface that is not occupied by the fuel. Some of this free area is actually occupied by the fuel cracks. Thus, the solid cylinder model overestimates the area of the fuel-cladding gap, resulting in an overestimation of the gap width and an underestimation of the gap conductance. Since the solid cylinder does not account for the cracks in the fuel, the effective thermal conductivity of the cracked fuel system is similarly overestimated. In short, the solid cylinder model does not adequately calculate the fuel temperature distribution.

Likewise, the calculated cladding axial elongations seem to rarely resemble in-reactor data because the solid cylinder model does not adequately account for the fuel cladding mechanical interaction (FCMI). The solid cylinder model predicts no FCMI until thermal expansion causes the fuel to contact the cladding. Thus, a plot of the calculated cladding axial elongation versus the rod linear heat rating will exhibit a discontinuous change in slope (elbow) that indicates the point where the fuel cladding contact occurs. This is usually in contrast to data obtained from in-reactor experiments, where the cladding elongation versus power plots rarely exhibit a well-defined elbow. The slope of the elongation versus power curve changes continuously, indicating a smooth transition as the degree of apparent FCMI increases with power/temperature level.

It is the purpose of this report to describe an alternate fuel model that includes both the modeling capabilities of the cracked fuel concepts, and the economic advantage of the solid cylinders approach.

Section 3.0 summarizes the observations that have been made from the in-reactor data. More detail is presented in the Appendices. In Section 4.0, some plausible mechanisms that explain the role of fuel cracking and relocation are proposed.

Section 5.0 quantifies the proposed mechanisms by developing a model that represents the effects of fuel cracking. This model is used in Section 6.0 to analyze the in-reactor temperature, power, and cladding elongation data. The effective radial and axial elastic moduli for the cracked fuel columns are calculated for a range of rod designs. The effects of fuel cracking on the effective fuel thermal conductivity are quantified, and the trends in conductivities and moduli with burnup are discussed.

Section 7.0 presents further evidence in support of the assumptions used and conclusions reached in previous sections. The results of further calculations using in-reactor data, observations from PIE data, and data from laboratory axial load-compliance tests are introduced. Section 8.0 discusses the limitations of the model and analysis method, and thus provides direction for future research. Finally, conclusions and recommendations are summarized in Section 9.0.

3.0 OBSERVATIONS FROM THE IN-REACTOR DATA

This section summarizes the observations made from the in-reactor data provided by the irradiations of IFA-431, IFA-432, and IFA-513. Brief descriptions of the thermal analysis methods used to analyze this data are presented in Appendix A. In-reactor measurements of the fuel center temperatures (in the form of the rod total thermal resistances) are shown in Appendix B, along with cladding axial elongations and rod power data.

Nearly complete fuel relocation seemed to occur within the first few ramps to power. Further gap closure (increases in FCMI) appeared to dominate the rod temperature changes within the first few GWD/MTM, fission gas release becoming more dominant thereafter.

Two other general observations were noted in the data, and provided the primary motivation for questioning the adequacy of the solid cylinder model. The first observation was that the fuel temperatures (at a given power) exhibited consistent increases during the first few ramps to full power. This occurred even for fuel that was stable with respect to densification and had negligible off-gassing. This rise in temperatures is shown schematically in Figure 1. No explanation for this event was immediately apparent.

The second observation is shown schematically in Figure 2. Figure 2a shows typical cladding elongation as a function of rod power during power increases. The typical data from the very first ramp in the rod's life is shown, together with data trends from several subsequent ramps. Note, first, that there is an offset between the first and subsequent zero-power cladding elongations (about 0.05 to 0.10% strain typically). Next, note that the slope of rod elongation versus power (in ramps after the first) is less than the axial thermal expansion of the cladding tubing itself. Finally, note that the overall character of the first-ramp curve is different from that of subsequent ramps. (The slope of the first-ramp curve changes more slowly than does that of subsequent ramps in the region of apparent FCMI initiation.)

Figure 2b shows the same schematic data curves with a typical (solid-cylinder model) code prediction added. This code-calculated curve is the same

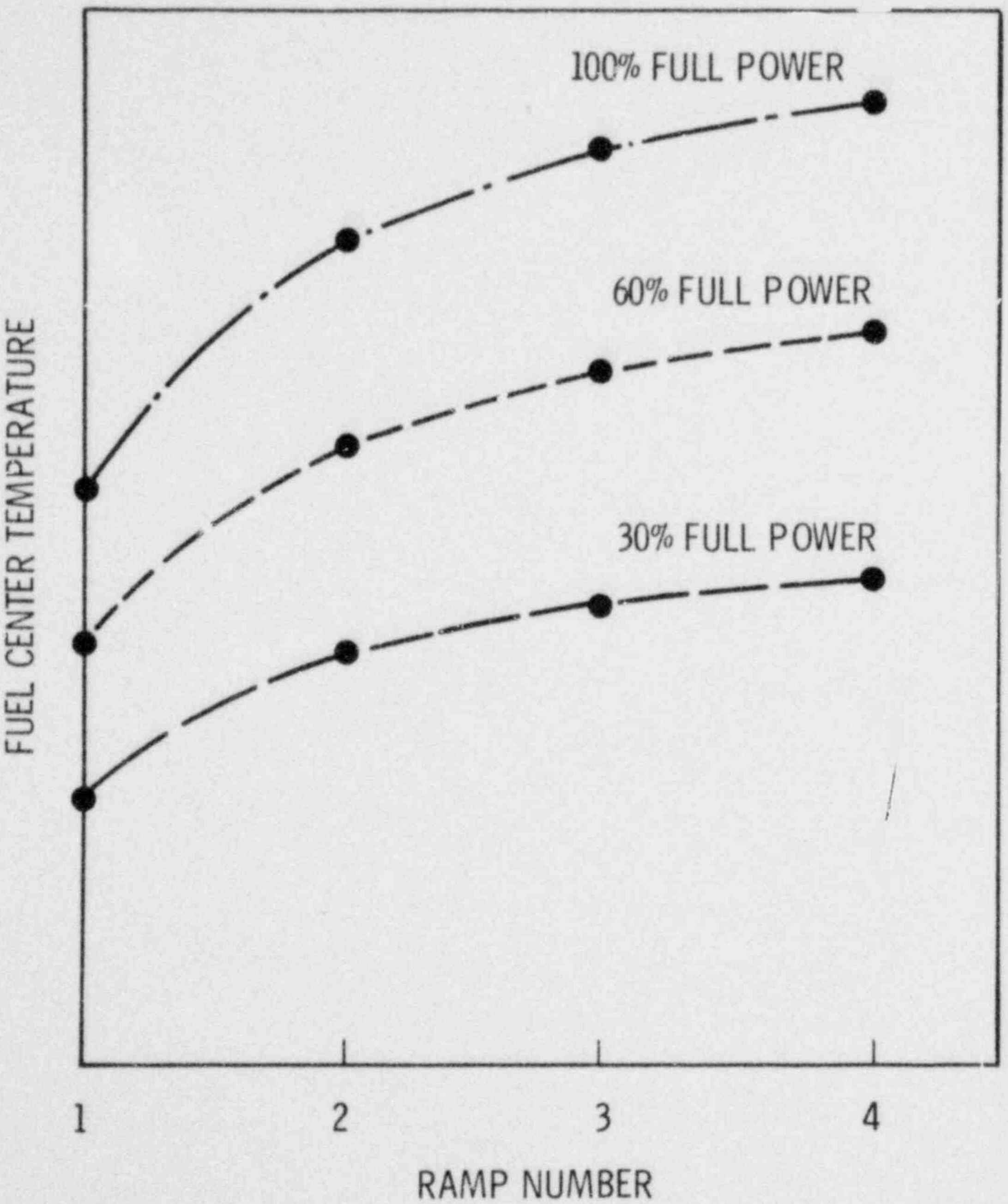

FIGURE 1. Fuel Center Temperature Behavior at Beginning-of-Life

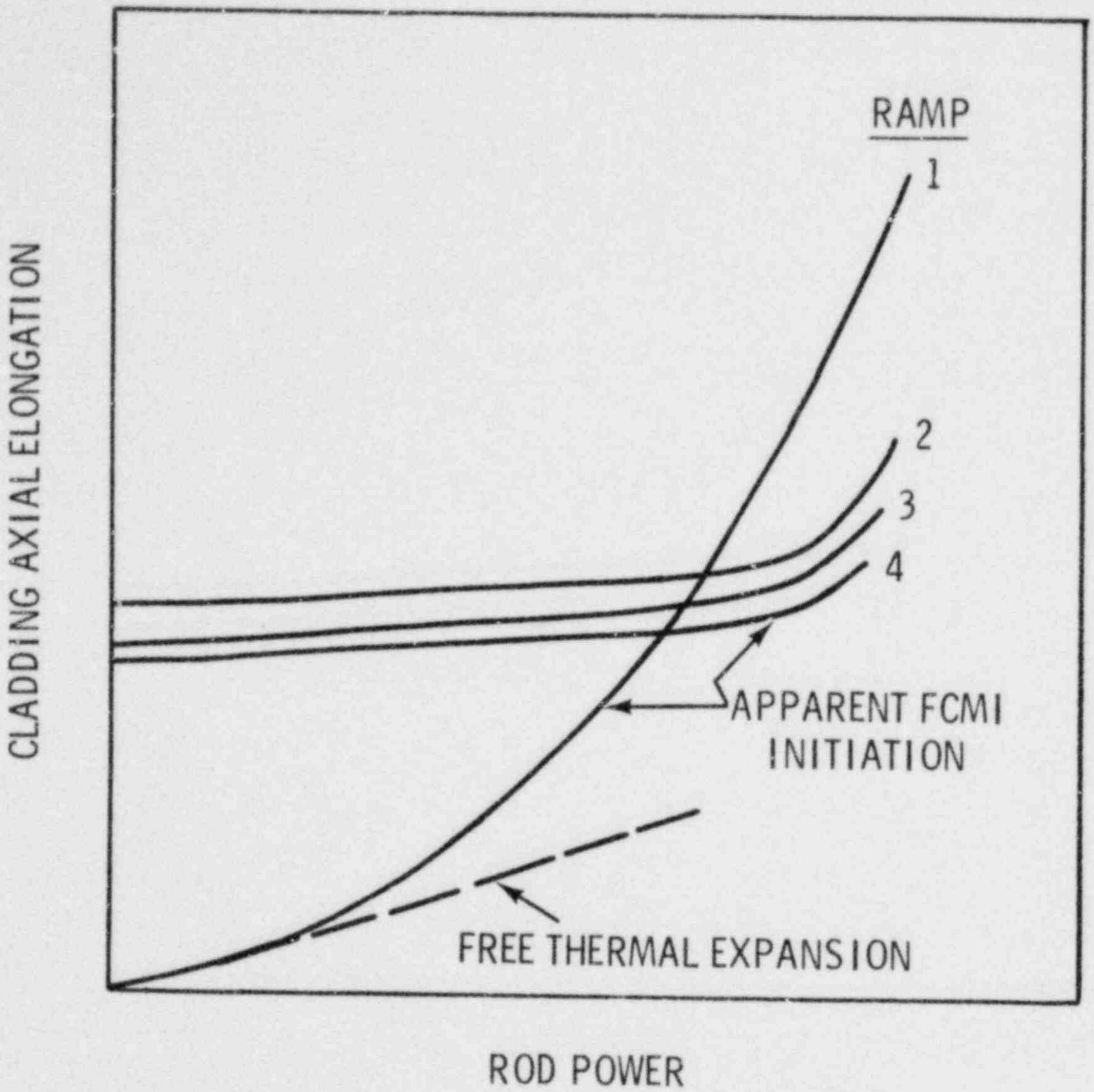

FIGURE 2a. Cladding Elongation Data at Beginning-of-Life

for all the ramps. First, note that the code predicts no zero-power offset (no permanent elongation). Second, note that there is no change in the code-predicted slope of the elongation curves from ramp to ramp. Neither the inhibition of elongation prior to apparent FCMI nor the slope change from ramp to ramp is predicted by the code.

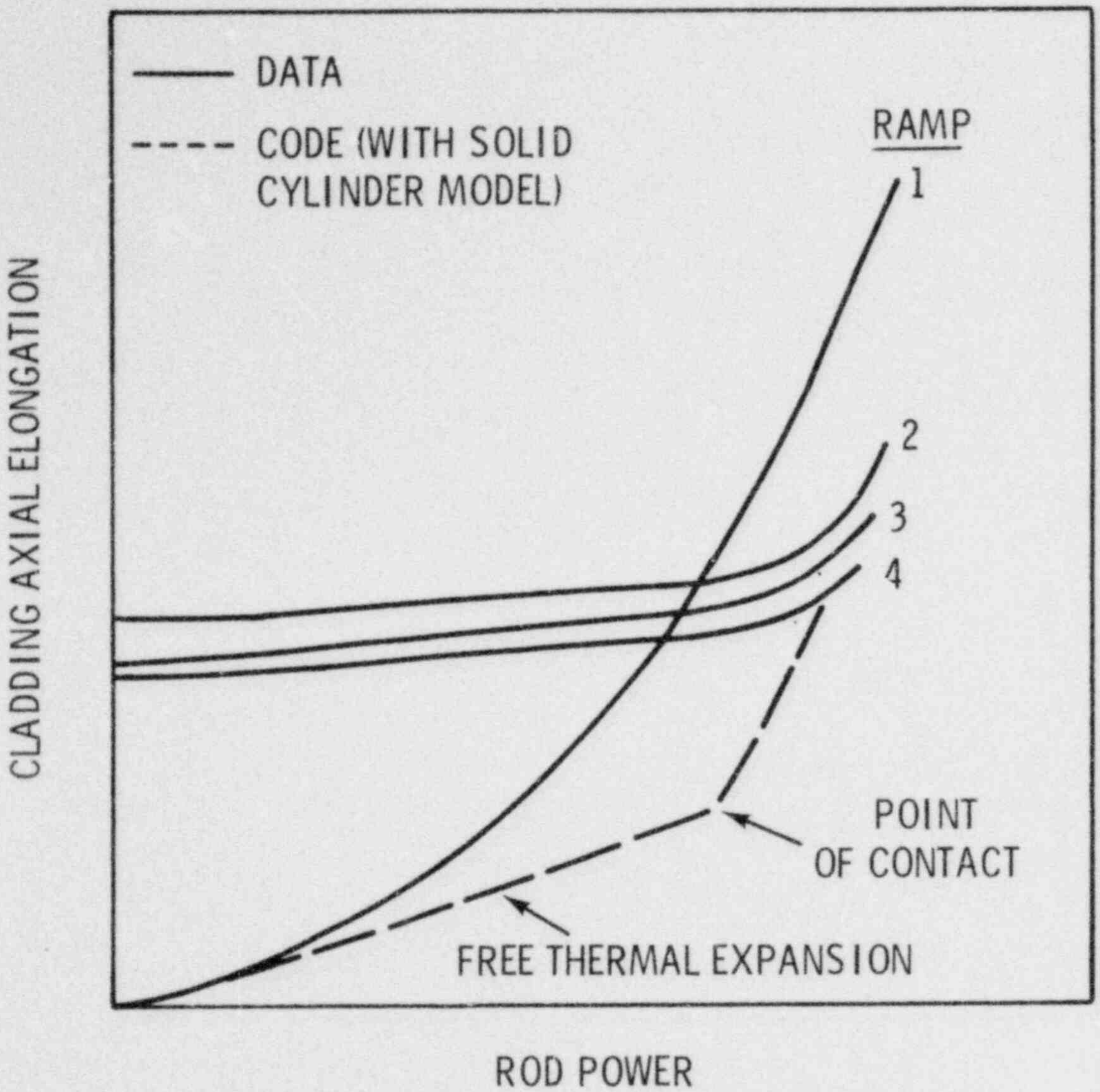

FIGURE 2b. Comparison of Cladding Elongation Data to Code Calculations

These behavorial characteristics were thought to be caused by the fuel cracking and its subsequent relocation. The following sections present alternate concepts intended to provide more suitable models for predicting the thermal and mechanical behavior of cracked nuclear fuel during operation.

4.0 EVOLUTION OF PELLETIZED FUEL SYSTEMS

In this section, we hypothesize a plausible combination of events that may occur during the ramp-to-ramp evolution of pelletized fuel systems in order to provide background for some of the analyses and models that follow. The phrase "evolution of pelletized fuel systems" is used here to emphasize that the fuel and cladding are components of a system, and that they experience changes in state throughout the life of the fuel rod.

In Appendix B, the thermal and mechanical data from IFA-431, IFA-432, and IFA-513 are presented in two basic forms. The full-life data illustrates the trends that are evident when the fuel mechanical evolution reaches its apparent asymptotic state and the thermal changes due to fission gas release became dominant. The beginning-of-life (BOL) data illustrates the period where the most dramatic changes in thermal and mechanical behavior occur in relatively short times under normal operating conditions. During the first few ramps to power, the fuel center temperatures for any specified power level have been observed to increase, as evidenced by the resistance versus power plots. The cladding axial elongation versus power plots exhibit significant and consistent reductions in slope during the first few power ramps. In many cases, these slopes have been less than that expected from the cladding axial free thermal expansion.[4]

Modern fuel performance codes have, in general, not succeeded in modeling these events to the satisfaction of the code authors. A possible source of this modeling difficulty may be inadequate representations of the cracked fuel. It is the purpose of this section to qualitatively describe alternate modeling concepts for cracked fuel pellets, thus serving as an introduction for the quantitative descriptions that follow. These alternate modeling concepts are approached from a strictly mechanical point of view (i.e., fuel cracking and relocation). Although other phenomena (i.e., densification or off-gassing) are sometimes used to explain some fuel behavioral characteristics, these variables have been controlled in these experiments.[5] This report is thus concerned only with fuel relocation, which is a thermally driven mechanical event.

MECHANICAL EVOLUTION

The life of a typical fuel rod begins with the loading of the pellets into the cladding. The completion of the rod and assembly fabrication and insertion into the reactor requires handling of the rod. During these loading and handling processes, the pellets probably stack stochastically within the cladding. The pellet-cladding eccentricity may thus be a random function of rod length.

It follows that during the first rise to power, the random eccentricity causes appreciable pellet-cladding contact that is distributed throughout the rod. As the fuel temperatures rise, the pellets begin to crack because of thermal strains induced by the radial temperature gradients. However, the cracked pellets have probably not yet separated into distinct fragments, at least not during the beginning of the first power ramp. This may be caused by the interlocking of the irregular fragments, or the radial and axial loads applied to the cracked (but still largely intact) pellets, or a combination of both. The expectation that many of the cracks will probably not extend from one free surface to another also tends to retard complete fragment separation during the beginning of the first power ramp. It may be possible for the fragments to begin separation as the fuel rod reaches higher operating powers, where the differential thermal expansions caused by the radial temperature gradient in the fuel may tend to push the fragments apart. However, the ratio of fragment size to fuel diameter is expected to remain sufficiently large enough to severely inhibit any "flow" of the fuel via relative motion between fragments. Thus, in general the fuel column is expected to retain much of its structural rigidity during the first power ramp.

The retained structural rigidity, when combined with the radial thermal expansion of the fuel, pellet-pellet end friction, and the random eccentricity, causes the pellet-cladding contact forces to increase throughout the rod as the power level increases. The pellet-cladding contact forces in turn provide a frictional resistance that prevents the fuel column from slipping axially with respect to the cladding. The prevention of axial slipping may also be caused by pellet chips becomming lodged in the gap, or by a region of locked pellets. However, it seems more probable that the accumulation of friction forces as described above is sufficient to prevent the fuel axial thermal expansion forces from causing axial slippage. Any inelastic accommodation of axial loads at higher power levels by the fuel may have a component due to the "flow" discussed above. The conservation of fuel volume then requires that as the axial length of the cracked pellet becomes shorter, the fuel is relocated radially outward via rigid body motion of the fragments. This in turn closes the gap and enhances the friction mechanism, which also impedes axial slippage.

The mechanisms postulated above would predict cladding axial elongations on the first ramp to power that become increasingly greater than the expected free axial thermal expansion of the cladding. This behavior would not be expected if the fuel and cladding geometry was truly that of concentric cylinders, with a pellet-cladding gap width that was symmetrically reduced as the power level increased, resulting in a sudden increase in cladding elongation when the gap closed.

The fuel structural evolution continues as the fuel rod is returned to a zero power state (hot standby). The reduction of the power/temperature level decreases the thermal expansion, and thus decreases the radial and axial forces imposed on the cracked pellets. This in turn allows the cracks to open and the fragments to separate. Once this occurs, the fuel can no longer be called a pellet. It has become a collection of irregular fragments. These fragments move relative to each other via translations and rotations so that their potential energy is minimized. The opening of the cracks is accompanied by misalignment of the fragment surfaces.

On the second rise to power, the radial and axial thermal expansion loads imposed on the fuel by cladding restraint must be transmitted across the cracks. But the crack surfaces are relatively rough and irregular, so that the contact between fragments is made through the surface asperities of adjacent fragments. The localized stresses on these asperities become very concentrated (References 6 to 10), and the cracks are consequently much more compliant than the solid fuel. The net result is that the effective elastic modulus of the cracked fuel is significantly lower than that for solid UO_2. It follows that the fuel-cladding interaction on the second and subsequent rises to power will be less severe than on the first power ramp. Thus the slope of the cladding elongation versus power curve will be reduced. This has been observed from in-reactor data.

Between the first and second power ramps, a permanent offset in cladding axial elongation is a common occurrence (see Appendix B). This may be explained by many phenomena, but the most probable seems to be that the permanent cladding axial elongation is due primarily to the relatively strong fuel-cladding interaction on the first power ramp. If there is no axial slipping on the first power ramp, the cracked pellets maintain their relative axial positions with respect to the cladding.

As the power decreases on the first shutdown, the fragments begin to move. The decrease in thermal expansion permits some fragments to rotate about their points of contact with the cladding. This in turn can lock the fragment collections into their respective axial positions. The end result is that the permanently elongated cladding provides some extra room for axial fuel cracks to open up. These axial cracks would be expected to be relatively small, and may not be detectable by gamma scans because they are probably not planar. Thus the axial elastic modulus of the cracked fuel column is also expected to be significantly less than that for solid UO_2.

The rates at which the radial and axial cracks close during subsequent power ramps may determine whether the fuel rod is radially or axially dominated. If at low powers, the radial cracks close faster than the axial cracks, there may exist a Poisson mechanism that would tend to reduce the total observed cladding axial elongation to a value less than that expected from free thermal expansion. If the axial crack closure dominates at higher powers, the cladding elongation would be expected to be greater than that for free thermal expansion. These manifestations of radial-axial dominance were observed from the in-reactor data.

THERMAL EVOLUTION

The thermal counterpart of the above described mechanical evolution is also of note. The fuel center temperatures on the first rise to power have been observed to be lower than those on subsequent ramps when compared at the same power levels. Since fuel densification and off-gassing have been controlled in these experiments,[5] a mechanical explanation may be proposed.

There are at least three possibilities, and all probably occur simultaneously. One possibility is that the mating of the cladding and (still largely intact) fuel surfaces on the first power ramp provides appreciable area for solid contact conductance to become a significant portion of the total gap conductance. Another possibility is that the axial forces imposed on the cladding induce Poisson effects that reduce its diameter by small amounts. In the azimuthal segments where there is still no fuel-cladding contact, the gap between the two surfaces is smaller than for the no-axial-load condition.[11] These two possibilities act to reduce the fuel temperatures on the first ramp to power.

There is also a third, more probable mechanism that can cause the fuel temperatures to exhibit a relative increase on subsequent ramps. This mechanism is the cracking of the fuel, and the filling of the cracks with gas, resulting in a reduction of the effective thermal conductivity of the fuel. The magnitude of the conductivity reduction depends on the fill gas composition, the crack widths, and the crack pattern (orientation).

The conductivity reduction may become significant at the first return to zero power, where the fragments may move relative to each other and open up the cracks. On the second rise to power, the fuel relocation (gap closure) is not necessarily complete, and the reduction in fuel thermal conductivity caused by cracking may have a greater effect on fuel temperatures than the partial closing of the gap. On subsequent power ramps, the partition of the total thermal resistance between fuel and gap may change. It is important to note that a change in gap conductance due to relocation will always be accompanied by a corresponding change in fuel thermal conductivity caused by the opening of cracks. The relative magnitudes of these changes will be discussed in Section 6.

GAP EVOLUTION

The evolution of the fuel-cladding "gap" also deserves attention, since it has been obscured by the assumption that the fuel and cladding are concentric cylinders throughout the life of the rod. The fuel is actually composed of irregular fragments which have moved about in the space allowed them during relocation. Since this motion is expected to have a rotation component, it follows that on the average, the fuel and cladding surfaces are probably not aligned. It is more likely that the cladding experiences contact by many relatively large "asperities" provided by the disoriented fuel fragments. Thus the "gap" also has an equivalent roughness, and responds to thermal expansion induced loads in a manner similar to the fuel cracks. The "gap" is symmetric only on the average, in a statistical or stochastic sense.

HYPOTHESIS

It is postulated that the extent to which the fuel effective thermal conductivity and elastic moduli can change is controlled primarily by the amount of free volume the fragments have in which to move about, and on the distribution of the free volume between the fuel cracks and the gap. The greater this free volume, the greater the reductions in effective fuel properties, when other variables are held constant.

The description of pelletized fuel system evolution in this manner is a departure from the conventional concentric solid cylinder approach, and it is the objective of the following sections to quantify and verify these concepts.

5.0 MECHANICAL MODELS: ELASTIC MODULI FOR CRACKED PELLETS

We begin by recognizing that Hooke's Law describes the behavior of a medium that is assumed to be continuous. This is not the case for cracked UO_2 pellets, but the use of these equations is justified for calculational economy in fuel performance codes. Hooke's Law in cylindrical coordinates reads:

$$\varepsilon r = \frac{\sigma_r}{E_r} - \mu r\theta \frac{\sigma_\theta}{E_\theta} - \mu rz \frac{\sigma_z}{E_z} \tag{1}$$

$$\varepsilon \theta = \frac{\sigma_\theta}{E_\theta} - \mu r\theta \frac{\sigma_r}{E_r} - \mu\theta z \frac{\sigma_z}{E_z} \tag{2}$$

$$\varepsilon z = \frac{\sigma_z}{E_z} - \mu rz \frac{\sigma_r}{E_r} - \mu\theta z \frac{\sigma_z}{E_z} \tag{3}$$

where ε is strain, σ is stress, E is Young's Modulus, and μ is Poisson's ratio.

In-reactor data yields three relevant simultaneous measurements: power, center temperature, and total cladding axial elongation. The number of unknowns in the above equations must therefore be reduced. This can be done by assuming that some symmetry exists. Specifically, we may assume that since the fuel is cracked, but still relatively tightly packed, a hydrostatic state of stress exists in the (r, θ) plane, i.e.,

$$\sigma_r = \sigma_\theta \tag{4}$$

We will allow the axial fuel stresses to be different from the (r, θ) stresses so that the cladding elongation data may be used to its fullest advantage for describing the state of the cracked fuel column.

Because the fuel cracks are nearly aligned with the principle axes, we assume that Poisson's ratio is the same between any two arbitrary principle axes:

$$\mu_{r\theta} = \mu_{rz} = \mu_{\theta z} = \mu \qquad (5)$$

We also assume that the radial and hoop elastic moduli are identical:

$$E_r = E_\theta \qquad (6)$$

Substituting equations (4), (5), and (6) into equations (1), (2), and (3), we get:

$$\varepsilon_r = \frac{\sigma_r}{E_r} - \mu \left[\frac{\sigma_r}{E_r} + \frac{\sigma_z}{E_z} \right] \qquad (7)$$

$$\varepsilon_\theta = \frac{\sigma_r}{E_r} - \mu \left[\frac{\sigma_r}{E_r} + \frac{\sigma_z}{E_z} \right] \qquad (8)$$

$$\varepsilon_z = \frac{\sigma_z}{E_z} - 2\mu \frac{\sigma_r}{E_r} \qquad (9)$$

The (r, θ) and the z components of the cracked fuel may be further separated by adding equations (7) and (8):

$$\varepsilon_r + \varepsilon_\theta = 2(1-\mu) \frac{\sigma_r}{E_r} - 2\mu \frac{\sigma_z}{E_z} \qquad (10)$$

Equation (9) may be substituted into equation (10) to eliminate the σ_z/E_z term,

$$\varepsilon_r + \varepsilon_\theta = \frac{2\sigma_r}{E_r} (1+\mu)(1-2\mu) - 2\mu\varepsilon_z \qquad (11)$$

This equation is then a form of Hooke's Law where the (r, θ) components are separated from the z components, and the only material properties involved are the effective radial elastic modulus and Poisson's ratio.

Because the cracked fuel was assumed to be in a hydrostatic state of stress in the (r, θ) plane, the concept of the bulk modulus[12] may be used to further relate equation (11) to in-reactor data. We assume that the closing (or opening) of the fuel cracks dominates the fuel strain, and that the strains of the individual fragments are negligible. The relationship between the cross-sectional area of the cracked fuel and the strain is:

$$A + \delta A = A(1 + \varepsilon_r)\ (1 + \varepsilon_\theta) \tag{12}$$

where A is the total cross-sectional area of the fuel, and δA is the cross-sectional area occupied by the cracks. When the higher order term in equation (12) is neglected, we obtain:

$$\frac{\delta A}{A} = \varepsilon_r + \varepsilon_\theta \tag{13}$$

where the term on the left is the fractional cross section area of the cracked fuel system that is occupied by the cracks. Substituting equation (13) into equation (11) results in:

$$\frac{\delta A}{A} = \frac{2\sigma_r}{E_r} (1 + \mu)(1-2\mu) - 2\mu\varepsilon_z \tag{14}$$

The determination of the effective radial elastic modulus (E_r) of the cracked fuel may be further specified by introducing a model that relates the cross-sectional area ($\delta A/A$) to the hydrostatic stress (σ_r). The total crack area is equal to the sum of the products of the crack lengths times the crack widths. The crack widths are related to the hydrostatic stress by a model given by Mikic[10]:

$$\frac{1}{2}\,\mathrm{erfc}\left[\frac{d}{R\sqrt{2}}\right] = \frac{\sigma_r}{\sigma_r + H} \tag{15}$$

where: d = separation of mean surface planes (crack width)

R = effective surface roughness of cracks (1 standard deviation)

σ_r = hydrostatic stress applied normal to crack plane

H = Meyer hardness of UO_2

erfc = complementary error function

The asperity heights of the crack surfaces are assumed to form a normal distribution. The left side of this equation encompasses the surface geometry factors, while the right side expresses the load dependency. The hydrostatic stress is thus related to the crack width, which is in turn related to the cross-sectional free area of the cracks. Since the fuel is assumed to be in a hydrostatic state of stress in the (r, θ) plane, all crack widths are equal if all effective roughnesses are equal. This is a "scalar" representation of crack area and should be expanded to a "vector" form in the future.

The Mikic model is also used to describe the surface contact stresses at the cladding ID. The controlling variable for each type of surface interaction is the effective roughness. Equilibrium is reached when the crack and gap widths are found such that thermal and mechanical equilibrium are reached simultaneously. However, there still exists a problem in this model: the proper definition of the strain of the cracked fuel pellet. In Hooke's Law, the reference strain is identically zero at the zero stress state. But the cracks modeled by equation (15) have no unique strain reference at zero stress. Any arbitarily large crack width will produce a zero stress state. Thus the $(\delta A/A)$ term in equation (14) has n reference value.

This lack of [illegible] strain reference for the cracks may be accommodated by incorporating an incremental method in the analysis. Changes in power/temperature produce changes in crack width. Subtracting the crack widths between two successive power levels cancels out the reference strain:

$$\left[\left(\frac{\delta A}{A}\right)_2 - \left(\frac{\delta A}{A}\right)_{Ref}\right] - \left[\left(\frac{\delta A}{A}\right)_1 - \left(\frac{\delta A}{A}\right)_{Ref}\right] \tag{15}$$

$$= \left(\frac{\delta A}{A}\right)_2 - \left(\frac{\delta A}{A}\right)_1$$

$$= \Delta A$$

The use of this method also requires that the hydrostatic stress and axial strain be expressed incrementally. Equation (14) in incremental form is thus:

$$\frac{\Delta A}{A} = \frac{2\Delta\sigma_r}{E_r}(1+\mu)(1-2\mu) - 2\mu\Delta\varepsilon_z \tag{16}$$

where the Δ represents the change in the variables from one rod power level to the next. The effective fuel moduli to be determined are thus the secant moduli between two power/temperature levels.

Assuming that the crack parameters are known so that $\Delta A/A$ and $\Delta\sigma_r$ may be determined, that leaves the axial strain as the next variable to be quantified.

The axial fuel strain (ε_z) may be determined from the cladding elongation data by assuming that there is no axial slipping between the fuel and cladding. We note that ε_z in equation (16) is the fuel axial strain due to mechanical loads only, so that the fuel axial thermal expansion must be subtracted from the total fuel strain. This axial fuel strain is actually the strain caused by the closing (or opening) of the axial cracks in the fuel. (Axial cracks are parallel to the (r, θ) plane, radial cracks are parallel to the (r, z) plane, and azimuthal cracks are parallel to the (θ, z) plane).

The axial strains for the fuel and cladding are as follows:

$$\varepsilon_{zfs} = \varepsilon_{zfm} + \varepsilon_{zft} \tag{17}$$

$$\varepsilon_{zcs} = \varepsilon_{zcm} + \varepsilon_{zct} \tag{18}$$

where: z = axial direction; s = sum; f = fuel; m = mechanical; c = cladding; t = thermal.

Since we have assumed that there is no axial slipping between the fuel and cladding, we have the following compatibility equation:

$$\varepsilon_{zfs} = \varepsilon_{zcs} \tag{19}$$

Substituting equations (17) and (18) into equation (19), the axial fuel strain of equation (16) can be determined from the cladding elongation data (ε_{zcs}):

$$\varepsilon_{zfm} = \varepsilon_{zcm} + \varepsilon_{zct} - \varepsilon_{zft} \tag{20}$$

The thermal strains for fuel and cladding may be determined from rod power and fuel temperature measurements.

The changes in crack area ($\Delta A/A$), the hydrostatic stress ($\Delta\sigma_r$), and the axial fuel strain ($\Delta\varepsilon_z$) now being known in equation (16), this leaves us with one equation and two unknowns (E_r and μ).

At this point, we must assume a value for Poisson's ratio. This may be made on the basis of soil and rock mechanics work. A value of 0.25 has been reported for sand.[13] If the fuel and cladding were completely locked together, the value of Poisson's ratio would be expected to be about 0.3.

Thus, the value for sand accounts for the looseness of the cracked fuel. Now we may use the in-reactor data to solve for the effective radial elastic modulus of the cracked fuel system.

The effective axial elastic modulus of the cracked fuel system may be determined by making use of the assumption that there is no axial slipping between the fuel and cladding. This non-slipping assumption requires that the fuel and cladding be in axial force equilibrium. Since at each power (temperature) level, axial equilibrium must hold, we may write the equation in incremental form:

$$\Delta F_{zc} = \Delta F_{zf} \tag{21}$$

where the subscripts f and c represent the fuel and cladding, respectively. We also rewrite equation (9) in incremental form, and a similar equation for the cladding:

$$\Delta \varepsilon_{zf} = \frac{\Delta \sigma_{zf}}{E_{zf}} - 2\mu_f \frac{\Delta \sigma_{rf}}{E_{rf}} \tag{22}$$

$$\Delta \varepsilon_{zc} = \frac{1}{E_c} \left[\Delta \sigma_{zc} - \mu_c \left(\Delta \sigma_{rc} + \Delta \sigma_{\theta c} \right) \right] \tag{23}$$

The radial and hoop stress changes for the cladding are known from $\Delta \sigma_{rf}$ and the coolant pressure, and may be found from thick wall formulas.[14] The sum of the hoop and radial stresses is the first stress invariant, so that (for plane stress)

$$\Delta \sigma_{rc} + \Delta \sigma_{\theta c} = \Delta I_{1c} \tag{24}$$

The elastic modulus and Poisson's ratio for the cladding are known. The change in cladding axial strain is the mechanically induced portion of the cladding elongation, the thermal expansion increment having been subtracted. Equating axial force changes for fuel and cladding yields:

$$\left[\Delta\varepsilon_{zf} + 2\mu_f \frac{\Delta\sigma_{rf}}{E_{rf}}\right] E_{zf} A_{zf} = \left[\Delta\varepsilon_{zc} E_c + \mu_c \Delta I_{1c}\right] A_{zc} \qquad (25)$$

where A_{zf} and A_{zc} are the cross-sectional areas of the cracked fuel and cladding, respectively. All other symbols are as previously defined. Since the effective radial elastic modulus for the fuel was determined in equation (16), equation (25) may then be used to solve for the effective axial elastic modulus of the cracked fuel system.

Equations (16) and (25) are used in the next section to calculate the effective elastic moduli for a range of fuel rod designs.

6.0 ANALYSIS OF IN-REACTOR DATA

In this section we combine the in-reactor thermal and mechanical data to solve for the material properties that were discussed in the previous sections. Because the evolution of pelletized fuel systems is frequently subtle, fuel rod data from BOL was used, where fuel structural changes caused by cracking are greatest, and fission gas release is minimized. This type of data lends a greater sensitivity to the analysis of fuel cracking and relocation.

The data that we have analyzed is shown in Appendix B. It consists of the simultaneous measurement of rod powers, centerline temperatures, and total cladding axial elongations. Because of the necessity to cast the equations for elastic moduli in incremental form, data from power ramps was required. The data from IFA-513 were corrected for the response lag of the vanadium SPND's,[15] while those for IFA-431 and 432 were not. It will be seen that the scatter in the data is greater than the small errors in power levels. Most power ramp rates were slow enough to be classed as steady state, the power between data points changing by less than 16 kW/m/hr.

A computer code was written to analyze the data. A flow diagram for program BM2DNS (Bulk Modulus in 2 Dimensions with No Slip) is shown in Figure 3. The two convergence loops are for the thermal conditions in the gap and the hydrostatic stress condition of the fuel. The program first reads in a set of temperature, power, and cladding elongation data for a rod at a particular time during a power ramp. Then a gap size (Dg) is assumed and the stress at the cladding ID (PRG) is calculated using the Mikic surface response model. A value for the effective roughness of the gap must be assumed. This has been found to be dependent on the design gap size, and will be discussed later in this section. Then the radius of the cracked fuel at thermal and mechanical equilibrium, (RFM), is calculated from the assumed gap and the cladding ID, which has been corrected for thermal expansion and the deformation due to coolant and FCMI pressures. Using this gap size, the temperature drop across the gap (ΔTg) is found in an inner convergence loop. A temperature drop is first assumed, and the gap conductance components due to conduction, radiation

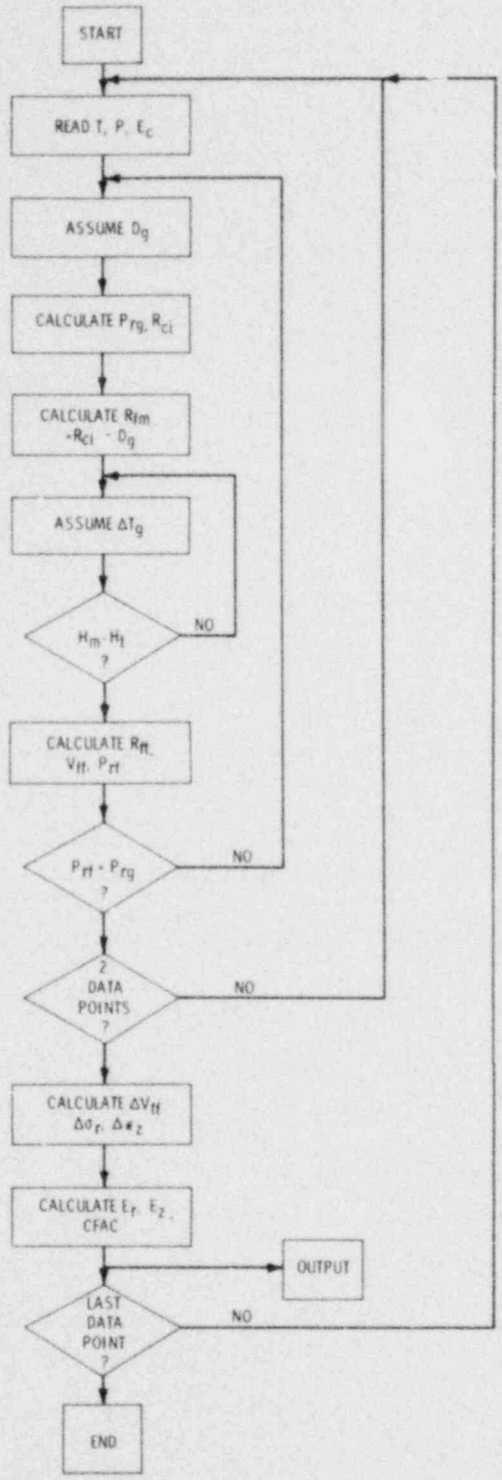

FIGURE 3. Flow Diagram for Program BM2DNS

and solid contact[2] are summed to find the total gap conductance from mechanical considerations (H_m). This is compared with the total gap conductance from thermal conditions (H_t), which is found by dividing the heat flux by the gap temperature drop. Convergence is reached when the two total gap conductances are the same. Then the fuel volume average temperature is estimated from the center and surface temperatures, and input to a thermal expansion model[16] to calculate the stress-free thermally expanded radius of the solid fuel (RFT). The area difference between RFT and RFM is the free area within the fuel that is occupied by cracks:

$$VFF = \pi(RFM^2 - RFT^2)$$

The total free area that is occupied by the cracks plus the gap is defined by the cladding inner radius:

$$VFC = \pi(RCI^2 - RFT^2)$$

The crack area (VFF) is then divided by the total crack length to find the widths of the cracks. Since the stress is the same throughout the fuel, the cracks will all be of the same width, according to the Mikic model. This crack width is applied in the Mikic model, along with an assumed crack roughness, and the hydrostatic stress in the fuel is found (PRF). When this value equals the radial stress at the cladding ID, mechanical equilibrium is reached.

The above calculations are performed for two successive data points which are usually less than 1.5 kW/m apart in power level. Then incremental values of the crack area (VFF), stress, and strain are computed. (The incremental VFF is the same as ΔA of Section 5.) These values are used in Equation (16) to calculate the effective radial elastic modulus for the cracked fuel. The elastic modulus for the axial direction of the cracked fuel is determined by Equation (25), where the mechanical portion of the cladding axial strain is found by subtracting the calculated thermal expansion portion from the total cladding axial elongation data.

It is known that voids or cracks in the fuel reduce its thermal conductivity below that for solid polycrystalline UO_2. Thus a value for this factor (CFAC) is computed using the Robertson integral[17] and Lyons thermal conductivity:[18]

$$\mathrm{CFAC} \int_{\mathrm{TFS}}^{\mathrm{TCL}} K_{\mathrm{Lyons}} \, dT = \mathrm{QF}/4\pi$$

For these experiments, the flux depression, F, had a value of 0.835.

Some important assumptions are necessary in order to use the above methods to solve for the effective elastic moduli of the cracked fuel. These assumptions originate from a need to define the free area and its distribution within the cladding ID.

The assumptions that are necessary are those of a crack pattern in the fuel, and the effective roughnesses for the fuel internal cracks and outer surface (gap). The crack pattern that was chosen for this initial study consisted of eight radial cracks and one circumferential crack, as shown in Figure 4. When the circumferential crack occurs at about 0.56 of the fuel radius, the total crack length is nearly equivalent to seven radial cracks extending to the fuel center. Since the widths of all cracks are equal under hydrostatic stress conditions in the (r, θ) plane, the value of VFF will be the same for both crack patterns. This model was chosen for its ability to represent both cases, and its resemblance to in-reactor conditions (Figure 5).

The selection of roughness values required that the results of the transient data analysis be used. The distribution of the free area between the cracks and gap determines the radial temperature distribution in the fuel, which in turn determines values for the effective fuel thermal conductivity and gap conductance. The effective conductivities and gap conductances had previously been deduced by the analysis of fast power drop data from IFA-432[19] and IFA-513.[15] Surface (gap) roughnesses were chosen so that the gap conductances calculated by BM2DNS corresponded to those found by analysis of fast power drop data. The same roughnesses were used in a contact conductance model based

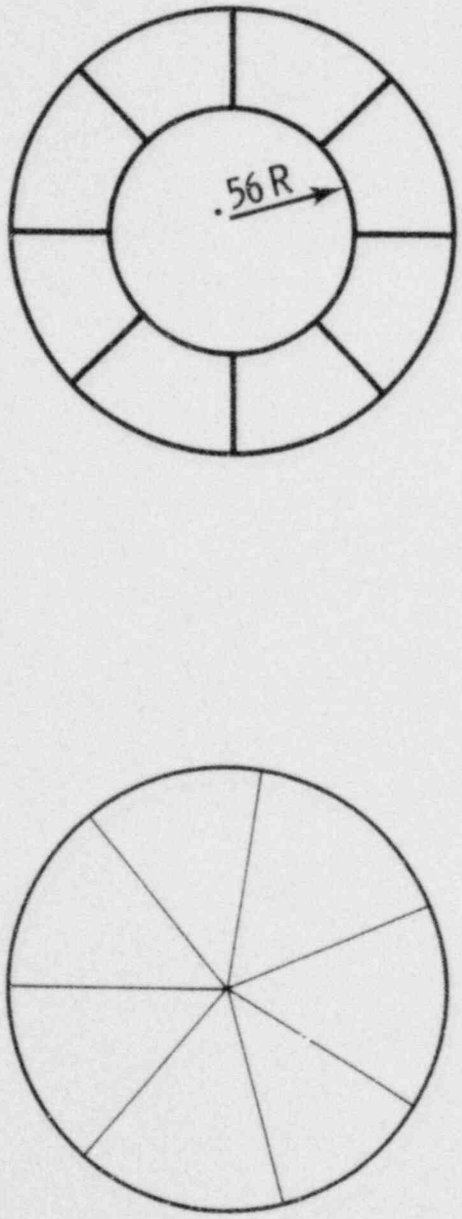

a.

b.

FIGURE 4. Top: Crack Pattern With Circumferential Crack
Bottom: Radial Cracks Only

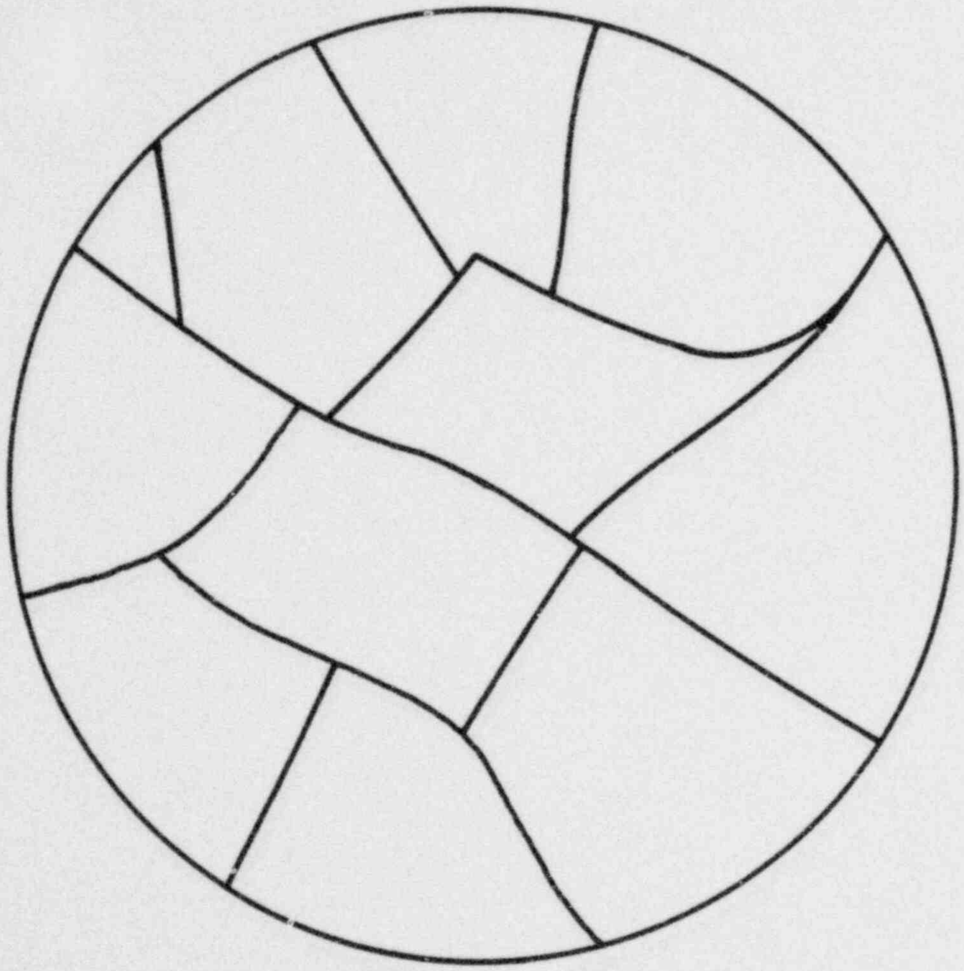

FIGURE 5. Crack Pattern of Pellet 39 from Rod 6 of IFA-431

TABLE 2. Determination of Gap Roughness

Rod Design			Conditions at 30 kW/m			
Rod Number	Gap (mm)	Fill Gas He:Xe	Hot Gap (mm)	H Gap kW/m^2 K	Fraction H Solid	Gap Roughness (mm)
3	0.038	1:0	0.005	25.80	0.226	0.003
1	0.114	1:0	0.031	8.70	0.260	0.014
6	0.114	0.77:0.23	0.030	6.55	0.405	0.014
2	0.190	1:0	0.054	5.76	0.271	0.023

on recent data.[20] Table 2 shows that the dependence of gap roughness on initial radial gap size is nearly linear when found by this approach.

It was also necessary to specify values for the surface roughness of the internal fuel cracks. As in the case of the gap, the crack roughness is defined by the misalignment of irregularly shaped fragments. It would again be expected to be influenced by the magnitude of the relative motions between fragments, and thus by the amount of available void (free area). The exact definition of this dependence is an unsettled matter that requires further investigation. The crack roughness was taken to be equal to 1.6 times the gap roughness for this initial study. The suitability of this assumption is shown by comparing the fuel thermal conductivity factor derived by transient methods with that calculated by BM2DNS, as shown in Table 3. Agreement is within the uncertainty for the transient data.

The dependence of the thermal conductivity factor CFAC on the hydrostatic stress for Rods 1, 2, and 3 of IFA-432 and Rod 6 of IFA-513 is shown in Figure 6. An array of gap size and fill gas effects is thus displayed. The increased xenon content of Rod 6 causes an expected decrease in CFAC due to the

TABLE 3. Comparison of CFAC Values

	CFAC at 30 kW/m	
Rod Number	Transient ($\pm 1\sigma$)	BM2DNS
3	1.000 ($\pm$0.3)	0.964
1	0.836 ($\pm$0.3)	0.806
6	0.746 ($\pm$0.2)	0.736
2	0.724 ($\pm$0.2)	0.711

lower thermal conductivity of the gas filling the fuel cracks, while the other rods form a consistent pattern. Figure 6 also indicates that each rod maintains a finite stress level throughout its power/temperature range.

There is always contact between the fuel and cladding due to the roughness of the cracked fuel surface. This is a result of the hydrostatic stress condition required for equilibrium in the (r, θ) plane of the cracked fuel. This constant contact condition results in an effective gap size which remains relatively constant throughout the power/temperature range (Figure 7). As the power and temperature increase, the cladding diameter changes because of thermal expansion and the stresses imposed on it. Since there must be hydrostatic equilibrium, the fuel radius tends to follow the cladding diameter. The slight decrease in gap size with increasing power is caused by the compression of the "surface asperities" of the gap, as dictated by the surface response model. This recognizes three events that are not adequately modeled by the solid concentric cylinder approach. The first is that since there is always contact between the fuel and cladding, the gap conductance will always have a finite contribution from solid conductance. The second is that the gap will not open during a severe power decay transient. This has also been shown by the analysis of scram data.(19) Since the thermal expansion is localized within each distinct fragment, there is no driving force to pull the fuel away from the cladding as the power is reduced. There should be no tension in a medium composed of separated fragments. The third event is that the changes in the available void (free area) occur in both the gap and in the fuel. The opening and closing of the fuel cracks (via the Mikic model) is just as important as for the gap.

The effect of the amount of crack void (VFF) on the radial elastic modulus is shown in Figure 8, where the crack void is plotted as a percentage of the total cross sectional (r, θ) area of the cracked fuel. The vertical axis is the base 10 logarithm of the radial elastic modulus (Pascals) as derived in the previous section. The data points are identified by rod number. A distinct dependence on crack void can be seen. The radial elastic modulus for the typical BWR design Rods 1 and 6 is at least one order of magnitude less than that for solid polycrystalline UO_2.(16)

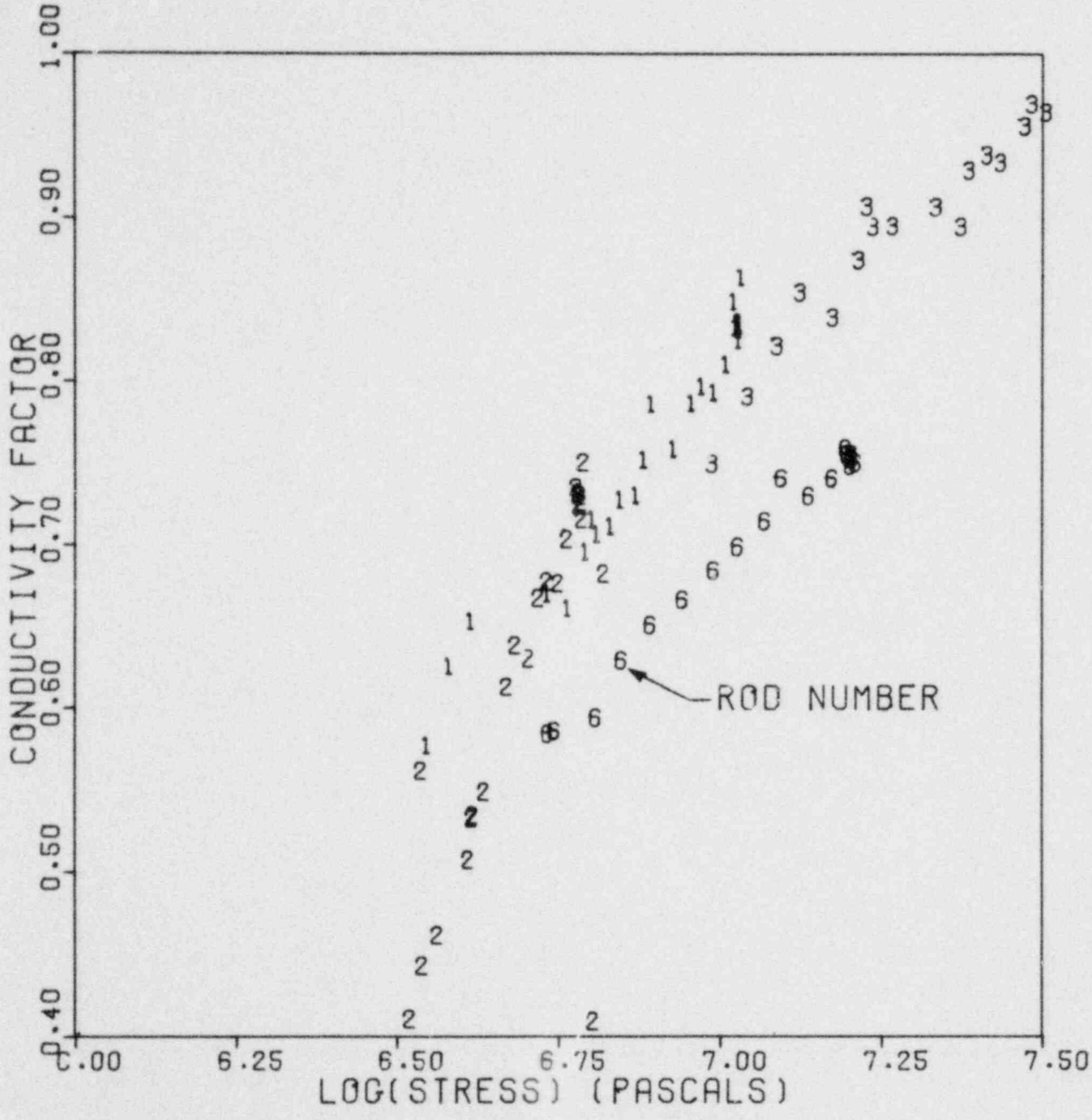

FIGURE 6. Thermal Conductivity Factor Versus Hydrostatic Stress (data points identified by rod number)

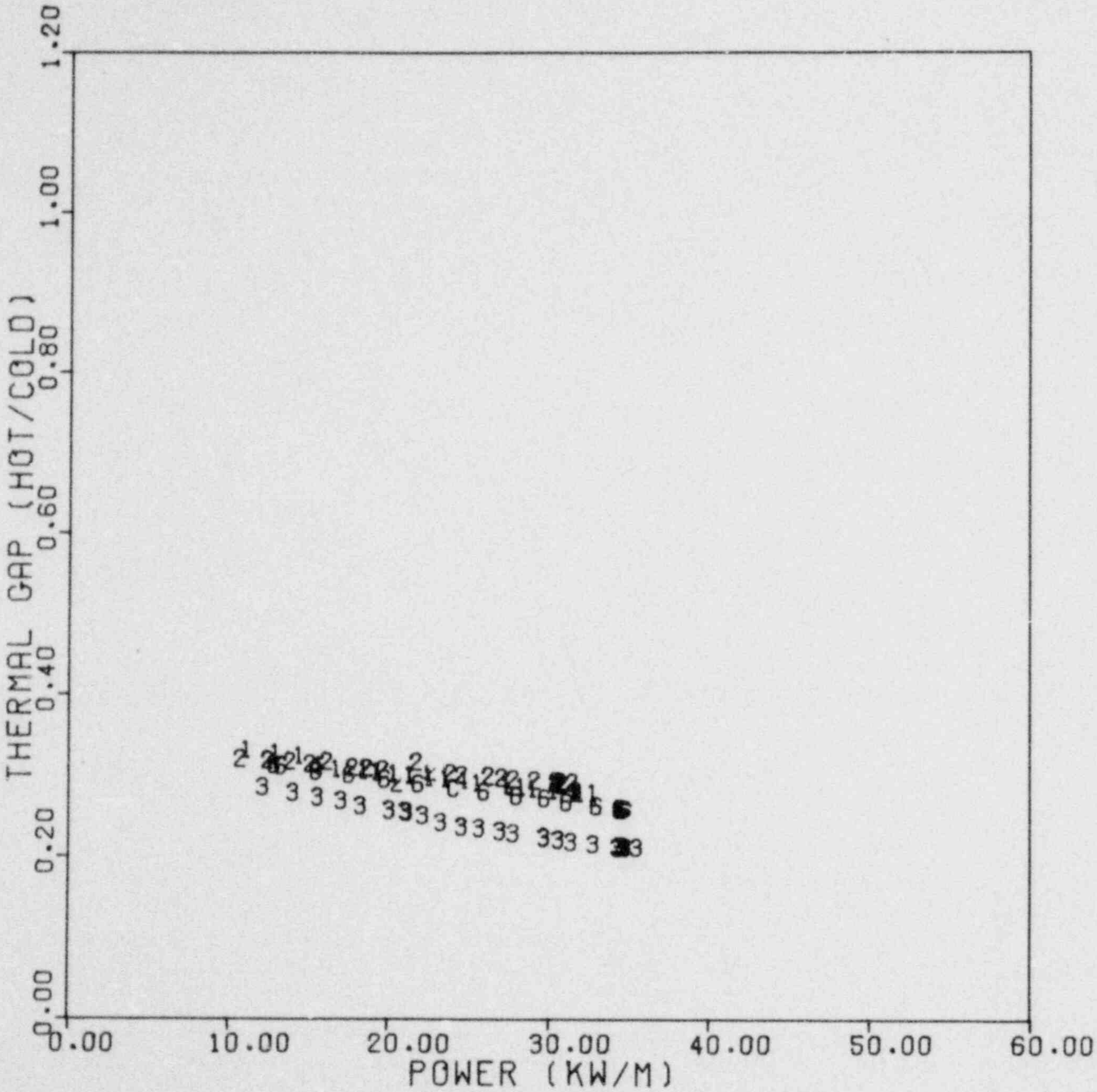

FIGURE 7. The Pellet-cladding Gap Under Hydrostatic Conditions (data points identified by rod number)

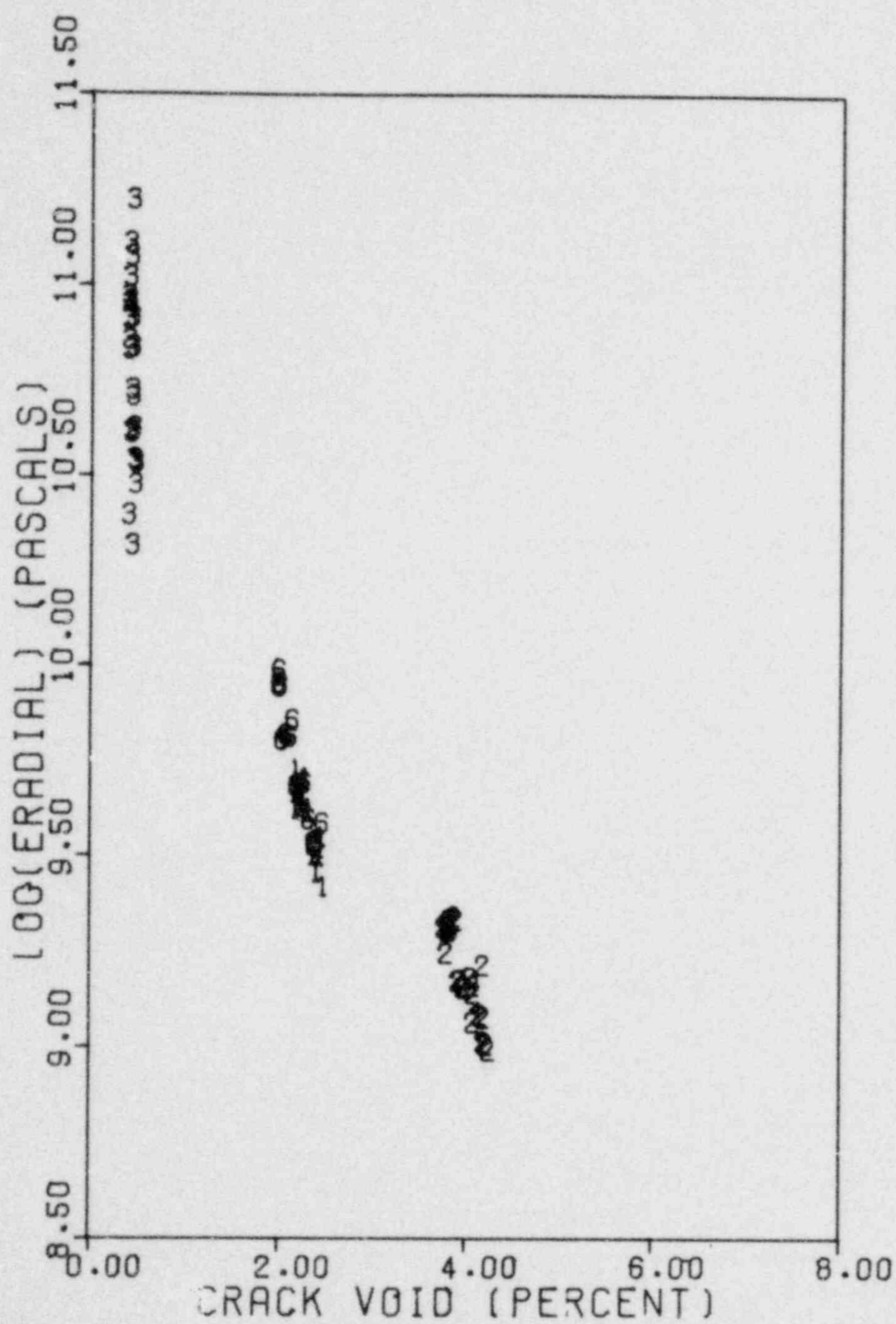

FIGURE 8. Radial Elastic Modulus as a Function of Fuel Available Void (data points identified by rod number)

The axial fuel modulus as a function of total available void (VF?) is shown in Figure 9, where the total void is plotted as the percentage of the cross sectional area defined by the cladding inner diameter. On the vertical axis is the base 10 logarithm of the axial fuel elastic modulus (Pascals). The trends are similar to those seen for the radial elastic modulus, with a slightly greater reduction. This slight anisotropy is shown in Figure 10.

We now turn our attention to the evolution of the fuel system, as discussed in a previous section. For this purpose, we have analyzed the first five power ramps for two rods typical of current BWR design. These are Rod 1 of IFA-432 and Rod 1 of IFA-513.

Rod 1 of IFA-513 was analyzed with constant crack and gap roughnesses and a constant crack pattern. These were discussed earlier in this section. The objective of this approach is to let the data reveal its own trends. The thermal conductivity factors for the first five ramps to power are shown in Figure 11, where the numbers plotted refer to ramp number. These are very similar to those shown in Figure 6. Through the scatter in the data, a trend toward decreasing CFAC can be seen with increasing ramp number. Since the model had a constant crack pattern and roughnesses, this trend reflects the increase in temperature gradient across the fuel with increasing ramp number. The magnitude and trends in CFAC are as expected. Precharacterization data indicates that densification and off-gassing of the fuel are expected to be negligible.[21]

The evolution of the radial elastic modulus for Rod 1 of IFA-513 is shown in Figure 12 where the vertical axis is the base 10 logarithm of the modulus. There appears to be an envelope that decreases in width with increasing ramp number, indicating that the fuel mechanical behavior is becoming more stabilized as time passes. The expected decrease in modulus with increasing ramp number is not clearly manifested in this figure. This type of evolution would signal the fuel's passage from solid to cracked states. The impact of the assumed constant crack pattern and roughnesses on modulus is apparently greater than the effects of the temperature gradient rise shown in Figure 11. Figure 13 indicates that the radial modulus is apparently slightly dependent on temperature. However, since the Meyer hardness of the UO_2 is independent of

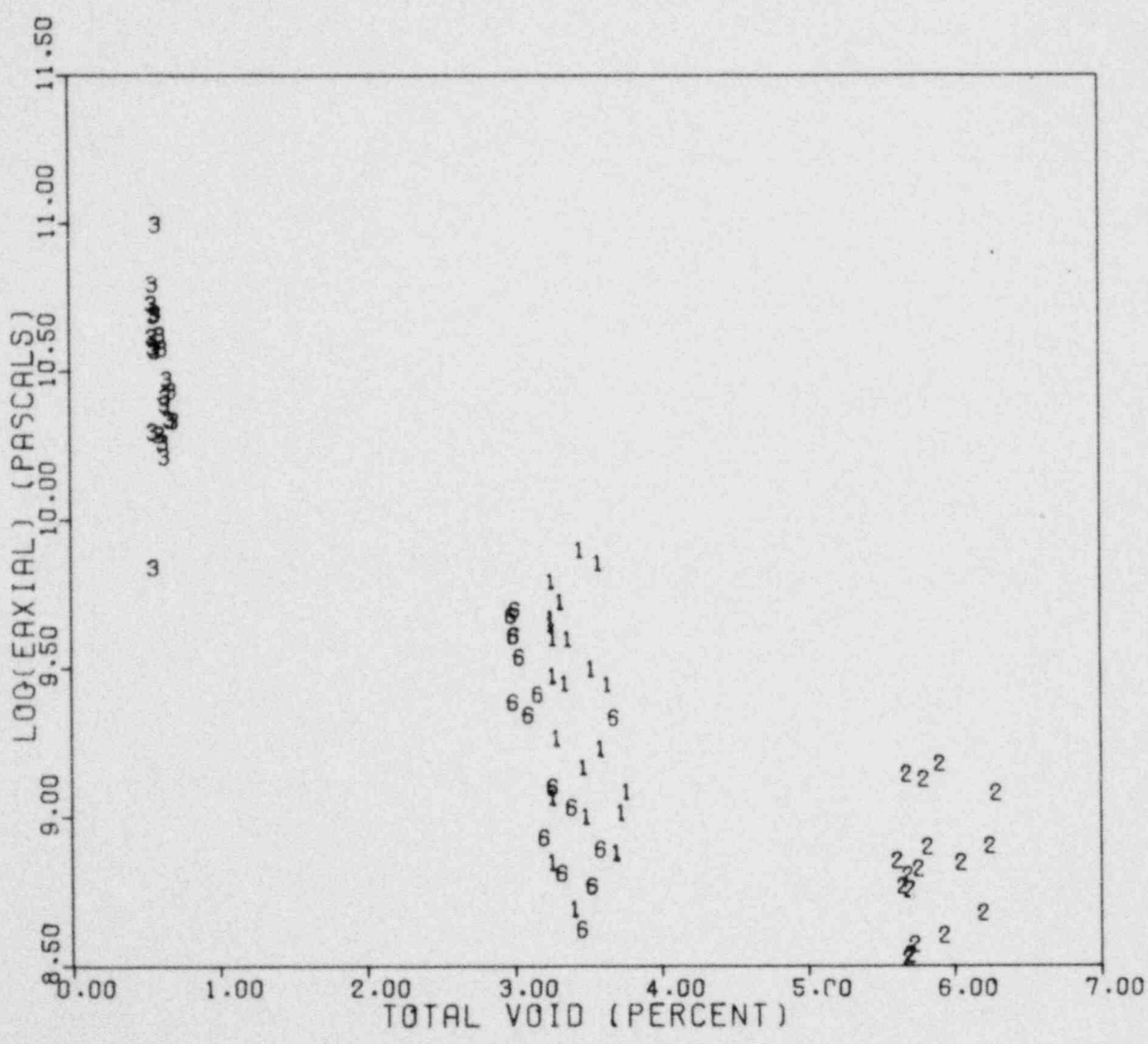

FIGURE 9. Axial Elastic Modulus as a Function of Total Available Void (data points identified by rod number)

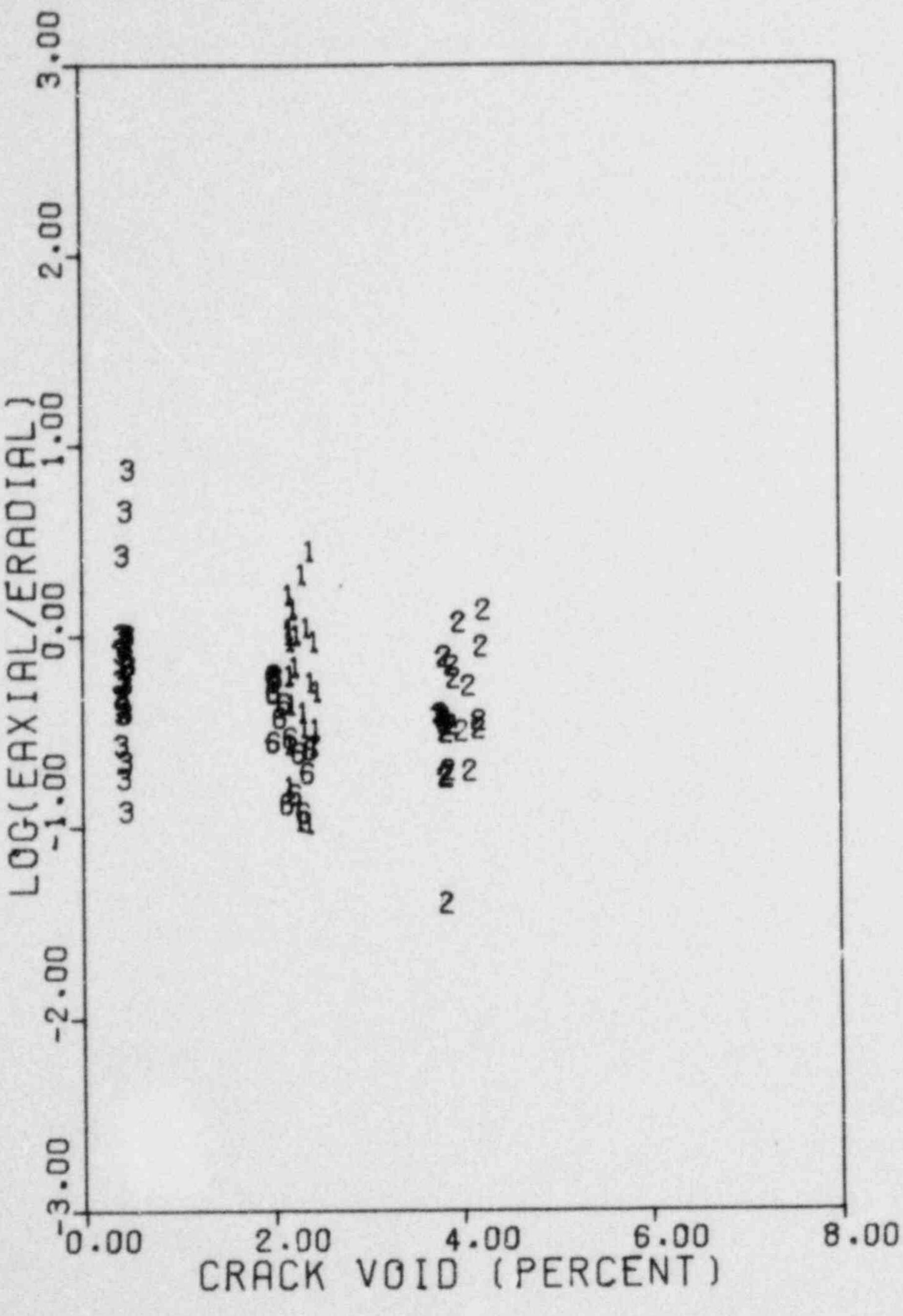

FIGURE 10. Relationship Between Radial and Axial Elastic Moduli for Cracked Pellets (data points identified by rod number)

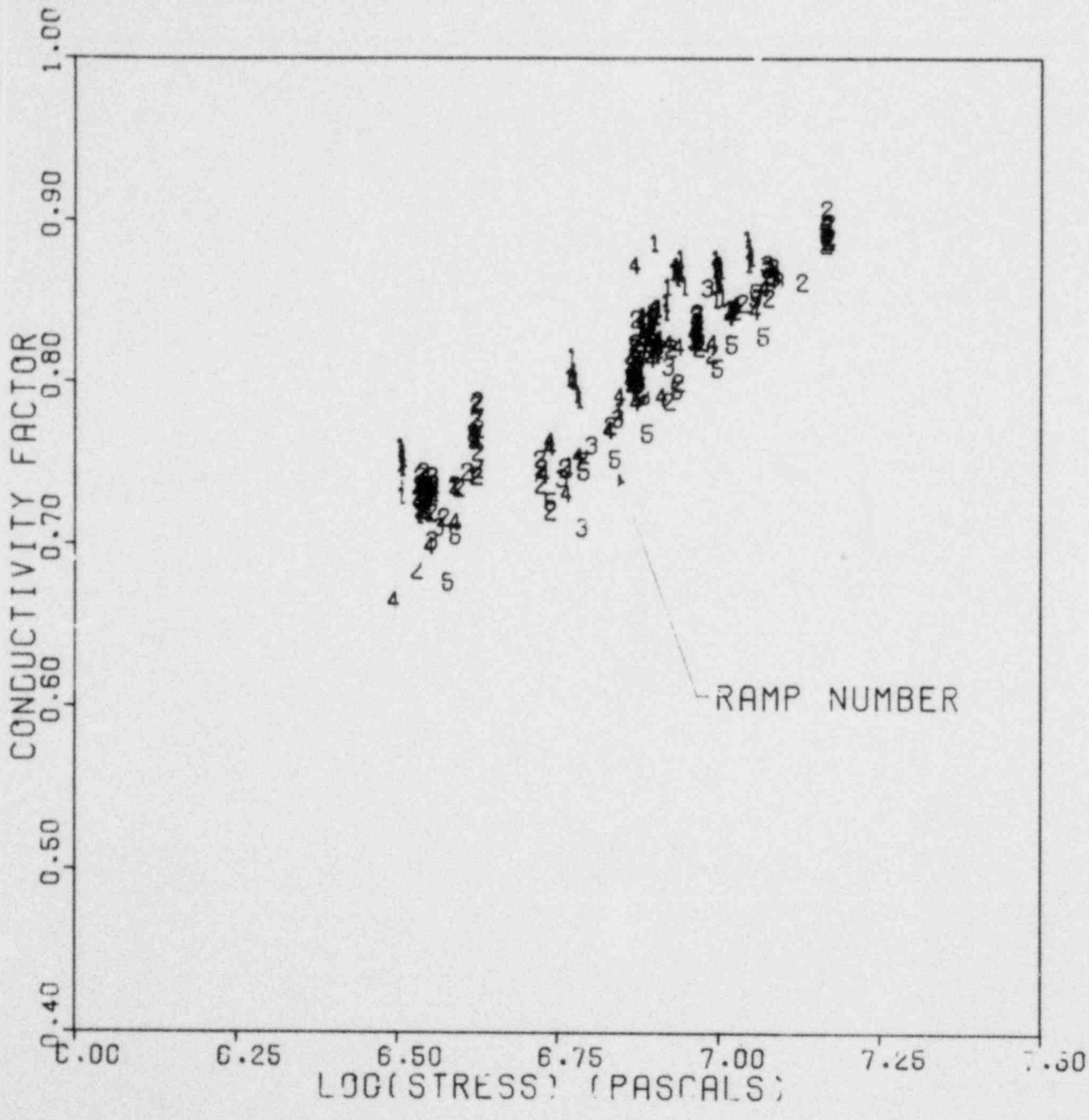

FIGURE 11. CFAC for the First Five Ramps of Rod 1, IFA-513 (data points identified by ramp number)

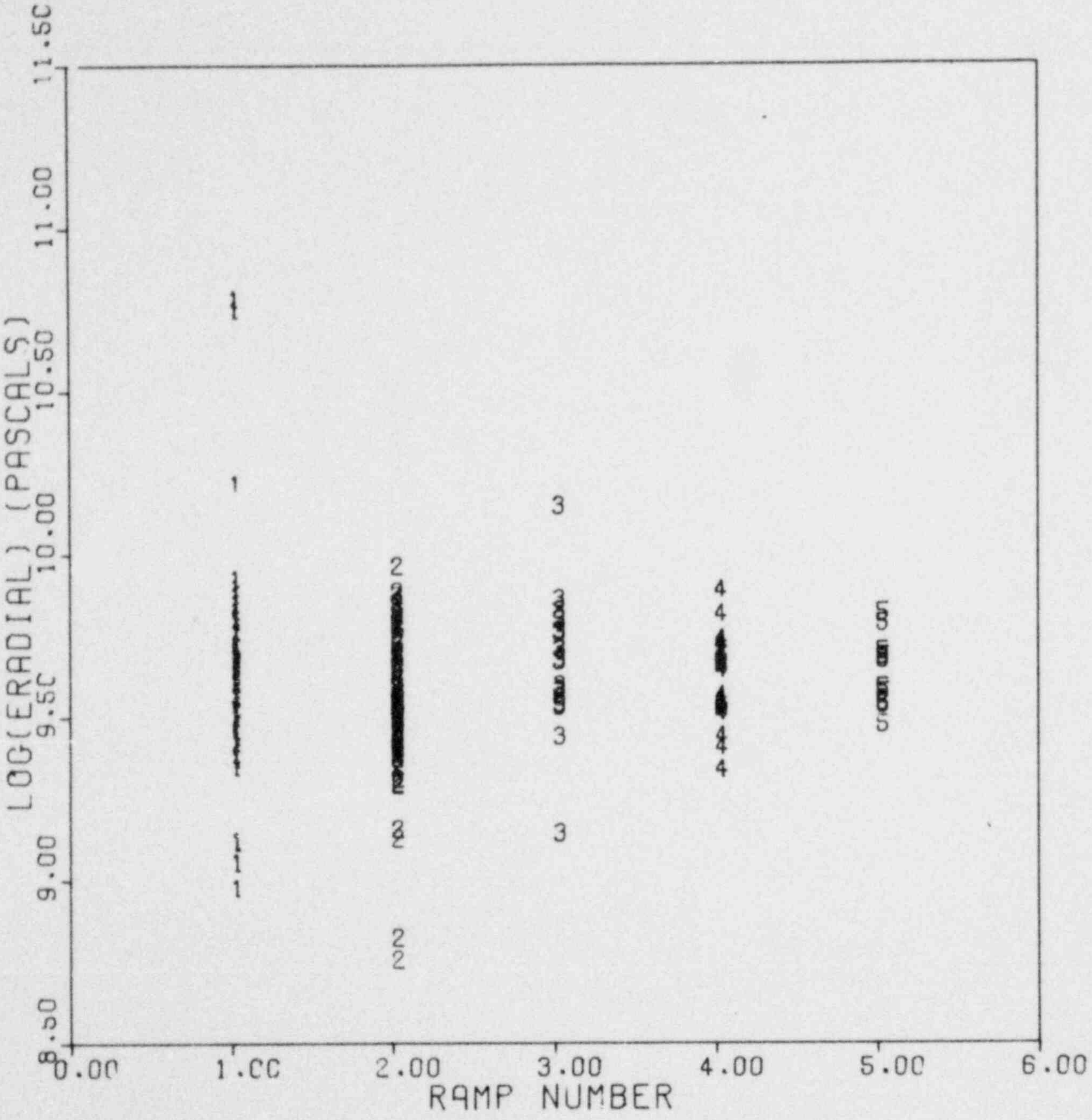

FIGURE 12. Evolution of Radial Elastic Modulus for Rod 1, IFA-513
(data points identified by ramp number)

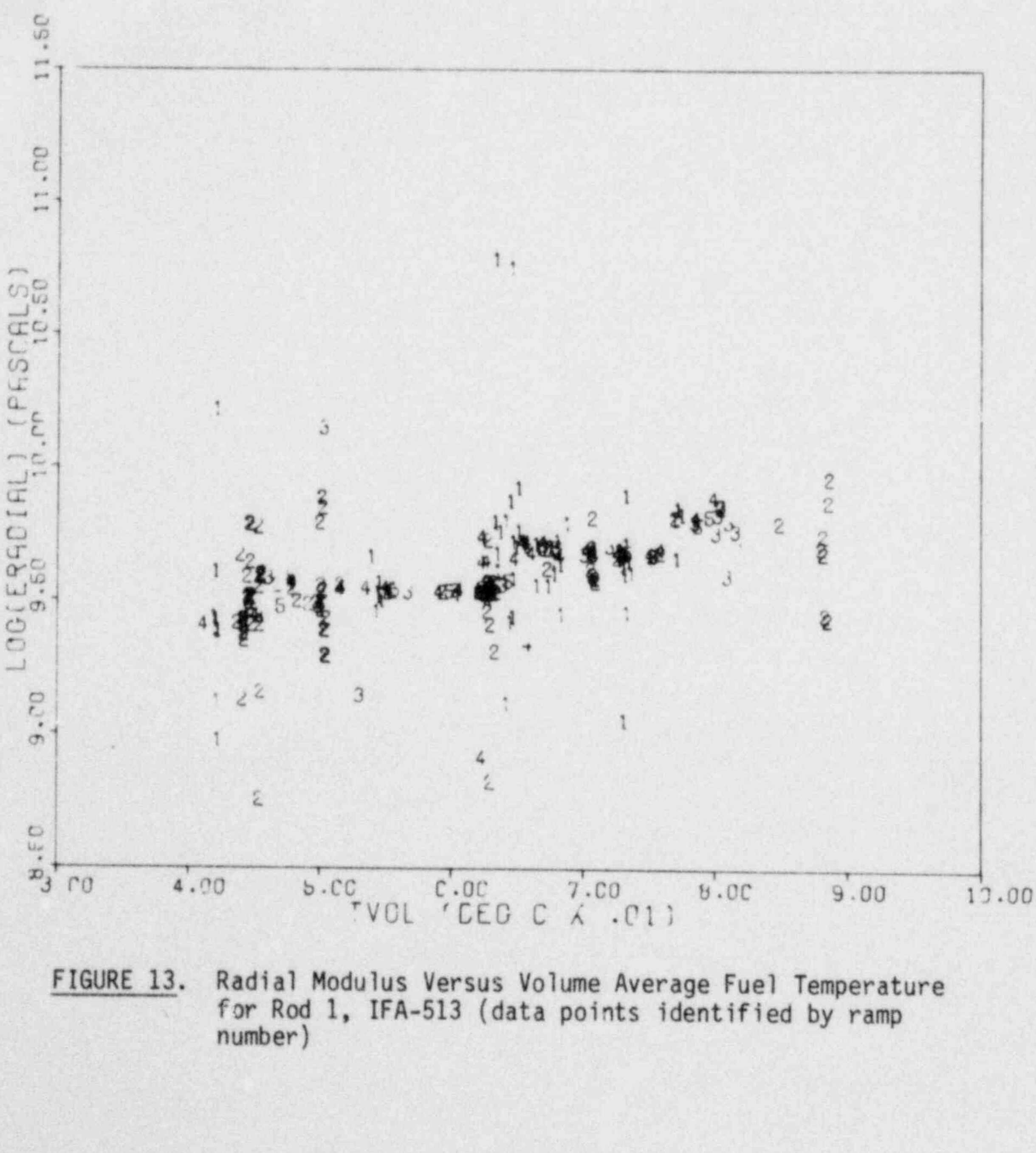

FIGURE 13. Radial Modulus Versus Volume Average Fuel Temperature for Rod 1, IFA-513 (data points identified by ramp number)

temperature above 700°C,[16] this is actually a manifestation of the increasing stress level. Figure 14 shows that the radial modulus appears to be independent of the power ramp rate. The evolution of the axial elastic modulus for Rod 1 of IFA-513 is shown in Figure 15. The envelope does not converge as quickly as for the radial modulus. However, there does appear to be a generally decreasing trend with respect to ramp number, indicating that the cracked fuel column is becoming softer in the axial direction while simultaneously exhibiting variablity from ramp to ramp. An interesting feature is noticed from Figure 16, where axial modulus is plotted versus ramp rate for the first five ramps of Rod 1. The axial modulus can be interpreted to exhibit a reduction in magnitude near the mid-range of the ramp rates shown. We suspect a pattern to be emerging, although its exact mechanism is at this time unclear. The use of rod average values for power, temperature, and cladding elongation may contribute to the confusion of the pattern. Stress relaxation of fuel and cladding may be instrumental in causing this effect.

The analysis of Rod 1 for IFA-432 was used to study the effects of varying the crack pattern and roughnesses. Calculations were first performed with the same constant crack pattern and roughnesses as for Rod 1 of IFA-513 (Figures 17, 19, 21). The analysis was then repeated with variations that were intended to more closely represent reality and are consistent with the hypotheses of Section 4. For ramp 1 only, the circumferential crack in Figure 4a was deleted, leaving only the radial cracks that begin at 0.56 radius. The gap roughness for ramp 1 was increased by 65% to represent the initial eccentricity from the stochastic stacking of the pellets during loading and handling (see Section 4). The crack pattern and roughnesses for the remaining ramps were not changed from the previous analysis. The results of these variations are seen in Figures 18, 20, and 22.

The comparison of Figures 17 and 18 shows that CFAC values are strongly affected by the changes made for the second analysis. The attempt at a more realistic representation of crack pattern evolution has resulted in a quite dramatic change in CFAC between ramp 1 and following ramps. The change in radial elastic modulus is shown in Figures 19 and 20. The fewer cracks of the more intact fuel of ramp 1 have combined with the greater equivalent gap roughness due to eccentricity (increased stress level) to produce a greater radial

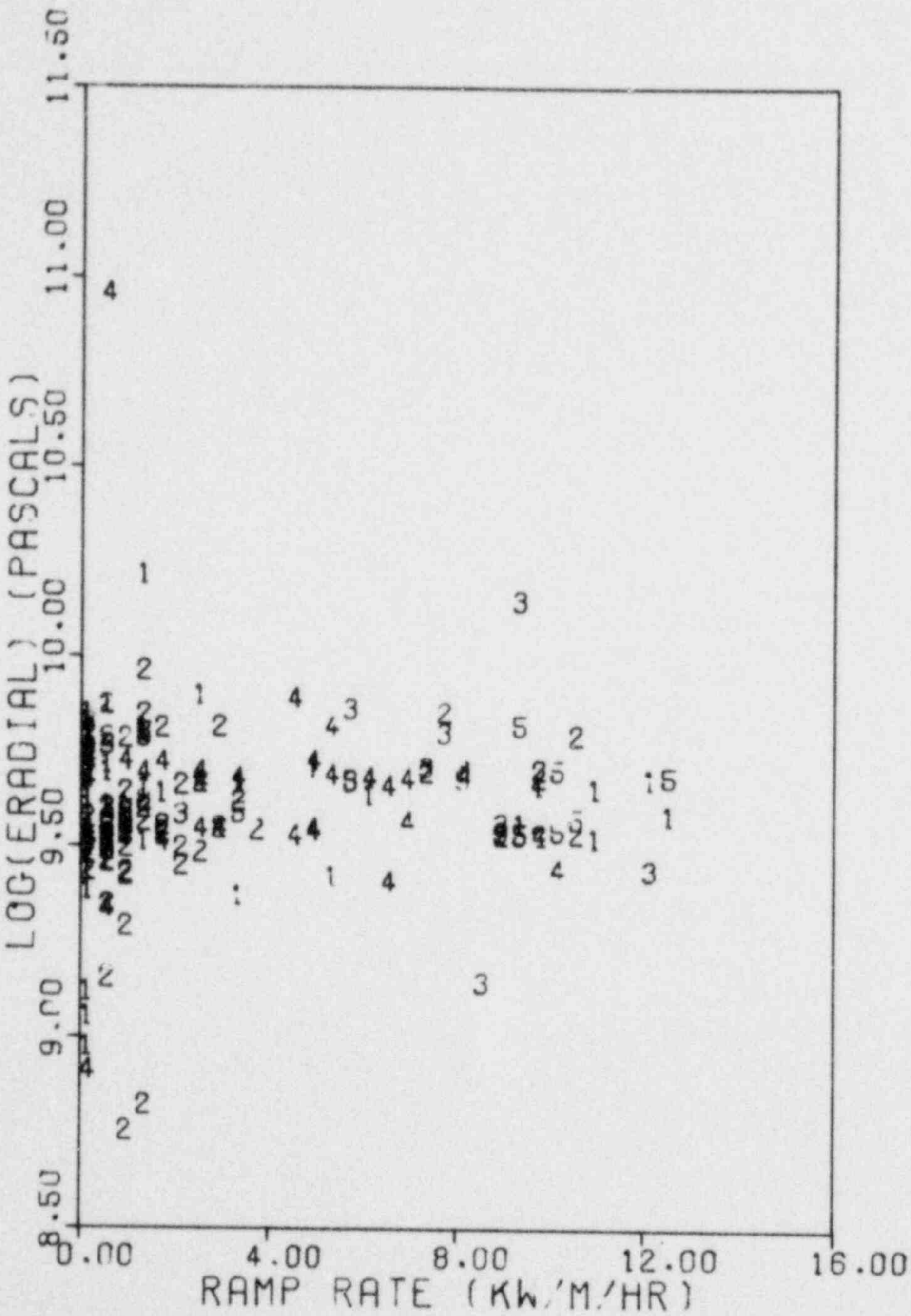

FIGURE 14. Effects of Ramp Rate on Radial Modulus of Rod 1, IFA-513 (data points identified by ramp number)

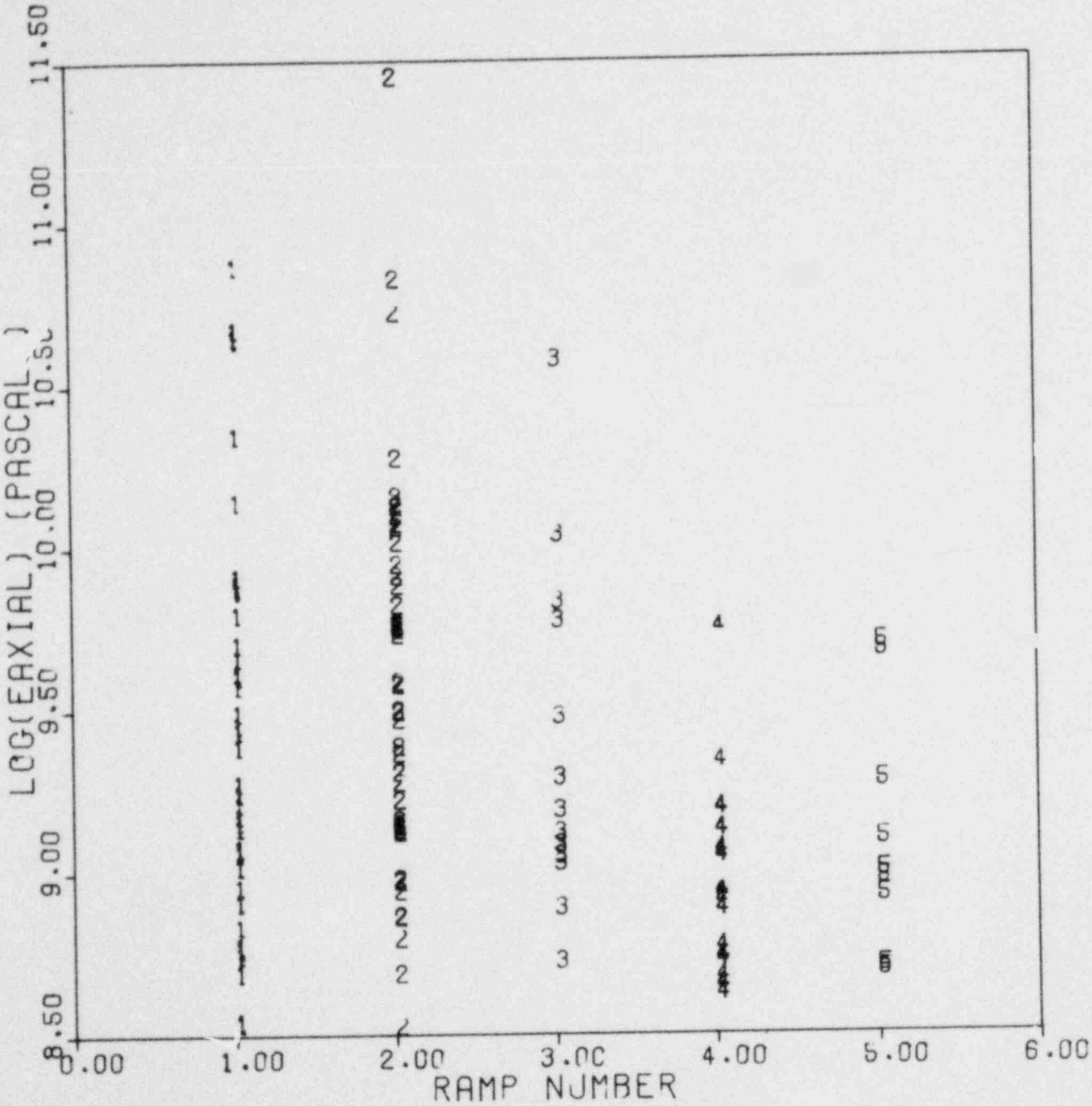

FIGURE 15. Evolution of Axial Modulus for Rod 1 of IFA-513 (data points identified by ramp number)

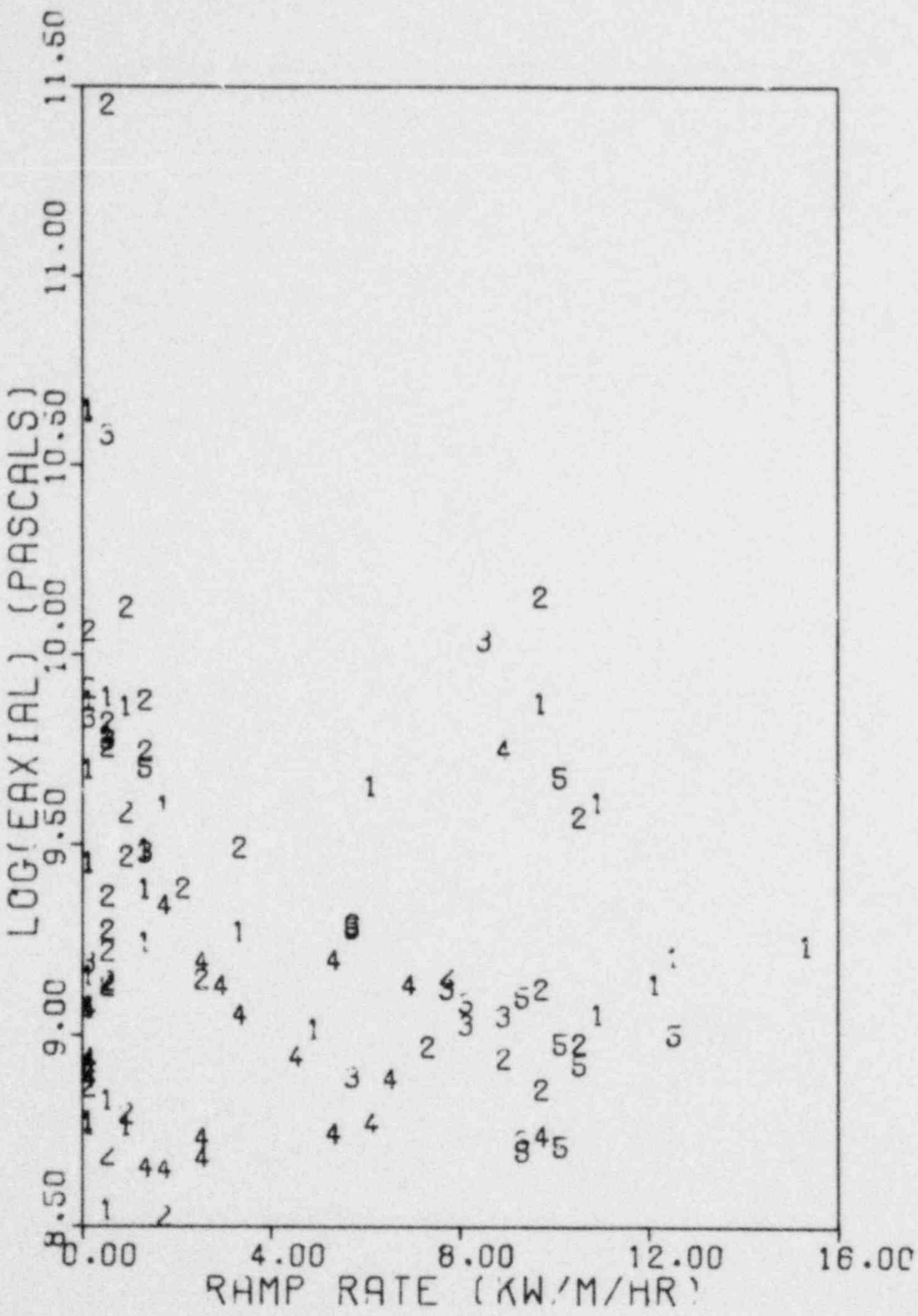

FIGURE 16. Axial Modulus Versus Ramp Rate for Rod 1 of IFA-513 (data points identified by ramp number)

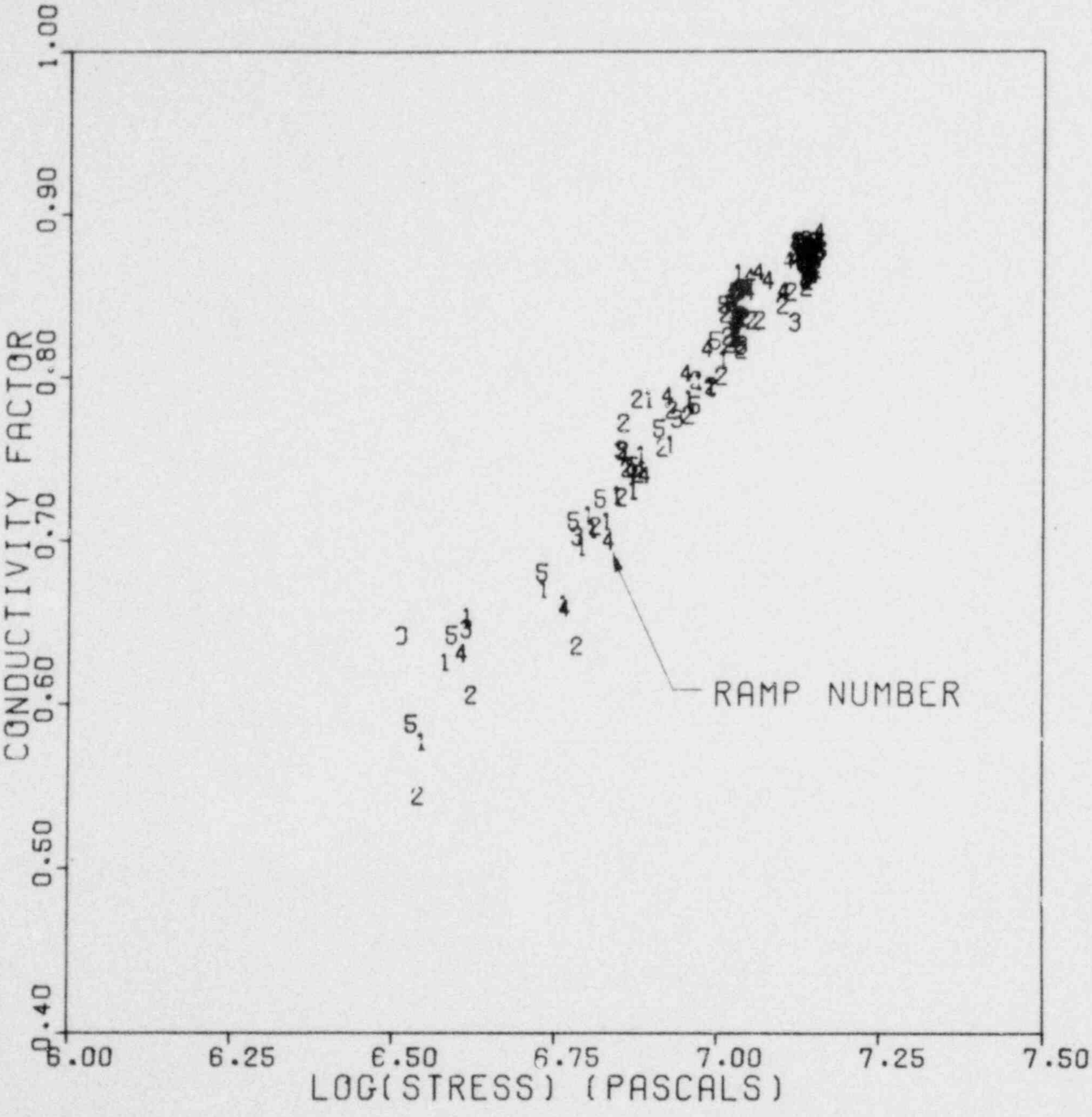

FIGURE 17. CFAC for Rod 1, IFA-432 - Standard Analysis (data points identified by ramp number)

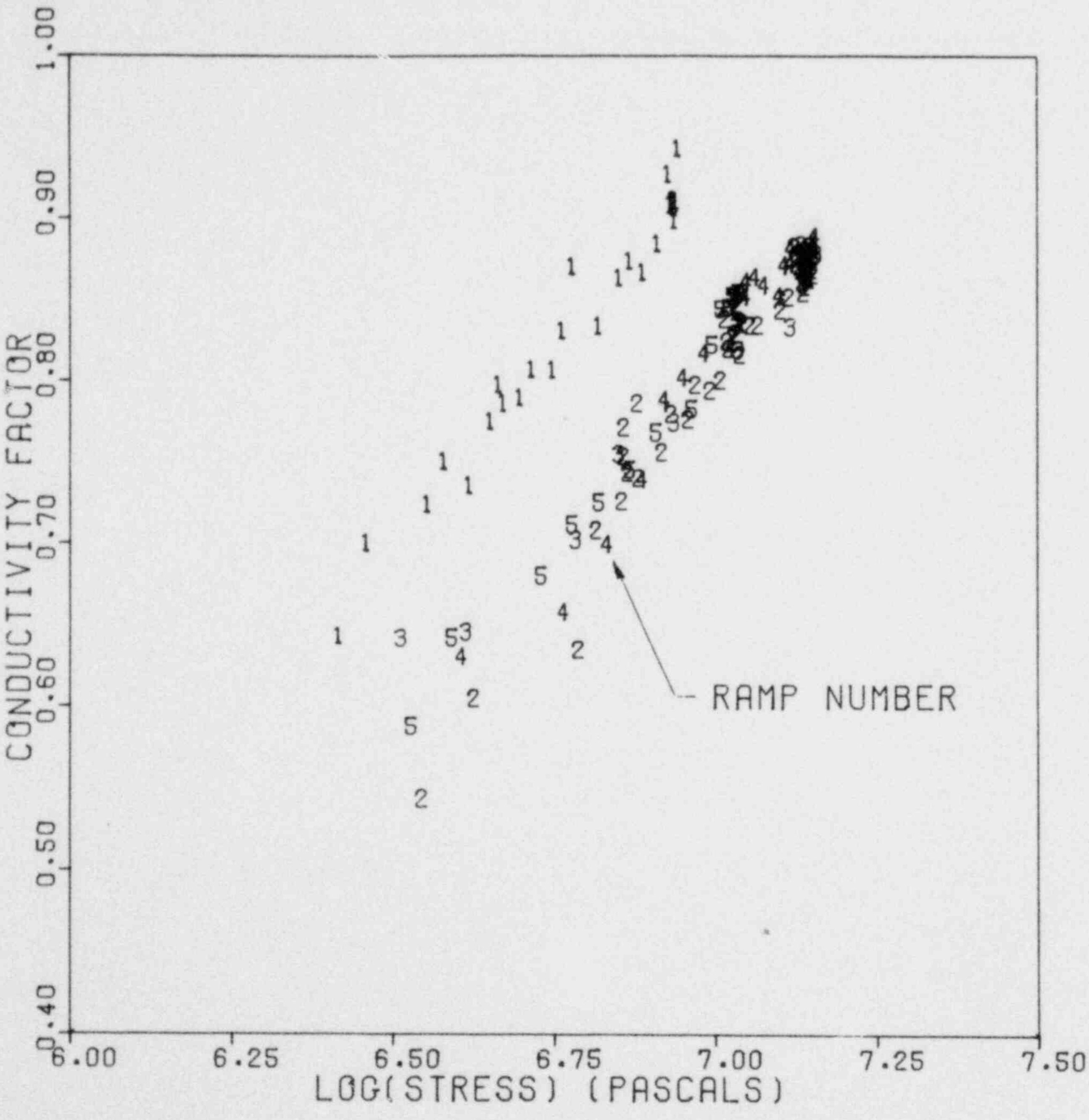

FIGURE 18. CFAC for Rod 1, IFA-432 - Ramp 1 Variations
(data points identified by ramp number)

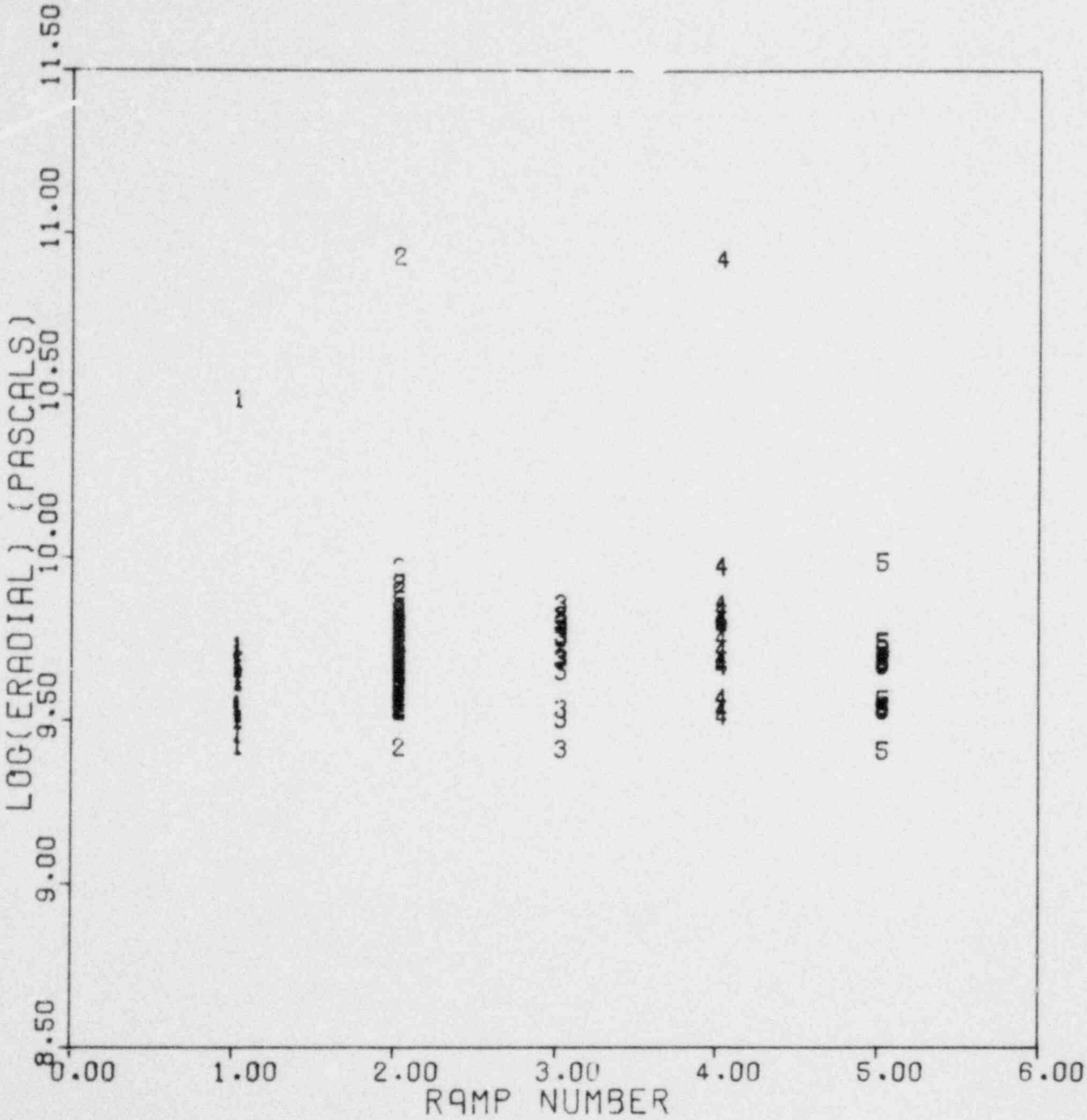

FIGURE 19. Radial Modulus Evolution for Rod 1, IFA-432 - Standard Analysis (data points identified by ramp number)

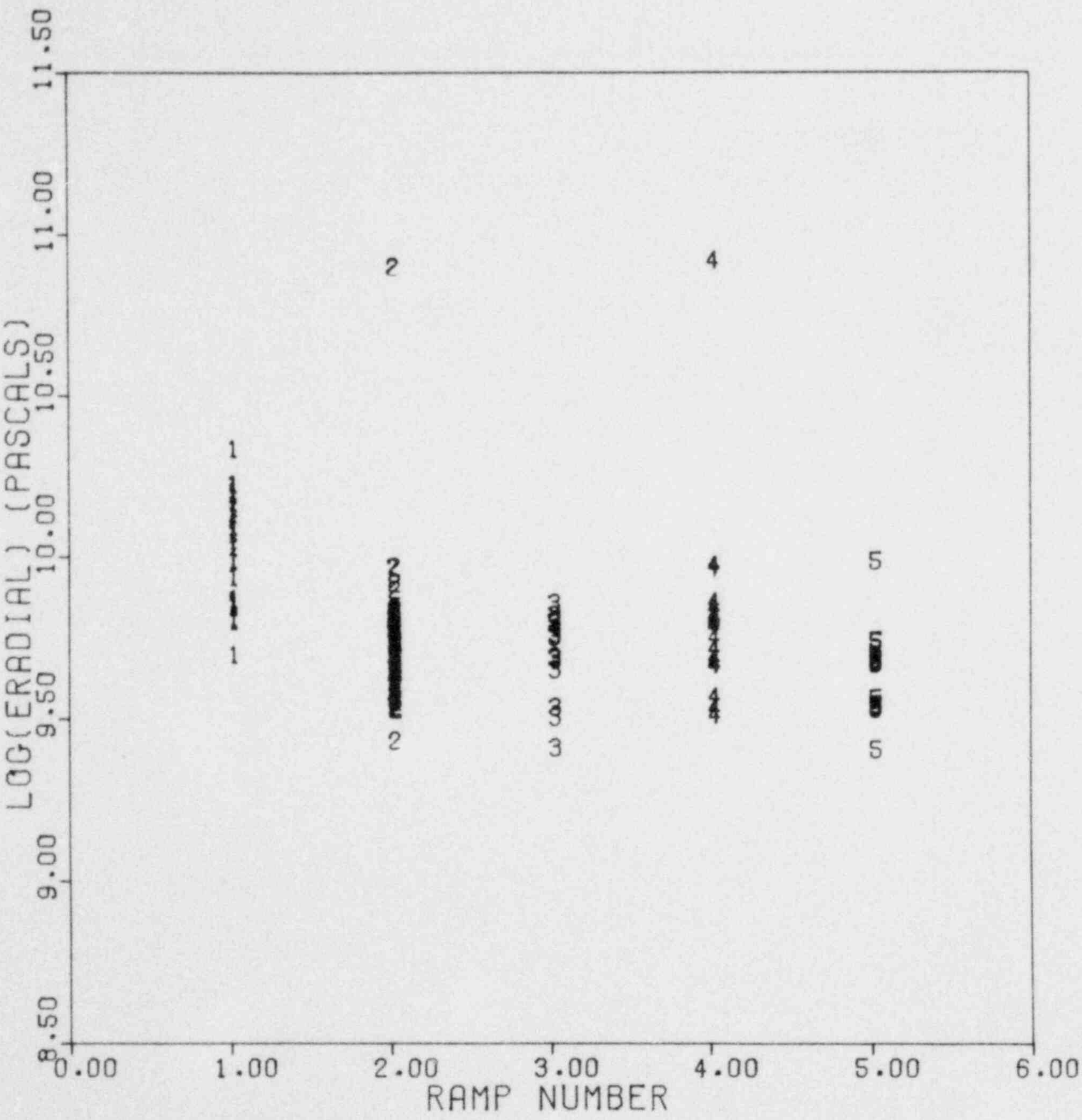

FIGURE 20. Radial Modulus Evolution for Rod 1, IFA-432 - Ramp 1 Variations (data points identified by ramp number)

elastic modulus for ramp 1. This trend clearly reflects the passage of the fuel from relatively solid to more cracked states. However, the evolving crack pattern and roughnesses have not resulted in any significant change in the axial elastic modulus of the cracked fuel, as shown in Figures 21 and 22. The axial modulus still retains its unexpected behavior from ramp 1 to ramp 2 before it begins to asymptotically approach its reduced level due to cracking. This analysis indicates that the radial and axial moduli are relatively decoupled for this rod.

The above analyses have thus demonstrated that the changes in the effective thermal conductivities and elastic moduli for the cracked fuel are primarily dependent on the amount and distribution of the free void within the fuel rod. The hypothesized ramp dependency of crack pattern and gap roughness was shown to result in the expected evolutionary behavior for effective thermal conductivity and radial modulus. The axial elastic modulus exhibited a lesser sensitivity to the model parameters, probably due to the use of rod averaged values for powers, center temperatures, and cladding elongations.

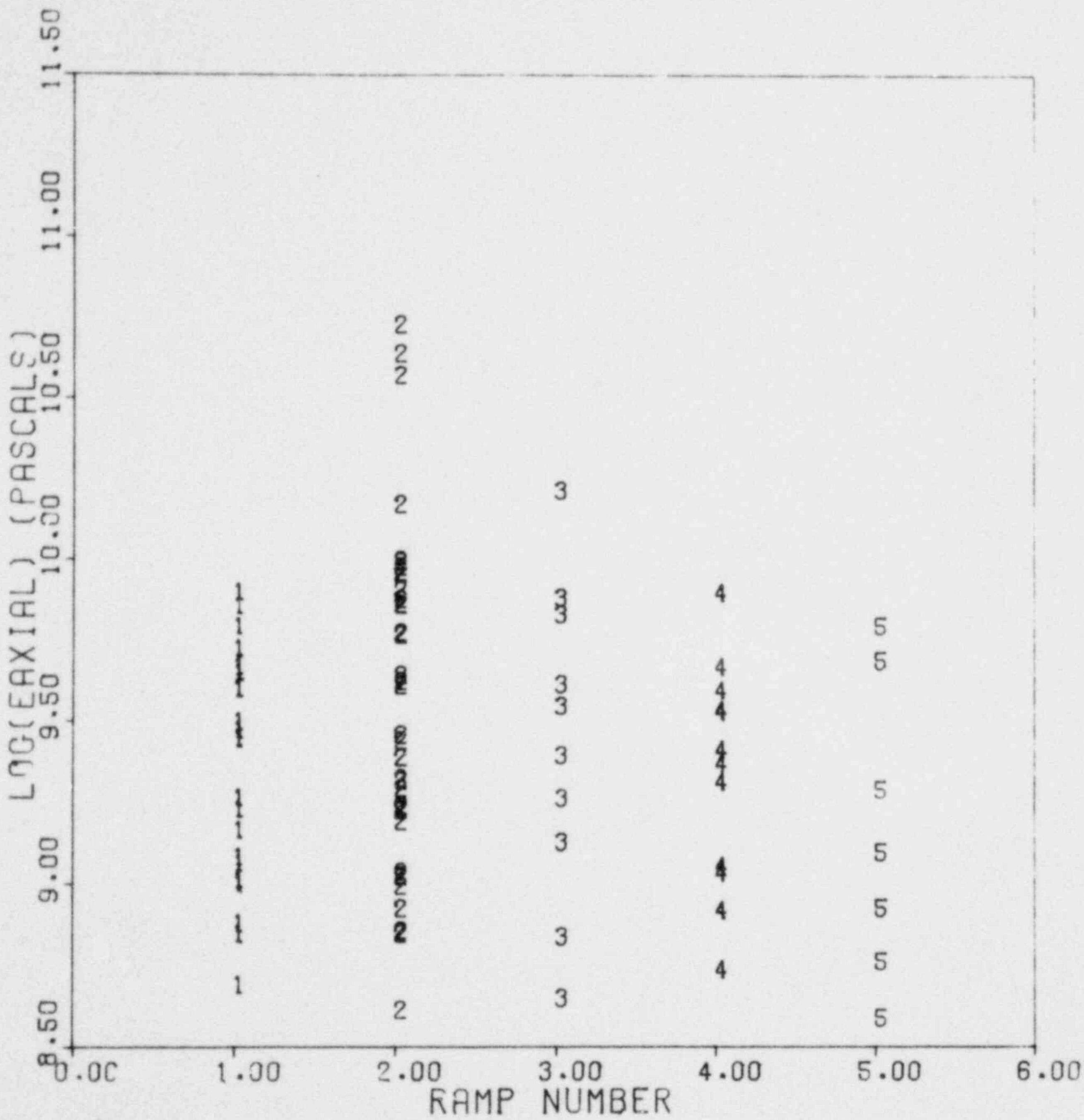

FIGURE 21. Axial Modulus Evolution for Rod 1, IFA-432 Standard Analysis (data points identified by ramp number)

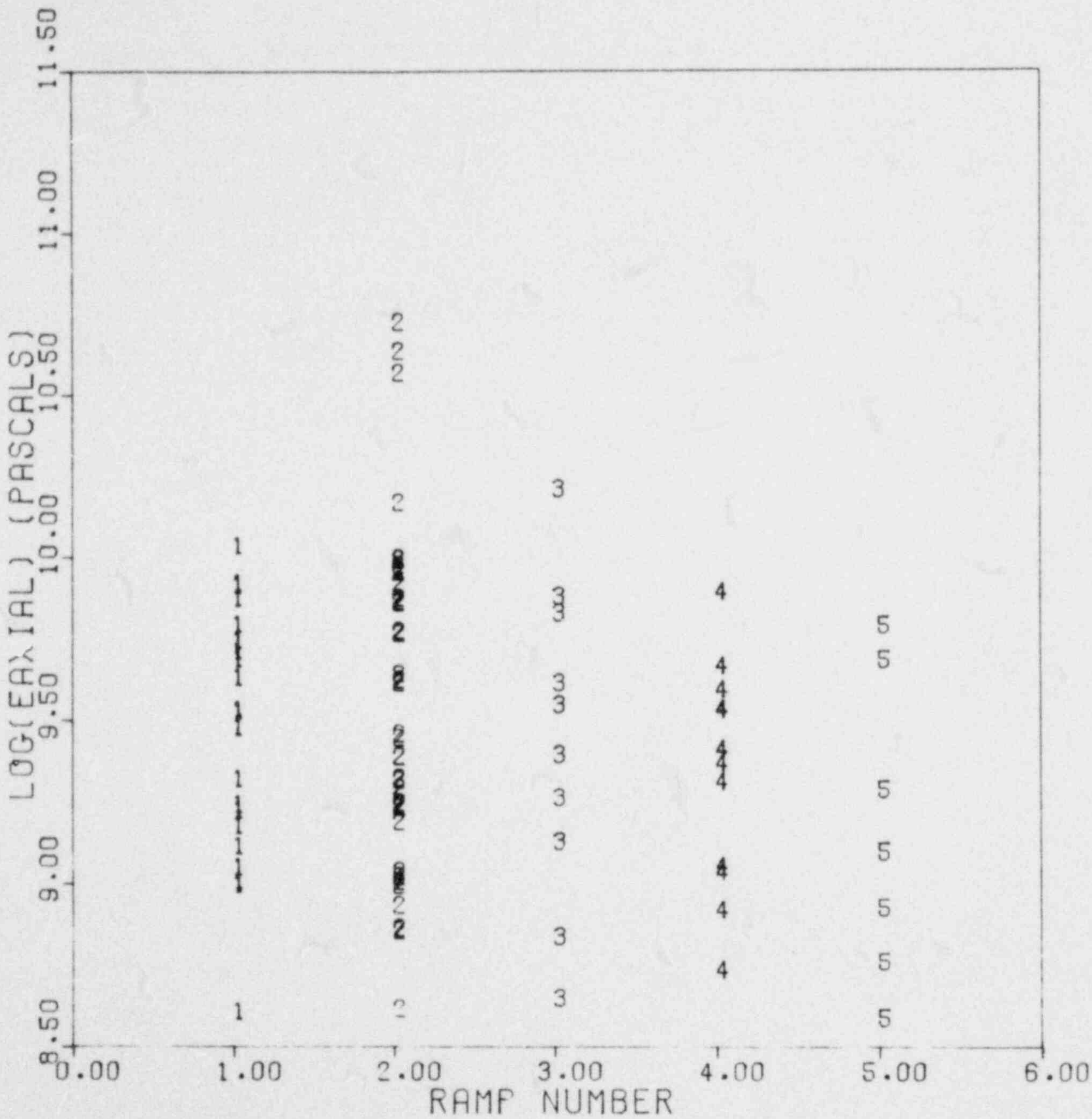

<u>FIGURE 22</u>. Axial Modulus Evolution for Rod 1, IFA-432 - Ramp 1 Variations (data points identified by ramp number)

7.0 VERIFICATION: SUPPORTING EVIDENCE

Observations have been made from PIE data, from laboratory experiments (out-of-reactor), and from calculations that lend support to the assumptions used and conclusions reached in the previous sections. These observations are presented below.

CALCULATIONS FROM IN-REACTOR DATA

Previous discussions have described mechanisms that may be active in causing the observed thermal and mechanical behavior of nuclear fuel rods. The changes in slope of the cladding elongation versus power data were explained on the basis that the rod may experience radial domination at low powers and axial domination at higher powers. If the radial elastic modulus of the cracked fuel dominates over the axial elastic modulus at low powers, then a cladding Poisson mechanism may cause reductions in the observed cladding axial elongation. When there is a transformation to axial modulus domination at higher power levels, the cladding elongation data will exhibit a noticeable increase in slope. The elastic moduli were found by assuming that there was no axial slipping between the fuel and cladding. This important assumption was checked by calculating friction coefficients that must prevail to prevent slipping in the in-reactor rods analyzed above.

The friction coefficients were calculated using the following equation:

$$Fax = f_f \cdot PRG \cdot A_{CID}$$

where: Fax = the axial force calculated by BM2DNS in establishing axial equilibrium between the fuel and cladding,

f_f = the friction factor,

PRG = the radial (hydrostatic) stress at the cladding inner surface (calculated by BM2DNS), and

A_{CID} = the area of the cladding inner surface that is in contact with the fuel.

The area in contact, A_{CID}, was calculated from the cladding inner circumference and an assumed length of contact along the cladding axis. Friction factors for two cases of contact lengths were calculated. One case assumed that only the top 10 mm of the fuel column was in contact with the cladding, and that the total contact area was equal to the cladding inner circumference times this contact length. This is in accordance with the usual definition of the friction coefficient. The second case was calculated by assuming that the entire fuel column length was in contact with the cladding, but that only the asperities caused by the gap roughness actually contacted the cladding. Thus the area in contact for the second case was

$$A_{CID} = \text{circumference} \times \text{length} \times A_F$$

where: A_F is the fraction of area that is in actual contact via asperity tips. (A_F is calculated by the Mikic surface response model.)

The results of these two calculations to find the friction factor that is required to prevent axial slipping are shown in Figure 23 (case 1) and Figure 24 (case 2). The friction factors are plotted versus the rod average power. The decreasing friction factor of Rod 3 in Figure 24 is caused by an asperity contact area fraction (A_F) that is increasing faster than usual because of the high stress levels experienced by this small gap rod. Either case yields friction factors that are less than 0.5.[22] Larger friction factors that have been reported[23] would thus further reduce the chance of axial slipping between the fuel and cladding. It thus seems reasonable to assume that there should be no axial slipping between the fuel and cladding.

An illustration of the radial-axial dominance that was previously discussed is shown in Figure 25. The base 10 logarithm of the ratio of the effective axial to the effective radial modulus is plotted versus power level for Rod 1 of IFA-432. The first four ramps to power are shown. The crack pattern and roughnesses from the "standard analysis" of Section 6.0 were used for all ramps. The scatter of ramp 1 data indicates the transition from solid to cracked fuel. Subsequent ramps show the development of the trend where the radial modulus dominates at low power, and the axial modulus dominates at

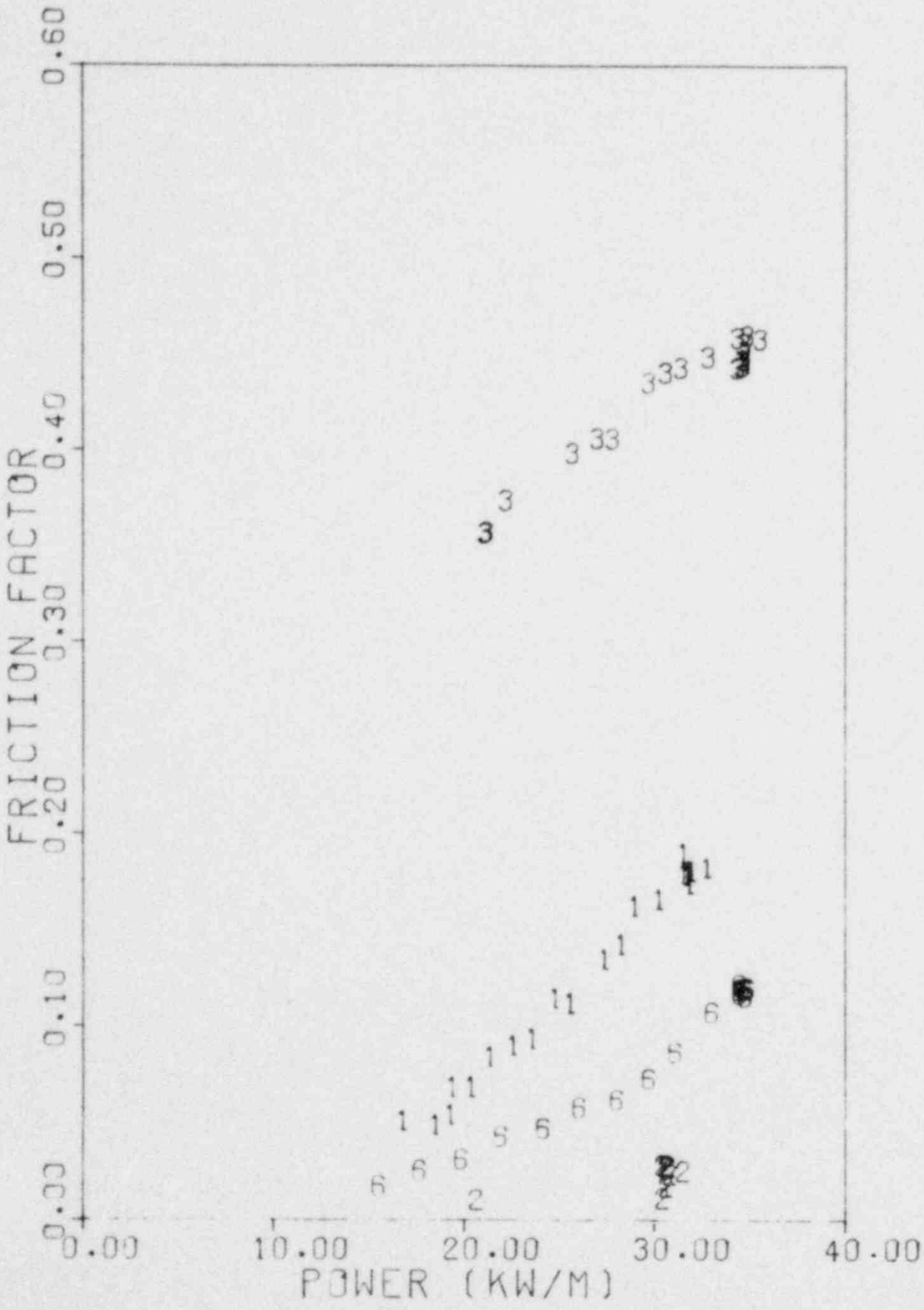

FIGURE 23. Friction Factors for 10 mm Contact Length (Case 1) (data points identified by rod number)

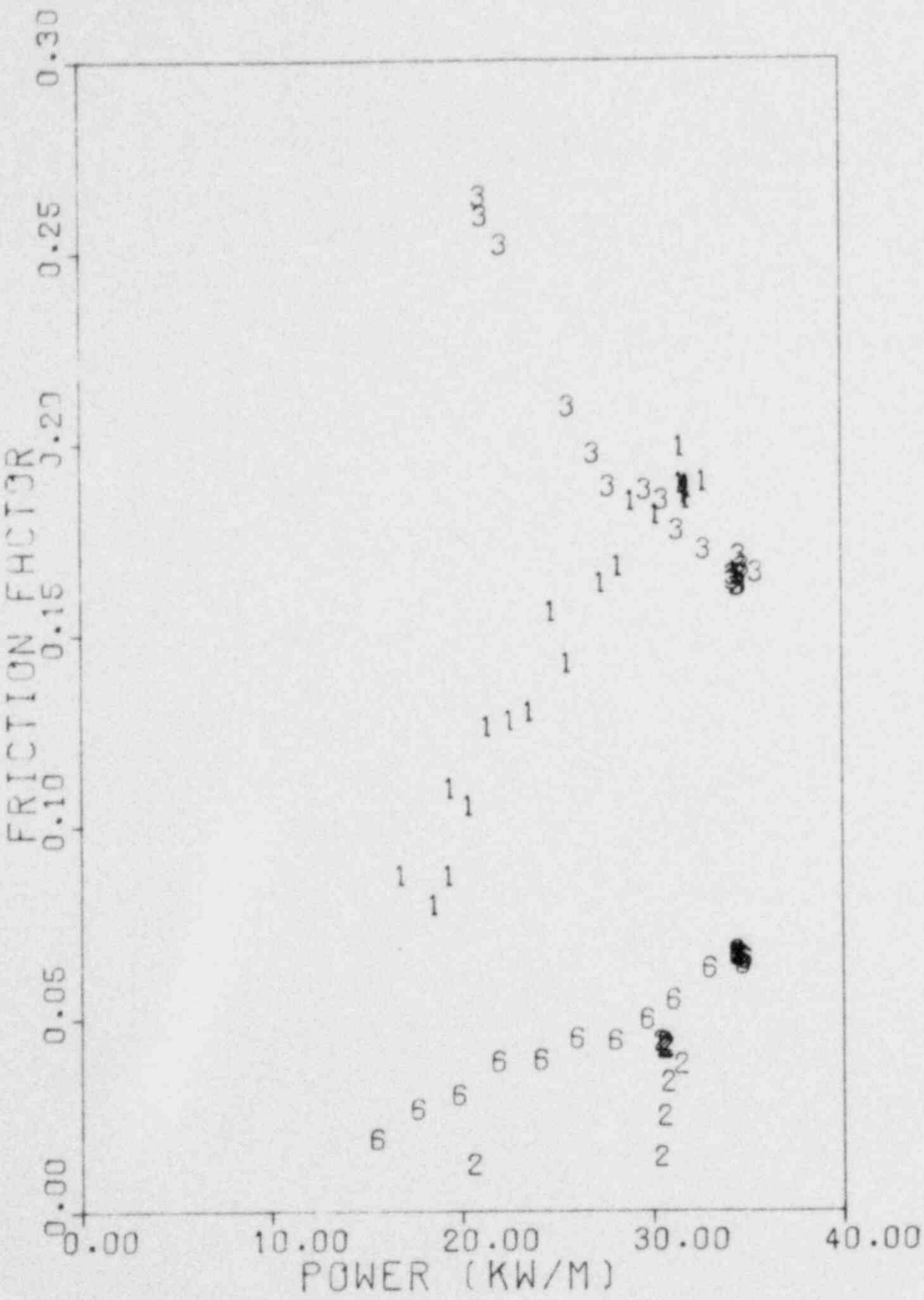

FIGURE 24. Friction Factors for Full Axial Contact Length (Case 2) (data points identified by rod number)

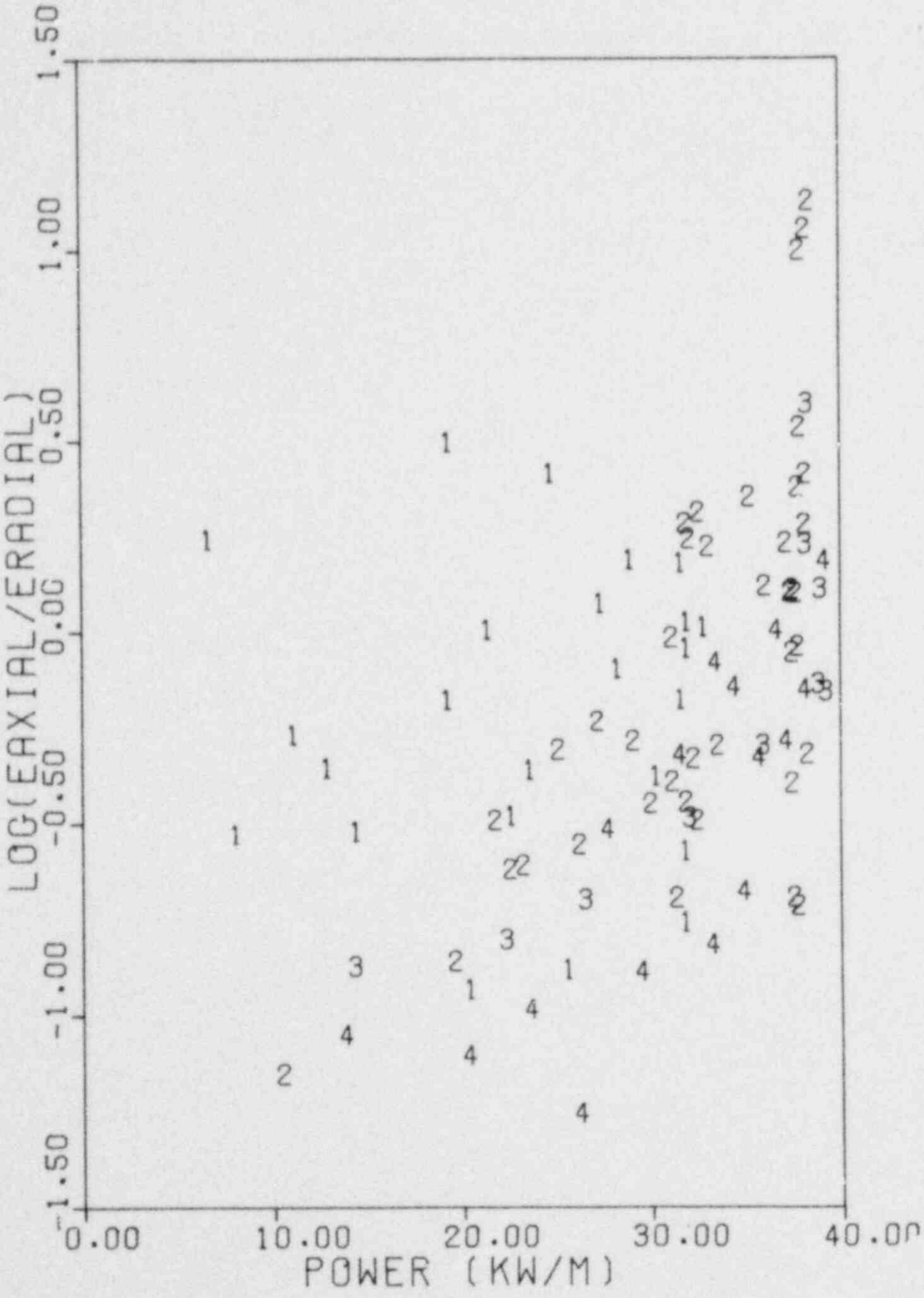

FIGURE 25. Radial-Axial Dominance for Rod 1 of IFA-432 (data points identified by ramp number)

higher powers. Note that a value of 1.0 on the vertical axis means a factor of ten in the modulus ratio. The power where the modulus ratio changes from negative to positive corresponds to the power where the cladding elongation exhibits a noticeable increase in slope. Figure 25 is thus a manifestation of the radial-axial domination characteristic, shown in terms of the effective material properties of the cracked fuel column.

POST IRRADIATION EXAMINATION DATA

A mechanism describing the "flow" of fuel fragments via rigid body motions was described in earlier sections. This flow mechanism is believed to be instrumental in the development of the radial-axial domination characteristics of fuel rods. Observations from PIE data that support this proposed mechanism will now be introduced. It will also be shown that the flow mechanism is consistent with observations made from thermal data.

The PIE of IFA-431[24] has shown that for BWR rods of typical design dimensions with non-densifying and unrestructured fuel, there is negligible change in fuel column length. Table 4 indicates this for Rods 1, 2, and 5. Rods 3 and 4 were special designs[5] and Rod 6 had densifying fuel. This lack of significant fuel length change implies that there was no axial slipping between fuel and cladding that would tend to increase the column length while forming axial cracks. Any axial cracks that reduce the cladding elongation response (axial fuel modulus) must have been formed in a different manner. The cracked pellets must have been axially shortened and radially expanded, and

TABLE 4. IFA-431 Fuel Column Length Changes from PIE Measurements

Rod	Length Change (mm)
1	-0.6
2	+0.1
3	+1.2
4	+2.1
5	-0.2
6	-6.5

they must have remained in their original axial positions. But the responsible mechanism (flow of fragments) could not operate the same throughout the whole rod without contradicting the observed axial variations of thermal conductivity and gap conductance found by thermal analysis methods. In Appendix B, it is noted that the upper portions of the rods appeared to have experienced a greater amount of fuel relocation than the lower portions.

Consistency between the thermal and mechanical evolution of the rods can be maintained by recognizing that the power/temperature levels of the upper portions of the rods were about 30% greater than the lower portions. The difference in temperatures may contribute to an explanation based on fuel creep. It also allows the axial variation of fuel properties to be explained on the basis of crack density. This is demonstrated by Figures 26 and 27. More cracks are observed at the upper thermocouple location, thus the fragment sizes are smaller on the average and may tend to "flow" (due to rigid body motion) more than those at the lower position. (Note that the amount of "flow" is still very small.) Also, the greater crack density at the upper thermocouple location requires that the fuel internal void be greater, and the gap void be smaller, than at the lower thermocouple position. This would result in higher gap conductance and more relocation at the upper position, which is exactly the conclusion reached from the transient data analysis.(19)

For consistency between thermal and mechanical evolution, it is then sufficient that the axial cracks (or gaps) that form should be more numerous toward the top (higher temperature) region of these rods than at the bottom. It follows that rigid body motion and friction between fragments contribute to the evolution of axial variations in mechanical properties that compliment the axially dependent thermal properties.

The formation of the axial cracks (or gaps) by rigid body motion allows ramps to power to be completed without the occurrence of axial slipping between fuel and cladding. There is a lag in axial cladding response while the axial cracks close up according to the Mikic model. These axial cracks may not be detected at PIE by gamma scanning because they are generally not planar. Slopes of cladding elongation versus power plots that are less than the calculated thermal expansion(4) occur because the hydrostatic (r,θ) forces of the

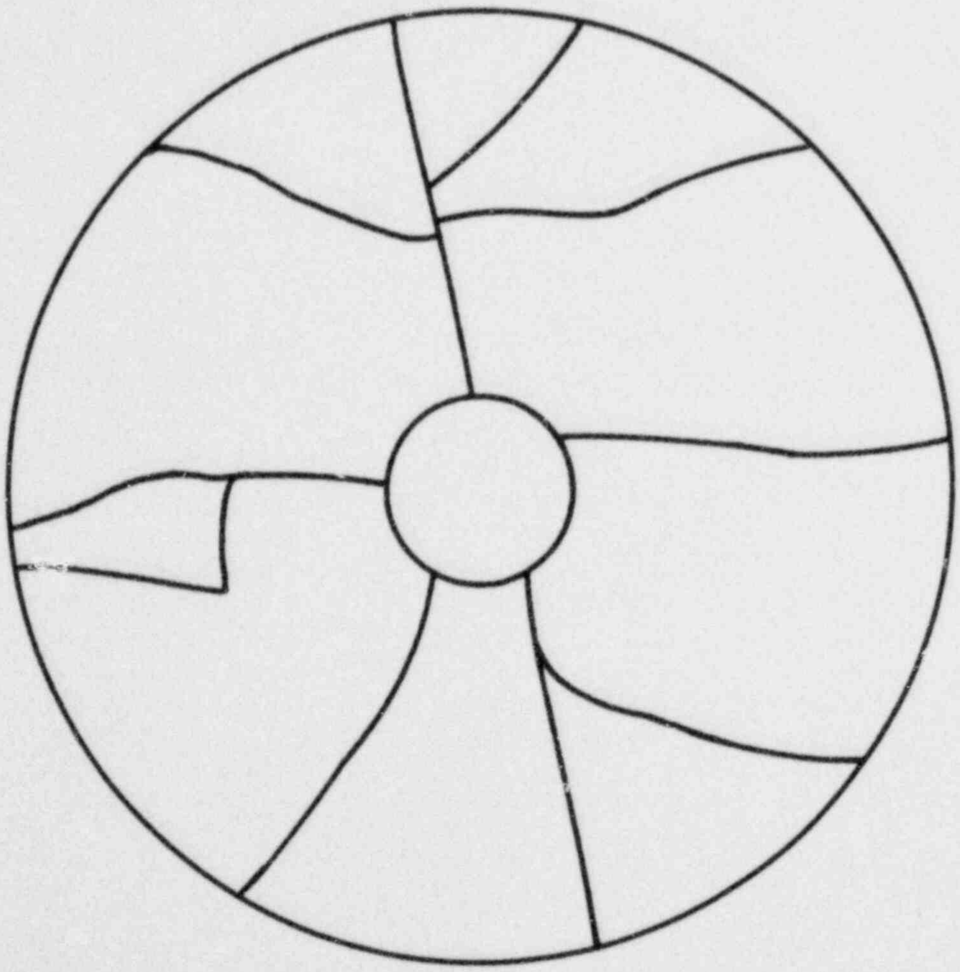

FIGURE 26. Crack Pattern of Pellet 42 of Rod 6 of IFA-431 Lower Thermocouple Region

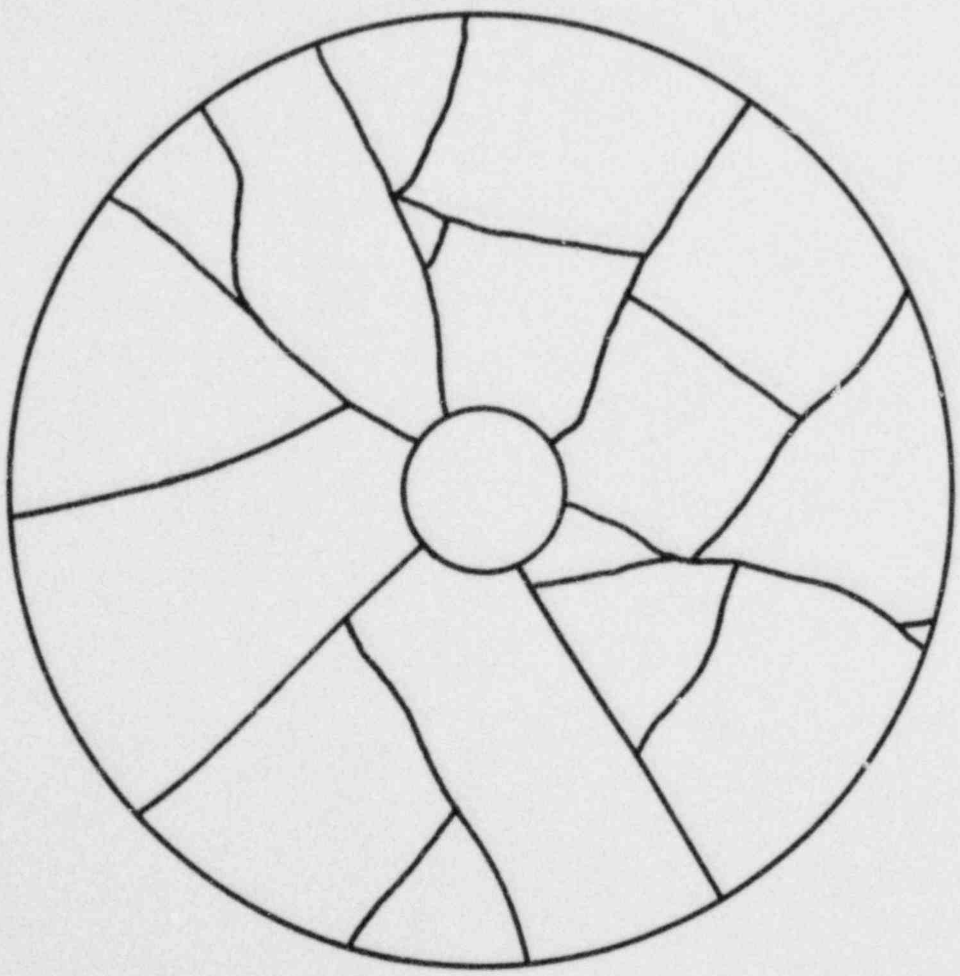

FIGURE 27. Crack Pattern of Pellet 9 of Rod 6 of IFA-431
Upper Thermocouple Region

fuel cause a Poisson shortening of the cladding, until thermal expansion closes the axial fuel cracks enough to transmit appreciable forces. The existence of these hydrostatic forces is demonstrated in the following paragraph.

The thermal conductivity factor of the in-reactor data has previously been plotted versus the hydrostatic stress (see Figure 6). It is apparent that there is always a finite stress level at the cladding inner radius, its magnitude depending on the crack and gap roughness parameters which yield acceptable thermal solutions. Radial stresses at low power (<3 kW/m) for the typical design Rod 1 were calculated to be between 7×10^4 and 3×10^6 pascals. These may have an interesting effect on cladding elongation data, as can be seen in Table 5. It is apparent that the post-irradiation permanent elongation is generally greater than that at hot standby just before discharge from the reactor. The elongation sensors were set to zero at hot standby at the beginning of irradiation. Calculation shows that about 1.5×10^7 pascals hydrostatic stress at the cladding ID is required to shorten Rod 1 by the amount shown via the Poisson mechanisms. This is not an unreasonable value when the variations in stress level with crack pattern and roughness values are considered. Stress levels of this magnitude could have an impact on present conceptions of PCI-SCC failure mechanisms, as evidenced by the failure of power reactor rods that have operated at low power only. The uncertainties in the results from Table 5 are currently under investigation at PNL.

TABLE 5. Permanent Cladding Axial Elongation for IFA-431

	Permanent Elongation (mm)	
Rod	25°C (PIE)	240°C (Hot Standby)
1	+0.24	+0.13
2	+0.17	+0.08
3	+0.25	+0.14
4	+0.39	+0.45
5	+0.18	+0.17
6	+0.16	+0.09

OUT-OF-REACTOR EXPERIMENTS

A series of simple laboratory experiments were conducted for the purpose of verifying the reduced elastic moduli calculated from in-reactor data. There were four independent variables of interest: the gap size, the applied load, the fuel design (flat or dished pellet ends), and the fuel initial state (cracked or uncracked). These four variables were distributed among the eight tests in order to form a half-repetition fractional factorial test matrix[25] (see Table 6). Of the four variables, only the applied axial load and cycle number had any significant effects. The test results at the lower stress levels were representative of the expected elastic modulus reductions for the cracked fuel columns.

A schematic of the test apparatus is shown in Figure 28. A short length of zircaloy tubing (10.9 mm OD x 9.5 mm ID x 152.4 mm long) was used to contain the stack of five pellets. The pellets were 94%-TD, 15.2 mm-long depleted UO_2 that were sized to provide the gaps shown in Table 6. Short lengths of drill

TABLE 6. Axial Compliance Test Matrix

Sample	Gap (mm)	Load (kg)	Fuel Design	Initial State
1	0.102	440	F	U
2	0.254	4400	F	U
3	0.254	440	D	U
4	0.102	4400	D	U
5	0.254	440	F	C
6	0.102	4400	F	C
7	0.102	440	D	C
8	0.254	4400	D	C

F = Flat ends
D = Dished Ends
U = Uncracked
C = Cracked

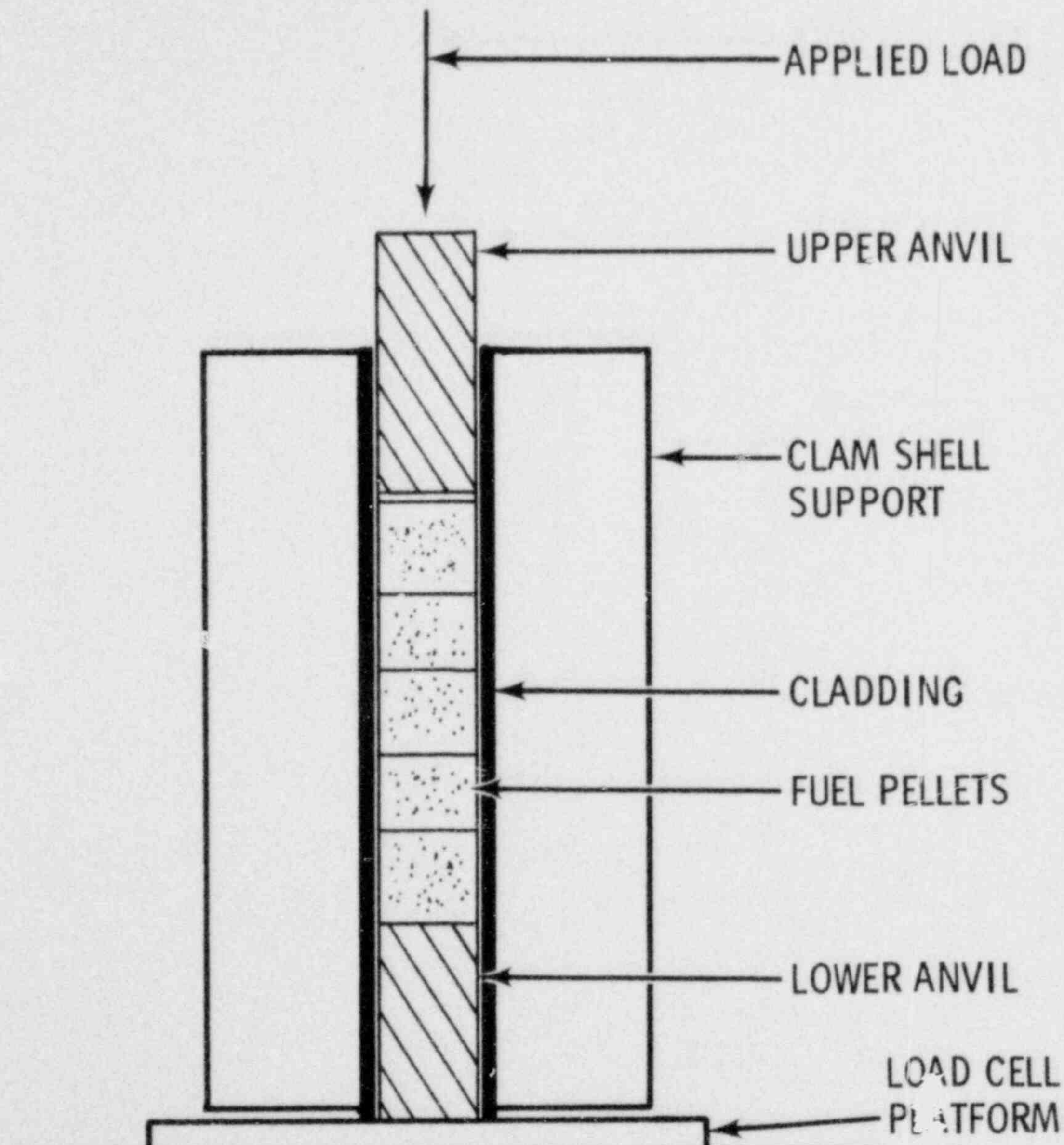

FIGURE 28. Schematic of Test Apparatus

rod were used as anvils, the lower one remaining stationary while the upper anvil compressed the fuel column. The assembled fuel column was h ld vertically in a clamshell support and placed on an Instron testing machine, where simultaneous measurements of applied load and fuel column axial deflection were obtained. All tests were conducted at room temperature.

A variable of interest was the initial state of the fuel, whether it was intact (solid) or precracked. Several methods of precracking the fuel were attempted. The most acceptable method was to crack the pellets as each was inserted into the cladding. This was accomplished by impacting the ends of the pellets with a star drill and hammer. Post-test destructive examination showed that there was no visible difference between the initially cracked and initially uncracked fuel. The load application had apparently cracked both fuel types to the same extent.

Each assembled fuel column was cycled through four loading sequences. As an example, the results from Test 4 are shown in Figure 29. The discontinuities in the cycle 1 curve are due to the fuel cracking under applied load, which was audible during the test. There is a similarity between these curves and the cladding elongation data plots presented in Appendix B. For any cycle past the first, there is a region of no response until the fuel column is contacted by the upper anvil. This is analogous to the in-reactor data, where the point of apparent FCMI initiation (the onset of axial domination) occurs at higher power levels than on the first power ramp. The axial deflection of the short samples (horizontal axis) corresponds to the closing of the axial fuel cracks for the in reactor data, while the stress level of the short samples (vertical axis) corresponds to the axial elongation data.

The results of the eight out-of-pile axial compliance tests are shown in Table 7. The elastic moduli were calculated for three stress regions for each test from the load-compliance curves. The effects of gap size, pellet design and precracking were negligible. However, significant changes in elastic modulus can be seen due to stress level and cycle number. Some of these scoping tests were conducted at loads that were up to two orders of magnitude higher than those calculated from in-pile data. This was done in order to magnify any effects on the cladding and to obtain information on fuel cracking methods.

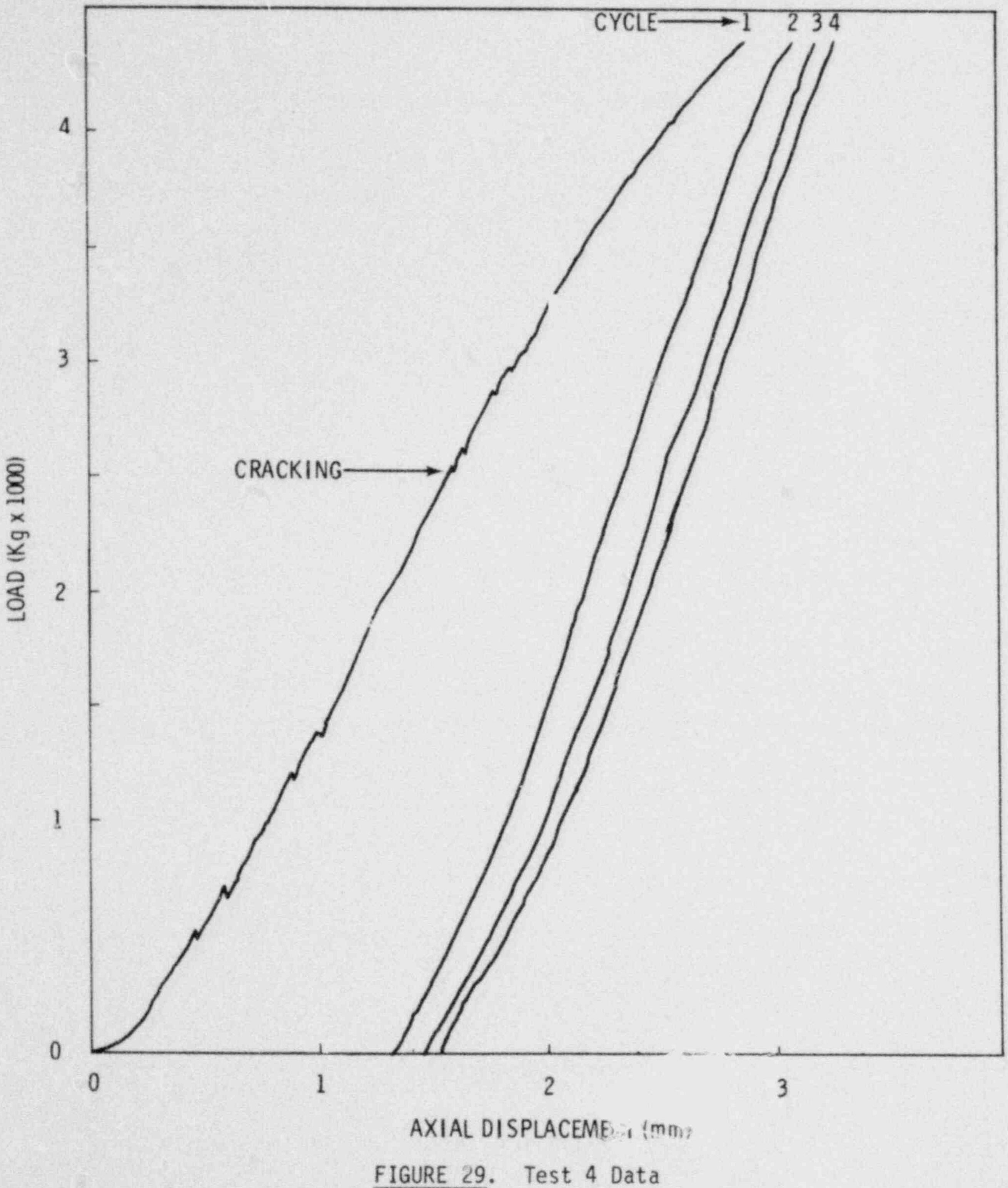

FIGURE 29. Test 4 Data

TABLE 7. Axial Elastic Moduli for Compliance Tests (in Pascals x 10^{-10})

Test	Stress Level (Pascals x 10^{-7})	Cycle Number 1	2	3	4
1	0 - 2	0.67	1.07	1.07	1.07
	2 - 4	1.65	2.14	2.14	2.14
	4 - 6	2.49	2.49	2.49	2.49
2	0 - 20	2.05	2.51	2.30	2.40
	20 - 40	1.45	3.07	3.16	3.16
	40 - 60	1.61	2.21	3.36	3.52
3	0 - 2	0.79	1.10	0.92	0.92
	2 - 4	1.38	1.84	1.84	1.84
	4 - 6	1.29	1.54	1.93	2.21
4	0 - 20	1.48	2.23	2.14	2.05
	20 - 40	1.94	3.05	2.97	2.97
	40 - 60	1.50	2.68	3.12	3.12
5	0 - 2	0.55	1.38	1.23	1.58
	2 - 5	0.85	1.70	1.70	1.70
	4 - 6	1.10	1.65	1.54	1.54
6	0 - 20	1.01	2.23	2.23	2.32
	20 - 40	1.70	2.81	2.97	2.89
	40 - 60	1.53	3.12	2.77	2.99
7	0 - 2	0.38	0.89	1.07	1.07
	2 - 4	0.77	1.65	1.53	1.78
	4 - 6	1.07	1.66	1.87	1.87
8	0 - 20	0.79	1.78	1.78	1.78
	20 - 40	1.49	2.91	2.91	2.83
	40 - 60	1.38	2.86	3.52	3.68

The axial elastic modulus is plotted versus cycle number for the lowest stress level of each test in Figure 30. The high load range tests are even numbered and the low load range tests are odd numbered. When compared at the same stress levels, the results of the out-of-reactor tests agree reasonably well with effective elastic moduli calculated from in-reactor data. The change in modulus due to temperature differences between the two data types is well within the scatter. This is taken as an indication that the analysis methods derived for in-reactor data are valid, and that the results are correct. Recall that it was not necessary to assume a crack model to find axial moduli for in-reactor data.

Another manifestation of rigid body motion was observed in the out-of-reactor tests that contributes both to anisotropy and to FCMI localization. Figure 31 shows sample 4 during post-test destructive examination. A longitudinal window has been removed from the cladding (Figure 31a), and then the cladding cut in half (Figure 31b). The pellet fragments and crack patterns have permanently deformed the cladding inner surface. Of special interest are the deformations due to fragment motion at the pellet-pellet interfaces. The cladding deformation is also visible on the outer surface of the rod. A bright ring can be seen around the tube in the right hand portion of Figure 31a. This was made visible by scratching that occurred during removal of the sample from the clamshell support. The cladding diameters at the ridges were 0.01 to 0.03 mm larger than the mid-pellet diameters. Since the tests were conducted at room temperature, there was no thermally induced pellet "hourglassing," and this effect is attributed to a "mushrooming" of the pellet ends due to the applied axial load. The fragments at the ends of the pellets had apparently rotated outward enough to cause plastic deformation of the cladding, which manifested itself in the form of bamboo ridges.

Under operating conditions in reactor, the thermal stresses of a cracked pellet are localized within each fragment, which would tend to reduce the thermal hourglassing effect. The bamboo ridges observed from in-reactor experiments are thus expected to have a component due to mechanically induced mushrooming (fragment rotation). Reductions in the effective axial modulus at low powers may be mitigated by the rotation of some fragments about their

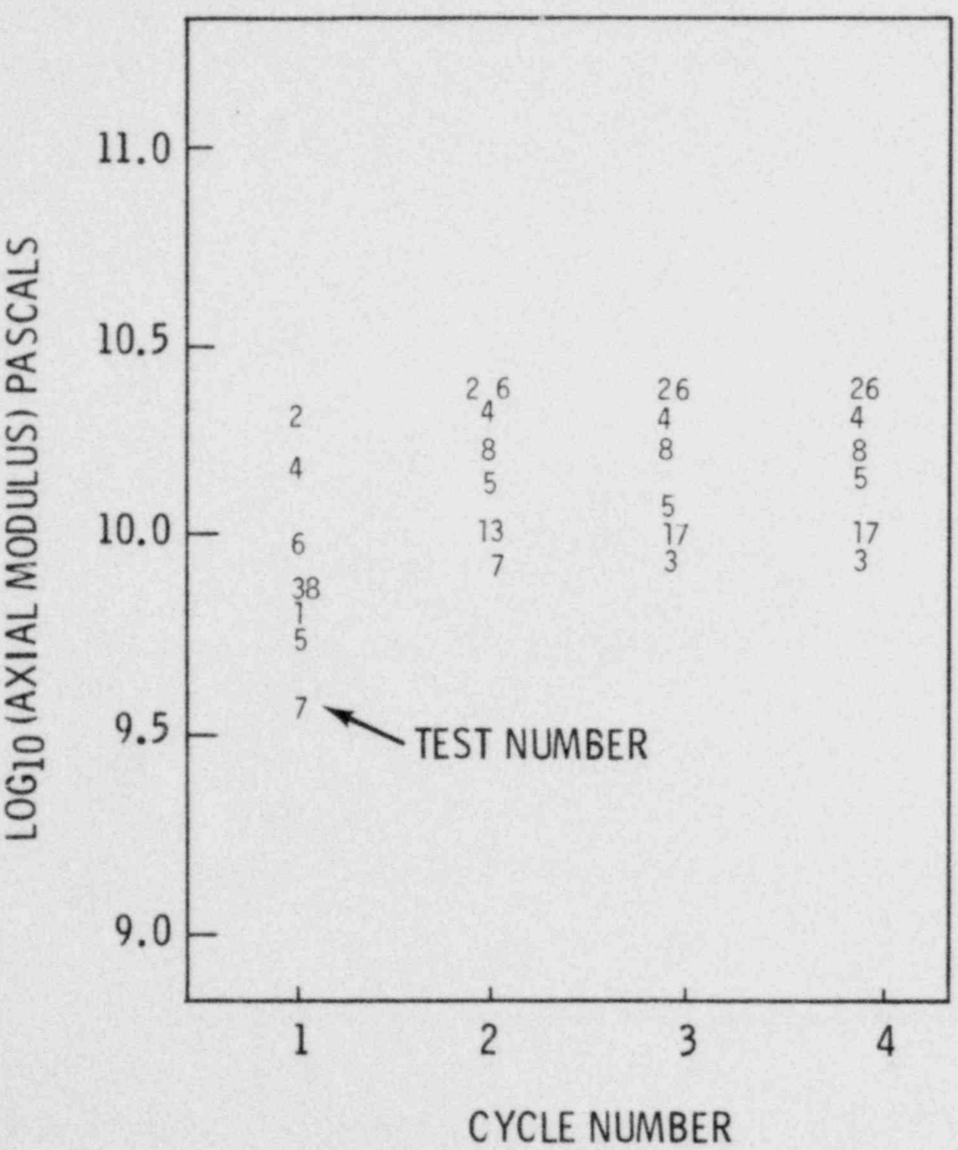

FIGURE 30. Axial Modulus Evolution for Out-of-Pile Tests - Low Stress Levels

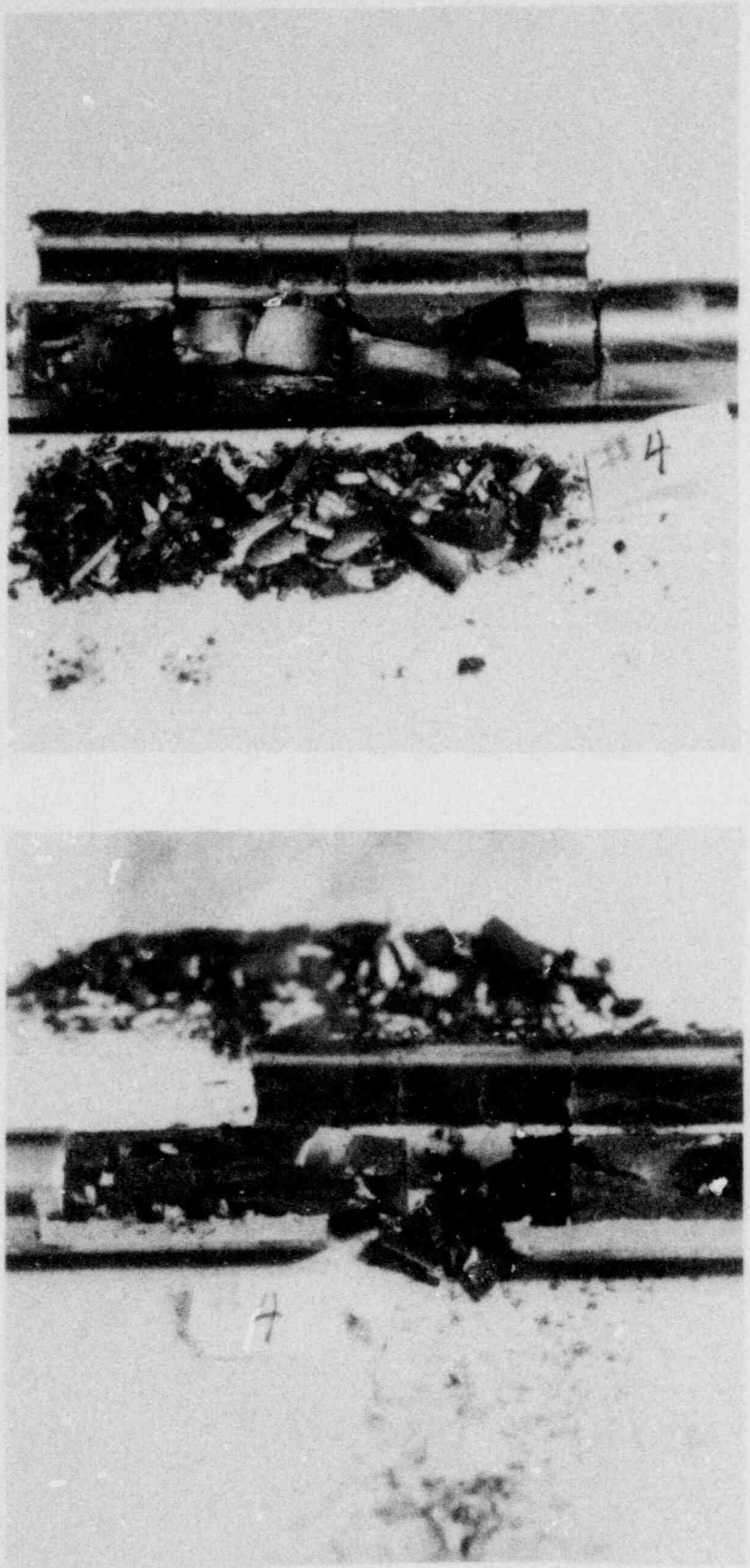

a

b

FIGURE 31. Sample #4 from Out-of-Pile Axial Compliance Tests

points of contact with the cladding, thus contributing to the radial-axial domination characteristics previously demonstrated. This effect would be enhanced with dish-ended pellets, where the resistance to rotations would be less. At higher powers, mushrooming would increase the fuel-cladding friction and thus contribute to the prevention of axial slipping. The mushrooming would also have an effect on Poisson's ratio for the fuel, and would cause a Poisson-induced reduction in cladding axial elongation. These effects are expected to be elastic for normally operating rods of typical design and low exposures.

8.0 DISCUSSION

In the foregoing analysis, we have recognized that pellet cracking has an effect on the thermal and mechanical performance of nuclear fuel rods. We have developed a model in order to quantify these effects. Analysis of in-reactor data shows that the effective thermal conductivity and elastic moduli of cracked fuel are significantly reduced from values for solid pellets. The magnitude of these effects depends primarily on the amount and distribution of free void within the fuel rod. The magnitude of the free void is determined by the initial design pellet-cladding gap and the power/temperature level, while the distribution of this void is determined by the crack pattern and the effective Mikic roughnesses.

Probably the most important assumption made was that the gap roughness was specified by forcing the gap conductance to agree with results obtained by transient analyses of data from the upper 20% of the power range. A check on the values used for crack roughness was obtained by comparison with effective thermal conductivities found by transient analyses. This approach was necessary because no values for roughnesses were known from strictly mechanical considerations. This implies that the mechanical results obtained are implicitly dependent on the thermal solutions. Future work should concentrate on the separation of thermal and mechanical results by providing values for mechanical parameters that more accurately represent physical reality.

In the (r,θ) plane, the assumption of a hydrostatic stress state permitted the use of bulk modulus concepts to reduce the number of unknowns. The hydrostatic assumption is considered reasonable by analogy with rigid body mechanics solutions for systems of comparable characteristic dimensions. The ratio of fragment size to cladding inner radius is comparatively large, and direct transmission of forces is expected. However, further characterization of fragment geometries (crack patterns) will be required in the future to adequately model the evolution of the fuel system and to separate out power/temperature history path dependencies.

The primary assumptions of the Mikic surface response model are that the interacting surfaces are nominally flat and have normal distributions of asperity heights. These should be considered first order approximations until they can be quantified by experimental measurement. However, they are justified from observations of PIE photo macrographs. Fuel fragments with curved surfaces remain relatively well aligned when compared to the random contact occurring in a pile of gravel. Most fracture surfaces are rough and irregular enough to be considered to have a normal asperity height distribution.

The Mikic model is intended to represent the elastic response of the surface interactions. Although there may be plastic flow or fission erosion of asperities, the small rigid body motions of the fragments are expected to result in new asperity interaction pairs with every change in power/temperature level until an asymptotic configuration is reached that establishes the lowest energy state of the cracked fuel system. Even then, stochastic effects may momentarily upset this preferred equilibrium configuration.[4] The roughness is thus an evolving variable and is probably path dependent.

The radial elastic modulus calculated from in-reactor data was found to be sensitive to variations in crack pattern and roughness. The expected decrease in inferred modulus with increasing ramp number was obtained by an approximation of crack pattern and roughness evolution that was consistent with the hypotheses of Section 4.0. The effective thermal conductivity also responded as expected, decreasing as the fuel became more cracked. The variations in radial modulus and thermal conductivity trends as they approached asymptotic values is taken as a display of their dependency on crack pattern and roughness evolution. Much of the data scatter is probably caused by the use of rod-averaged values for temperature, power, and cladding elongation, and this will receive greater emphasis in the future. In particular, the thermal conductivity factor (CFAC) needs to be more carefully defined.

The condition of no axial slipping between fuel and cladding for in-reactor data allowed the axial modulus to be derived independently of any assumed axial crack pattern or roughness values. The no-slip condition imposed on this data set is supported by four items. The first is that calculations have shown that the friction factors required to prevent axial slipping between fuel and cladding are within reasonable limits. The second is that fuel column length changes from PIE measurements are apparently negligible for rods of typical design. The third is the axially varying radial crack density (observed from PIE data) that accommodates the formation of axial cracks via rigid body motion (flow) of fragments. The fourth is the mechanically induced mushrooming observed from the out-of-reactor compliance tests that can contribute to the reduction of the effective axial modulus for the cracked fuel column.

The in-reactor effective moduli were calculated by using a value of 0.25 for the Poisson's ratio of the cracked fuel, based on soil mechanics research. We believe that the rigid body mechanisms described above will render the Poisson's ratio stress dependent. Further work is required in this area, as the results may significantly affect the degree of fuel anisotropy, and thus will dictate the level of complexity required for fuel performance codes such as FRAPCON.

The out-of-reactor tests have confirmed the axial modulus magnitude and the stress dependency that was found from the in-reactor data analysis. That the in-reactor and out-of-reactor data yielded similar values for axial modulus is taken as a strong indication that the analysis method used for the in-reactor data was valid.

Analytical and experimental results in general support the hypothesis that the fuel rod possesses distinct regimes of domination by the effective elastic moduli of the cracked fuel column. The transition from radial domination at lower powers to axial domination at higher powers is expected to affect the calculation of the stored mechanical energy in the fuel. This in turn affects the prediction of FCMI or PCI-SCC induced failures, which are a subject of interest for licensing and regulation.

9.0 CONCLUSIONS AND RECOMMENDATIONS

The effects of the thermally induced cracking and subsequent relocation of UO_2 fuel pellets on the thermal and mechanical properties of LWR fuel rods during irradiation were quantified in this report.

Data from the NRC/PNL Halden experiments IFA-431, IFA-432, and IFA-513 were analyzed. Beginning-of-life in-reactor measurements of fuel center temperatures, linear heat ratings, and cladding axial elongations were used in a new model to solve for the effective thermal conductivity and elastic moduli of the cracked fuel column. The following conclusions were reached:

- Pellet cracking allows the fuel fragments to relocate toward the cladding. This relocation redistributes part of the initial free void (gap) into the fuel in the form of cracks. The resulting reductions in fuel thermal conductivity and elastic moduli are primarily dependent on the amount and distribution of the free void, and always occur simultaneously.
- For a typical helium-filled BWR rod at BOL, the effective thermal conductivity of the cracked fuel was reduced to 70-90% of that for solid UO_2. The effective elastic moduli were correspondingly reduced by one to two orders of magnitude.
- The calculated fuel-cladding gap remained relatively constant (closed) with respect to power level, indicating that the fuel fragments do not retreat from the cladding when the power/temperature level is reduced. Thus, the concentric solid cylinder model traditionally used for fuel performance codes may not properly model the mechanical behavior of power reactor fuel rods, much less the mechanical-thermal interrelationships. This is expected to have an impact on PCI-SCC failure predictions with the advent of high exposure irradiation histories.
- Analytical results and experimental observations have in general supported the conclusion that the fuel rod response to power changes may be dominated by the effective radial elastic modulus of the

cracked fuel at low powers, and experience a transition to axial domination at higher powers. The importance of rigid body motions of the fuel fragments was demonstrated by the "mushrooming" observed from the laboratory axial compliance tests.

We also make the following recommendations:

- Since the primary independent variables (roughnesses and crack pattern) were not known, they were determined from limiting conditions provided by transient thermal data analysis results. Future work should quantify these parameters on stronger physical foundations to ensure no in-breeding between thermal and mechanical models.
- Much of the scatter in the results calculated from in-reactor data was caused by a lack of separating out effects due to power/temperature level. Refinements in the results may be obtained by more detailed analysis. In particular, the definition of the thermal conductivity reduction needs improvement, as do the elastic moduli dependencies on axial power profile shapes.
- More simple ex-reactor experiments should be performed. Since they have a distinct economic advantage over in-reactor experiments, the cost/benefit ratio is very good. The bench-top experiments are also directly observable and more easily measured, thus permitting more complete separations of individual phenomena. This is especially advantageous concerning the effects of rigid body motion of fragments and the study of Poisson' ratio for the cracked fuel.
- Although the in-reactor tests have yielded well-qualified and useful data, the uncertainties in thermal results could be significantly reduced by an assembly with xenon fill gas instead of helium. This would serve to refine the transient data results and thus provide a better thermal index for checking the three primary mechanical parameters.

ACKNOWLEDGMENTS

R. W. Miller has guided the assemblies to experimental success at the Halden Project. The many data plots were produced by W. D. Bennett. Technical editing was performed by Claude Dotson, and typing was done by Paulette Goodenough and Patti Giles. The support of C. R. Hann is also appreciated. Intense discussions with J. O. Barner have resulted in what we hope to be a clear and precise presentation of this work.

REFERENCES

1. Berna, G. A., M. P. Bohn and D. R. Coleman. 1978. FRAPCON-1: A Computer Code for the Steady State Analysis of Oxide Fuel Rods, CDAP-TR-78-032-R1, EG&G Idaho, Inc., INEL.

2. Lanning, D. D., C. L. Mohr, F. E. Panisko and K. B. Stewart. 1978. GAPCON-THERMAL-3 Code Description, PNL-2434, Pacific Northwest Laboratory, Richland, Washington.

3. Dearien, J. A., et al. 1977. FRAP-S2: A Computer Code for the Steady State Analysis of Oxide Fuel Rods. TREE-NUREG-1107, EG&G Idaho, Inc., INEL.

4. Hann, C. R., and R. K. Marshall. 1977. Comparative Analysis of Pellet-Cladding Interaction From IFA-431 and IFA-432 Halden Reactor Tests, BNWL-2240, Pacific Northwest Laboratories, Richland, Washington.

5. Hann, C. R., J. L. Bates, D. W. Brite, J. L. Daniel, N. C. Davis, P. E. Hart, R. K. Marshall, G. Mellinger and R. E. Williford. 1977. Test Design Precharacterization and Fuel Assembly Fabrication for Instrumented Fuel Assemblies IFA-431 and IFA-432. BNWL-1988, Pacific Northwest Laboratory, Richland, Washington.

6. Hertz, J. 1881. J. Math 92.

7. Greenwood, J. A., and J. B. P. Williamson. 1966. "Contact of Nominally Flat Surfaces," Proc. R. Soc. Lond 295:300-319.

8. Greenwood, J. A., and J. H. Tripp. 1971. "The Contact of Two Nominally Flat Surfaces," Proc. Inst. Mech Engng 185:625-633.

9. Pullen, J., and J. B. P. Williamson. 1973. Proc. R. Soc. Lond 327A:159-173.

10. Mikic, B. B. 1974. "Thermal Contact Conductance: Theoretical Considerations," Int. J. Heat Mass Transfer 17:205-214.

11. Williford, R. E., and C. R. Hann. 1977. Effects of Fill Gas Composition and Pellet Eccentricity, BNWL-2285, Pacific Northwest Laboratories, Richland, Washington.

12. Sechler, E. E. 1952. Elasticity in Engineering, John Wiley & Sons.

13. Barkan, D. D. 1960. Dynamics of Bases and Foundations, McGraw-Hill.

14. Timoshenko, S. P., and J. N. Goodler. 1970. Theory of Elasticity, 3rd Edition, McGraw-Hill.

15. Lanning, D. D., and M. E. Cunningham. 1979. Startup Data Report for NRC/PNL Halden Assembly IFA-513, NUREG/CR-0862, PNL-2948, Pacific Northwest Laboratory, Richland, Washington.

16. MacDonald, P. E., et al. 1976. MATPRO-Version-09 - A Handbook of Materials Properties for Use in the Analysis of Light Water Reactor Fuel Rod Behavior. TREE-NUREG-1005, EG&G Idaho, Inc., INEL.

17. Robertson, J. A. L. 1959. $\int k d\theta$ in Fuel Irradiations. CRFD-835, Chalk River, Ontario, CANADA.

18. Lyons, M. F., D. H. Coplin, T. J. Pashos and B. Weidenbaum. 1964. UO_2 Pellet Thermal Conductivity from Irradiation with Central Melting, GEAP-4624.

19. Lanning, D. D., B. O. Barnes and R. E. Williford. 1979. Manifestations of Non- Linearity in Fuel Center Thermocouple Steady State and Transient Data: Implications for Data Analysis, NUREG/CR-0220, PNL-2692, Pacific Northwest Laboratory, Richland, Washington.

20. Garnier, J. E., and Stefan Begej. 1979. Ex-Reactor Determination of Thermal Gap and Contact Conductance Between Uranium Dioxide: Zircaloy-4 Interfaces - Stage 1:Low Gas Pressure, NUREG/CR-0330, PNL-2696, Pacific Northwest Laboratory, Richland, Washington.

21. Cunningham, M. E., and D. D. Lanning. 1980. Precharacterization of the NRC/PNL Halden Assembly IFA-513, NUREG/CR-1077, PNL-3156, Pacific Northwest Laboratory, Richland, Washington.

22. Crouthamel, C. E. 1979. Fuel Performance Improvement Program, Quarterly/Annual Progress Report (October 1978-September 1979), COO-4066-13, UC-78, Exxon Nuclear Company, Inc., Richland, Washington.

23. Smith, E. 1979. The Fuel-Cladding Interfacial Friction Coefficient in Water-Cooled Reactor Fuel Rods, SMIRT-5 Conference, Berlin, Germany.

24. Nealley, C., D. D. Lanning, M. E. Cunningham, and C. R. Hann. 1979. Post-Irradiation Data Analysis for NRC/PNL Halden Assembly IFA-431, NUREG/CR-0797, PNL-2975, Pacific Northwest Laboratory, Richland, Washington.

25. Cochran, W. G., and G. M. Cox. 1957. "Experimental Designs," 2nd Edition. John Wiley and Sons, New York.

26. Lanning, D. D., et al. 1979. A Procedure for the Interpretation of Transient Fuel Centerline Thermocouple Data, NUREG/CR-1012, PNL-3096, Pacific Northwest Laboratory, Richland, Washington.

27. Lanning, D. D., C. R. Hann and R. E. Williford. 1978. "Qualitative Confirmation of Steady State Fuel Centerline Thermocouple Data from Transient Response," Trans ANS 30:177.

28. Bradley, E. R., M. E. Cunningham, C. R. Hann, D. D. Lanning and R. E. Williford. 1978. "In-Pile Measurements of Fission Gas Release From UO_2 Fuels," Trans. ANS 30:179.

29. Hann, C. R., D. D. Lanning, R. K. Marshall, A. R. Olsen and R. E. Williford. 1977. A Method for Determining the Uncertainty of Gap Conductance Deduced from Measured Fuel Centerline Temperature, BNWL-2091, Battelle, Pacific Northwest Laboratory, Richland, Washington.

30. Lanning, D. D., and C. R. Hann. 1977. Verification of Fuel Centerline Thermocouple Readings Through Response to Linear Power Decreases, BNWL-2189, Pacific Northwest Laboratory, Richland, Washington.

APPENDIX A

THERMAL ANALYSIS METHODS

APPENDIX A

THERMAL ANALYSIS METHODS

Two methods have been developed at PNL for the analysis of in-reactor thermal behavior of fuel rods. In the first method, the total thermal resistance of the rod is plotted versus its steady state power. The thermal resistances of the fuel interior and fuel-cladding gap have opposite slopes with respect to temperature. Thus the slope of the total resistance versus power plot reveals whether the rod is fuel or gap dominated.

The second method uses transient data. The center temperature response to power down ramps is cast into a normalized form. This response is compared with the expected response predicted by numerical calculations for chosen functions of fuel body and gap resistances. Two types of power decay ramps reveal whether the thermocouples are operating properly, and what the partition of the resistance is between fuel body and the gap. The transient behavior provides a qualitative confirmation of the steady state behavior.

In this report, the steady state method is applied in making observations from the data, and the transient results are used during data analysis.

TOTAL THERMAL RESISTANCE - STEADY STATE DATA

The "total thermal resistance," R_T, of a nuclear fuel rod is found by simply dividing the temperature difference (from centerline to coolant) by the local rod power, and its units are indeed those of resistance. From the Ohm's Law analogy with heat transfer, we find

$$Q = H\Delta T$$

where Q = Watts (current)

H = W/K (conductance)

T = K (potential)

The power can be made a local quantity by normalizing by length.

$$P = Q/L = W/m$$

Then the "total resistance" is $R_T = \Delta T/P = \text{mK/W}$, where ΔT is the temperature drop from centerline to coolant. This represents a very simple series electrical circuit with the rod power as the source and the coolant as the sink, the resistance connecting the two. Figure A-1 shows how the calculated components from fuel, gap, and cladding resistance contribute to the total thermal resistance for Rod 1 at beginning of life. The increase in fuel resistance (with increasing power) is due to decreasing fuel thermal conductivity, while the decrease in gap resistance is due to fuel thermal expansion closing the "gap" and increasing the amount of solid conductance between fuel and cladding. (The term "gap" refers to the thermally equivalent annulus between fuel and cladding, but does not necessarily imply that it is geometrically symmetric.) The cladding resistance rises nearly linearly. These combine so that the resultant total resistance, R_T, is nearly a constant for an "open gap" helium-filled rod. We will call this rod a "balanced rod." When the "gap" closes, R_T increases with power since the fuel resistance dominates and the change in gap resistance is minimal ("fuel dominated rod"). A xenon filled open "gap" causes

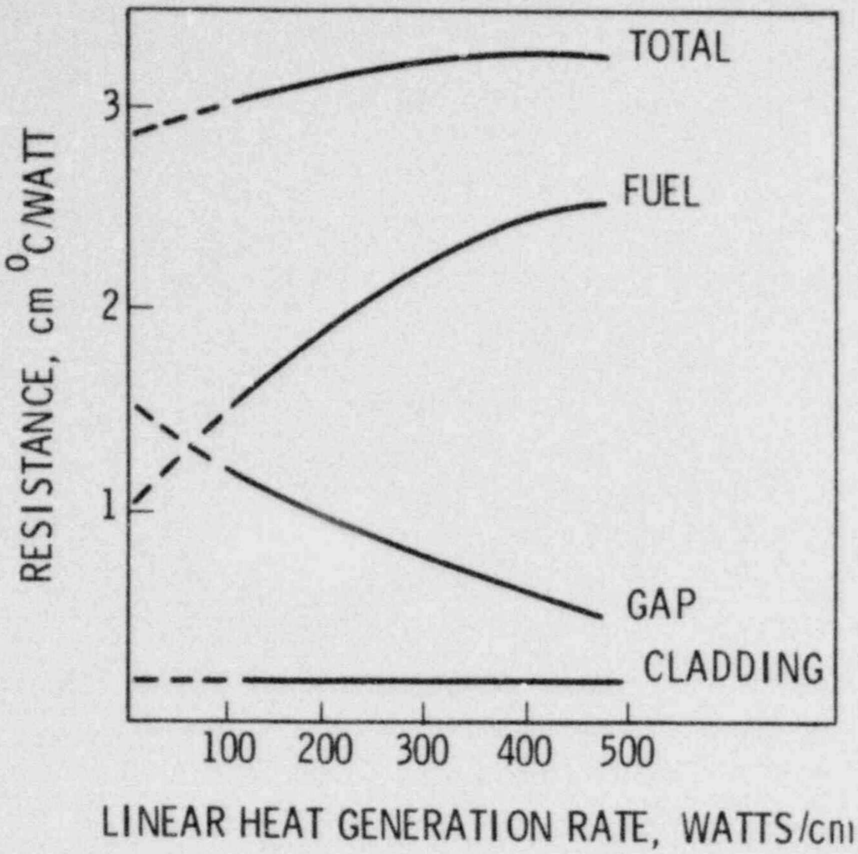

FIGURE A.1. Components of Resistance

the total resistance to decrease with increasing power ("gap dominated rod"). Plots of R_T vs. power can thus be used as an indicator of gap closure or low gas conductivity (Figure A.2).

The total resistance is in fact the only thermal "property" of the rod that is actually measured with centerline thermocouples. It is the ratio of measured temperature drop and measured power. All other thermal characteristics of the rod must be inferred. Gap conductance is an example of an inferred variable.

The sensitivity of the resistance when plotted versus power is also of note. Figure A.3a shows the form in which most data is received and plotted. It is difficult to determine from this plot what the fuel rod is actually doing because the data are sparce. However, Figure A.3b shows the same data in terms of resistance. Here the nonlinear character and scatter of the data are both evident.

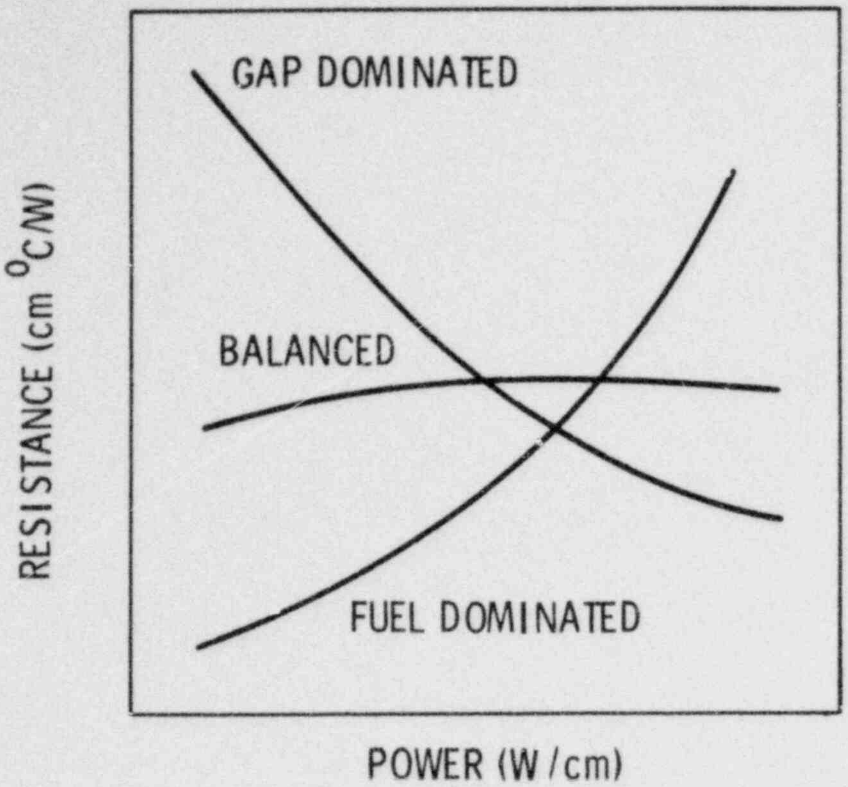

FIGURE A.2. Resistance Behavior of Various Rods

Since the total thermal resistance, R_T requires a minimum of assumptions and is a sensitive indicator or rod characteristics, it is used in this report to represent the events occurring during the lifetimes of the IFA-431, IFA-432, and IFA-513 rods.

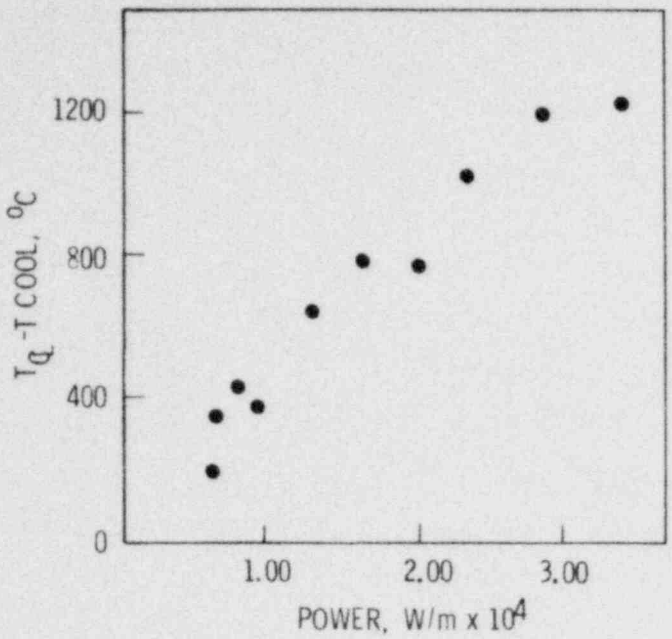

a. Conventional T vs P Does Not Discriminate Nonlinear Behavior

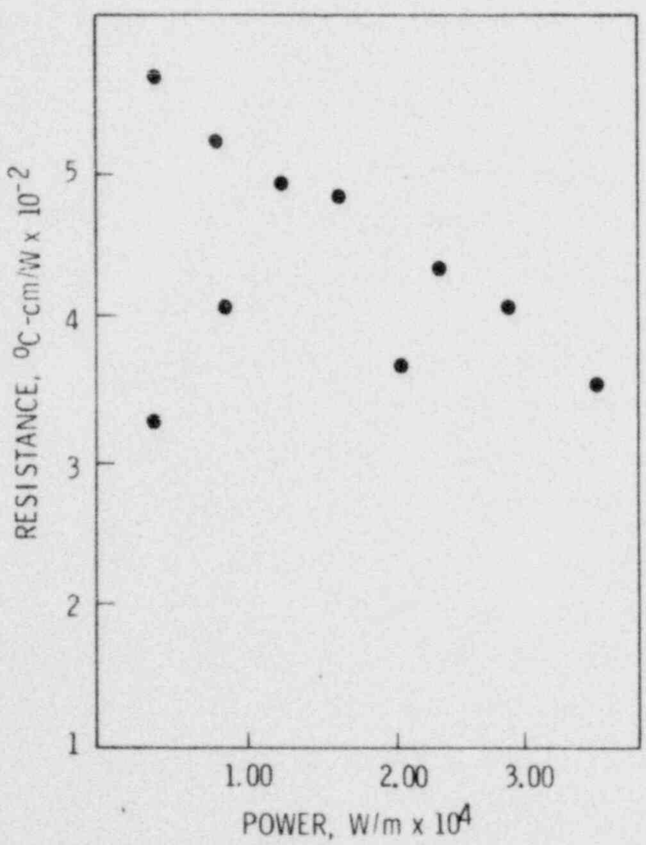

b. More Sensitive R vs P Shows Nonlinear Trends of T vs P

FIGURE A.3. The Sensitivity of Resistance

TRANSIENT ANALYSIS METHODS

The data for this analysis consists of fuel centerline thermocouple measurements and relative power measurements using a cobalt fast response SPND. The true power measured by vanadium SPND's may be checked to provide steady state values immediately before and after the transient period by comparison with the cobalt SPND readings.

The first step in this analysis is to normalize the temperature response. This is done in a classical manner.[26] The transient temperature difference between fuel center and coolant is divided by its steady state value before the ramp starts:

$$Tn = \frac{Tct - Tcool}{Tcs - Tcool}$$

where Tn = normalized temperature
$Tcool$ = coolant temperature
Tct = transient center temperature
Tcs = steady state center temperature at beginning of ramp.

This normalized temperature is used in the analysis of two types of power down ramps, linear and step.

The linear power down ramp is shown in Figure A.4 where the normalized power and temperature are plotted. The power decreases to about 80% of its initial value in about 30 seconds.

An indication of the state of the rod can be seen by comparing the slopes of the normalized power and temperature curves. If the Pn (normalized power) curve has a greater slope than the Tn curve, the rod is relatively sluggish in its response and is termed "gap dominated." If the two slopes are equal (within statistical limits of the data), the rod is termed "balanced." If the Tn slope is greater than the Pn slope, the relatively quick exhausting of fuel stored energy results in a "fuel dominated" rod, where the "gap" is "closed." However, this analysis is insensitive to reasonable variations in fuel and gap thermal properties that are used. Within statistical limitations of the data, this analysis cannot distinguish between solid or cracked fuel thermal conductivities.

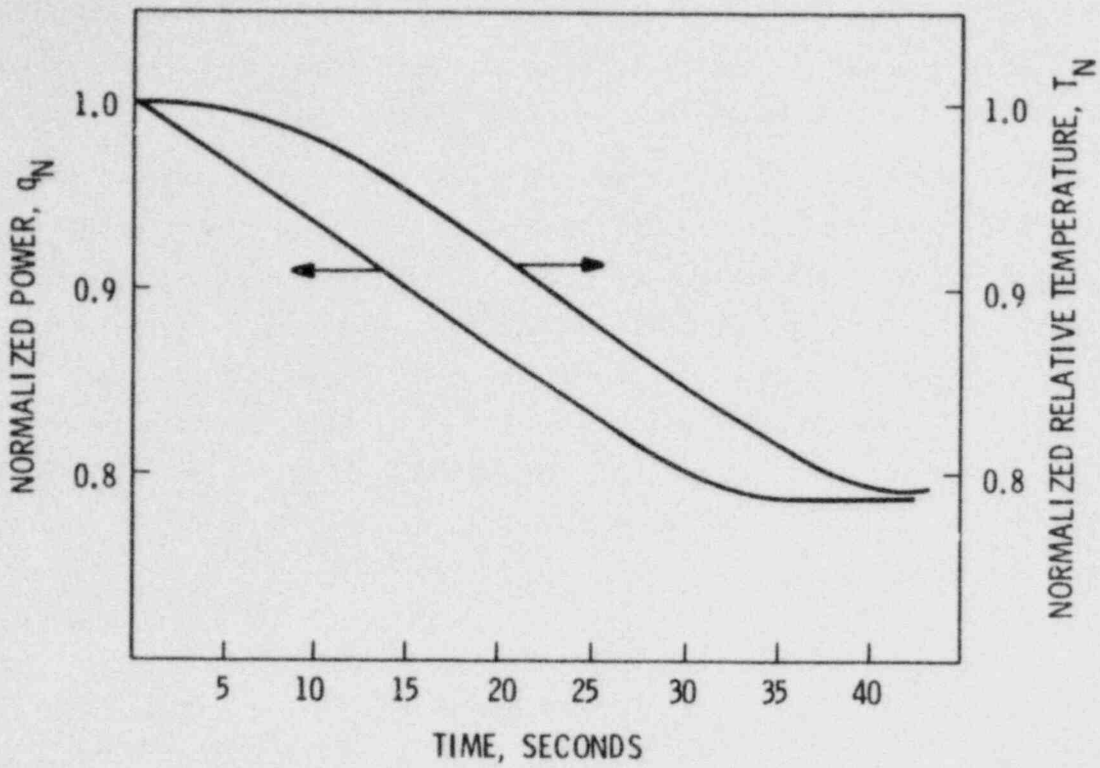

FIGURE A.4. Linear Power Down Ramp

Rather than being a detriment, this result can be used to verify that the thermocouple data is consistent with the power data,[26] providing a useful and necessary check on the health of the instrumentation.

The second type of transient analysis performed is for step power drops, as shown in Figure A.5. The classical lumped parameter solution (assuming constant thermal properties) for the idealized step power drop is[26]

$$Tn = a + (1-a)\, e^{-\alpha_F t}$$

where "a" is the fraction of initial power at the end of the step power drop. The normalized temperature data is plotted in the form

$$\ln(Tn-a) = \ln(1-a) + \ln e^{-\alpha_F t}$$

$$= \text{constant } -\alpha_F t$$

This means that plots of -ln(Tn-a) versus time should be linear. The thermocouple time constant causes the predicted line to be translated by a small amount, but does not affect the slope of the line.

While actual data is not ideal, there are useful ranges where the above plots are approximately linear. It is possible to determine the partition of resistance between fuel and gap by comparing measured and predicted plots of -ln(Tn-a) versus time. Although the decisive comparison is qualitative in nature, the results confirm the steady state resistance versus power behavior, and in general show that the effects of the cracks on fuel thermal conductivity and gap conductance are significant. The reader is referred to References 19, 26, and 27 for a complete discussion.

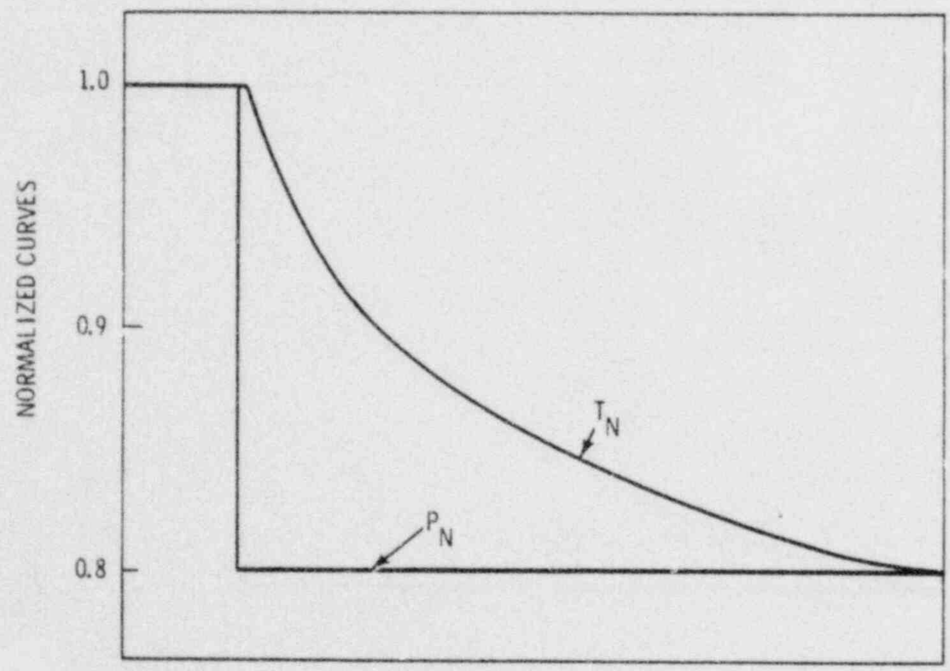

FIGURE A.5. Step Power Drop

APPENDIX B

OBSERVATIONS FROM THE IN-REACTOR

APPENDIX B

OBSERVATIONS FROM THE IN-REACTOR DATA

In this Appendix, data from IFA-431, IFA-432, and IFA-513 are presented. IFA-431 and 432 are shown in the form of total thermal resistance versus burnup plots in order to summarize the results obtained from these rods. References are cited pertaining to specific details of results. IFA-513 data are presented for beginning-of-life (BOL) conditions in more detail than for IFA-431 and IFA-432. Resistance versus power and cladding elongation versus power plots are shown. Observations and trends in the data are discussed on a rod-by-rod basis.

OBSERVATIONS FROM IFA-431 AND IFA-432

Figures B.1 through B.12 show resistance versus burnup plots for all rods of IFA-431 (to end-of-life) and IFA-432 (to ~18 GWd/MTM). These plots were constructed from steady state data only. That is, the data file was filtered so that the change in local linear heat rating varied by no more than 5% from one data point to the next.[a] The various symbols and numbers represent steady state data within 5 kW/m power increments (Table B.1).

TABLE B.1. Symbols Used in Figures B.6 Through B.12

Local Power (kW/m)	Symbols (upper TC)	Numbers (lower TC)
5-10	0	1
10-15	Δ	2
15-20	+	3
20-25	$\overline{x}$	4
25-30	◇	5
30-35	†	6
35-40	X	7
40-45	Z	8
45-50	Y	9
50-55	□	10

(a) Successive data points are separated in time by at least 15 minutes.

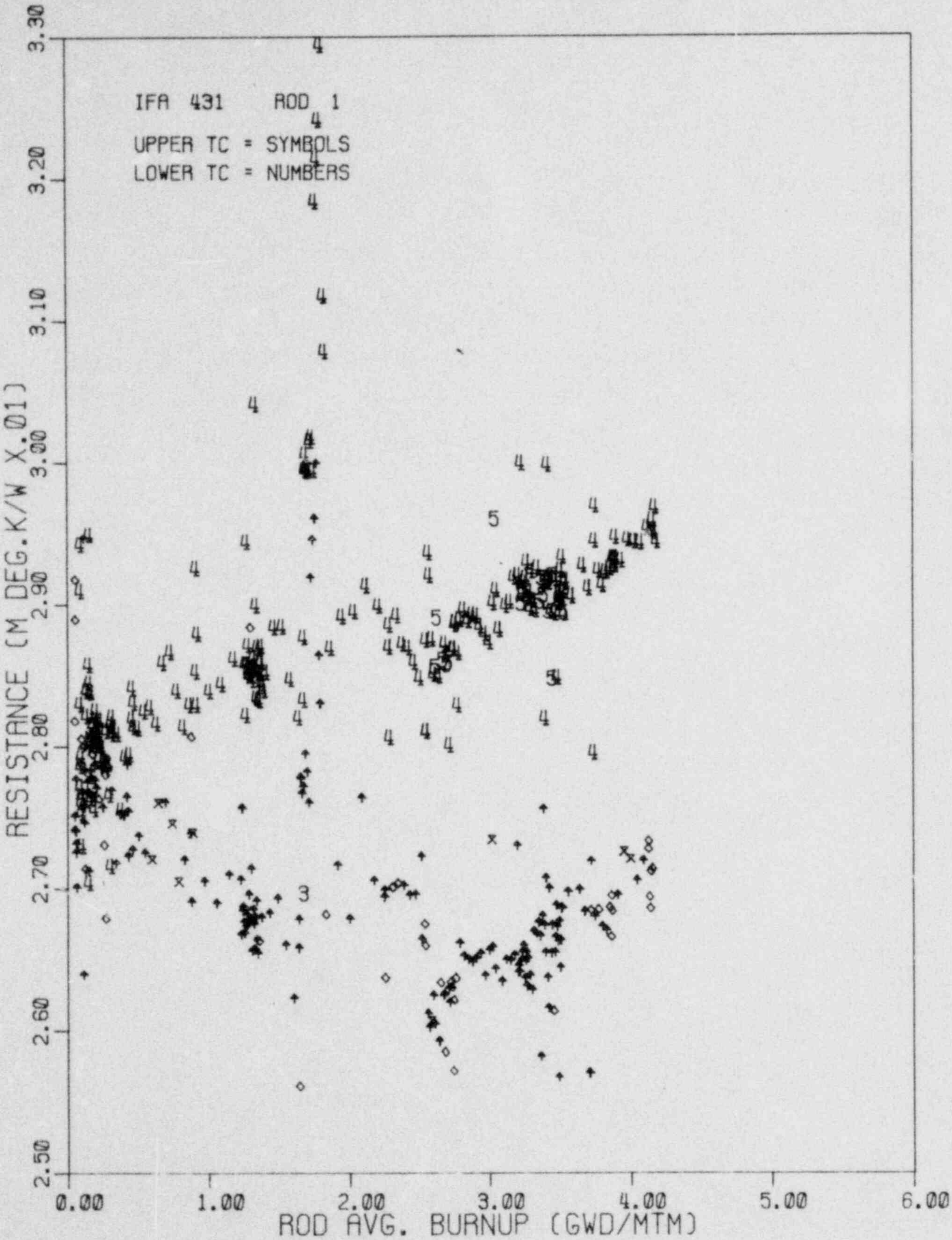

FIGURE B.1. Resistance History for Rod 1 of IFA-431

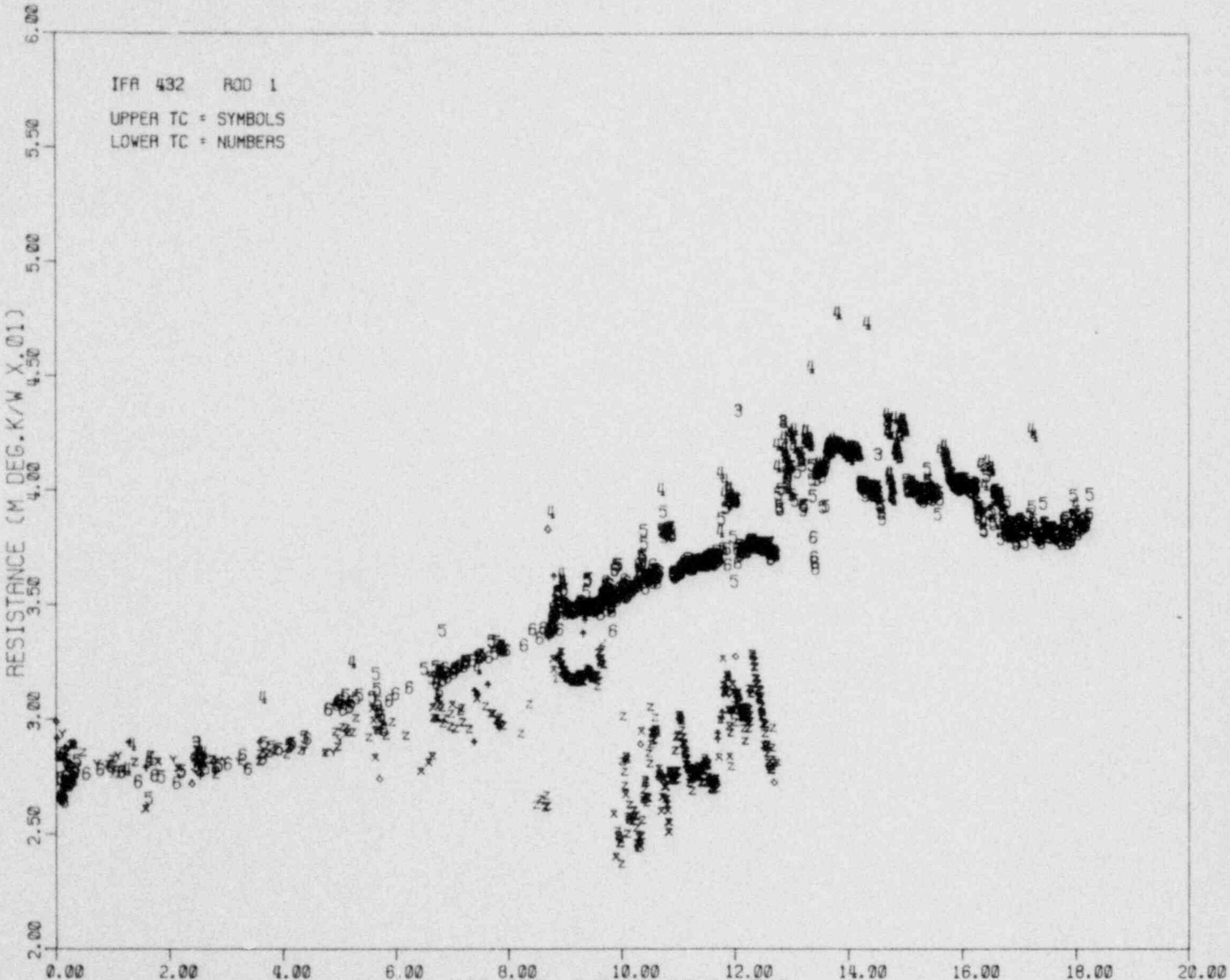

FIGURE B.2. Resistance History for Rod 1 of IFA-432

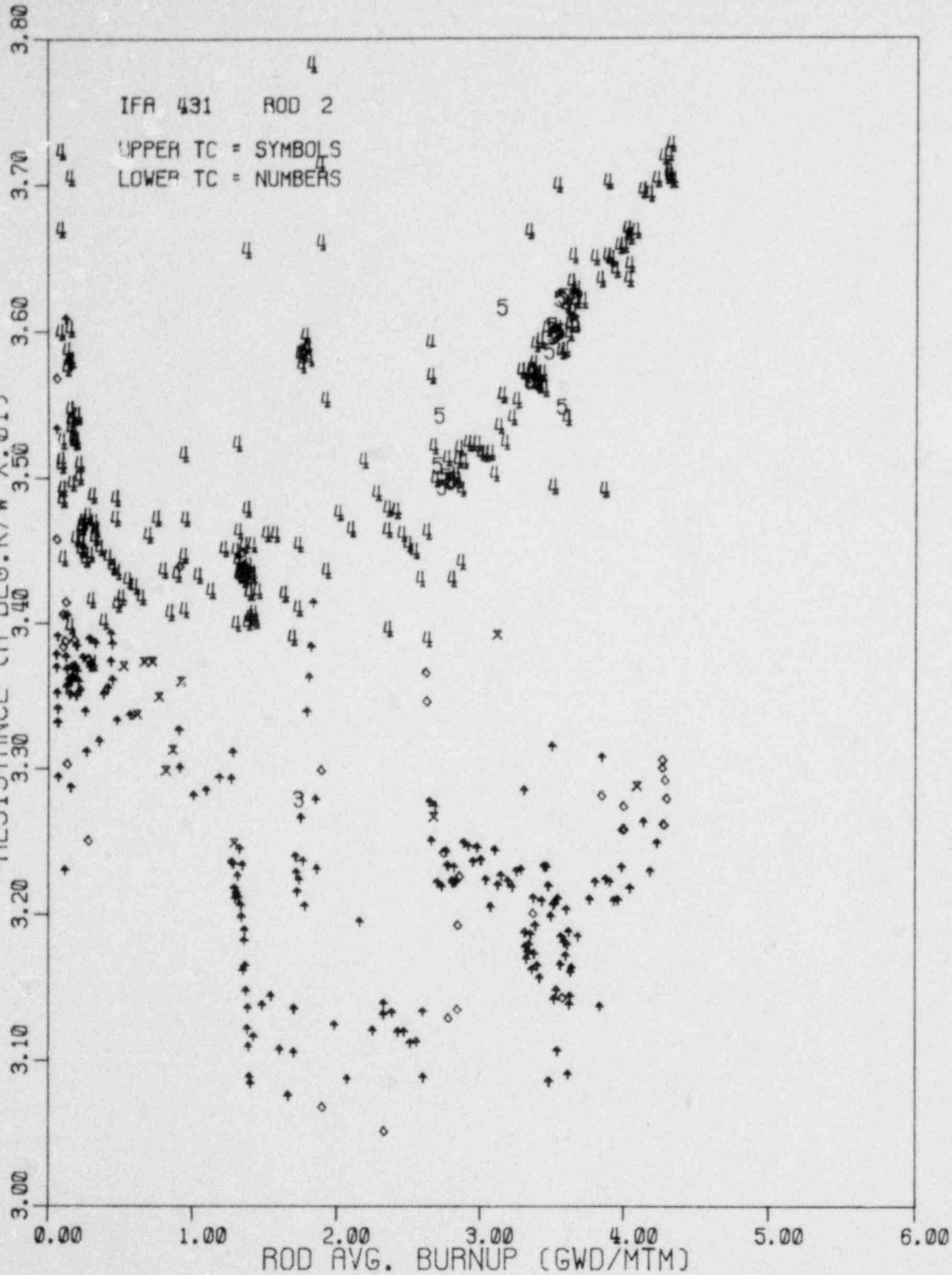

FIGURE B.3. Resistance History for Rod 2 of IFA-431

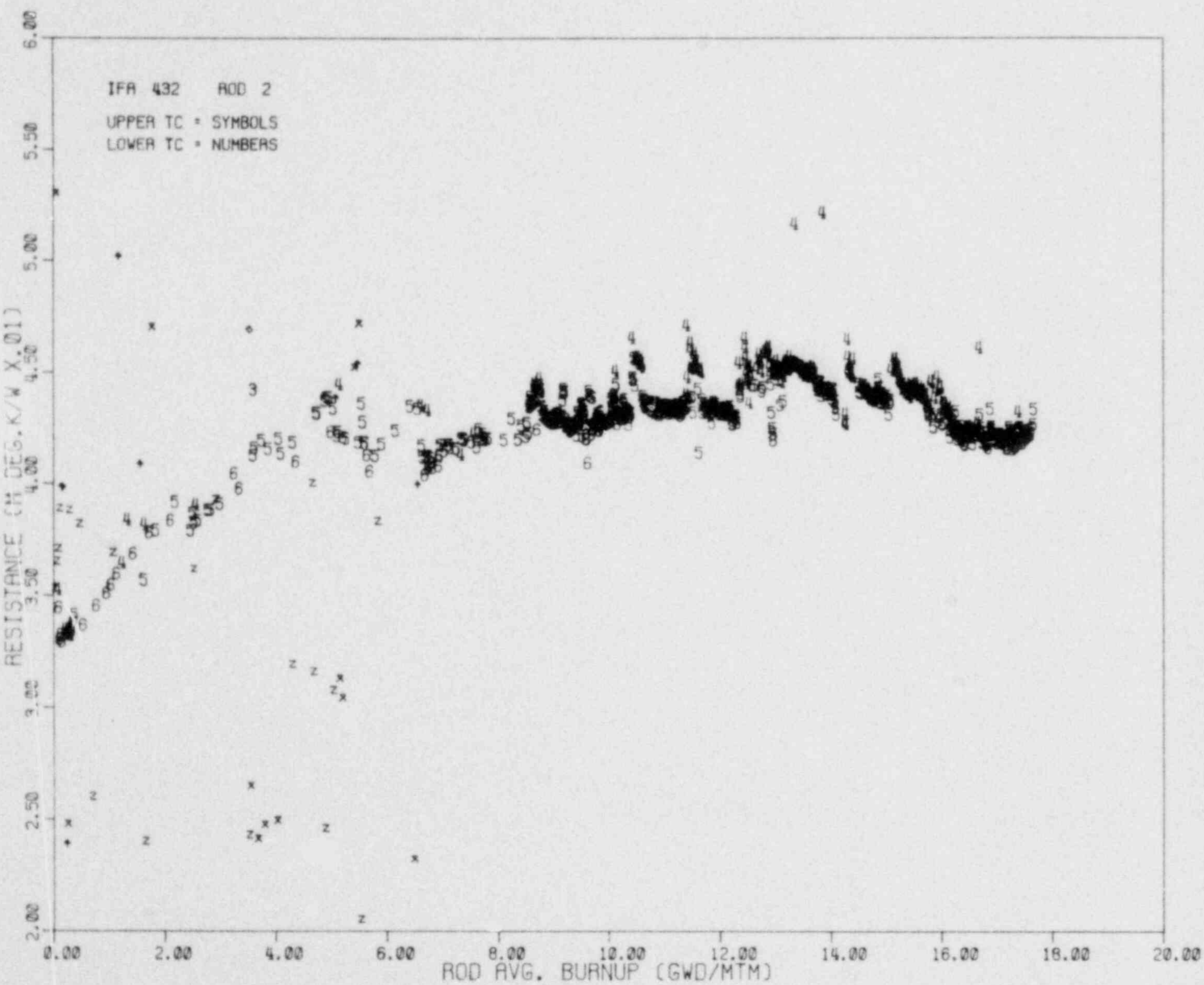

FIGURE B.4. Resistance History for Rod 2 of IFA-432

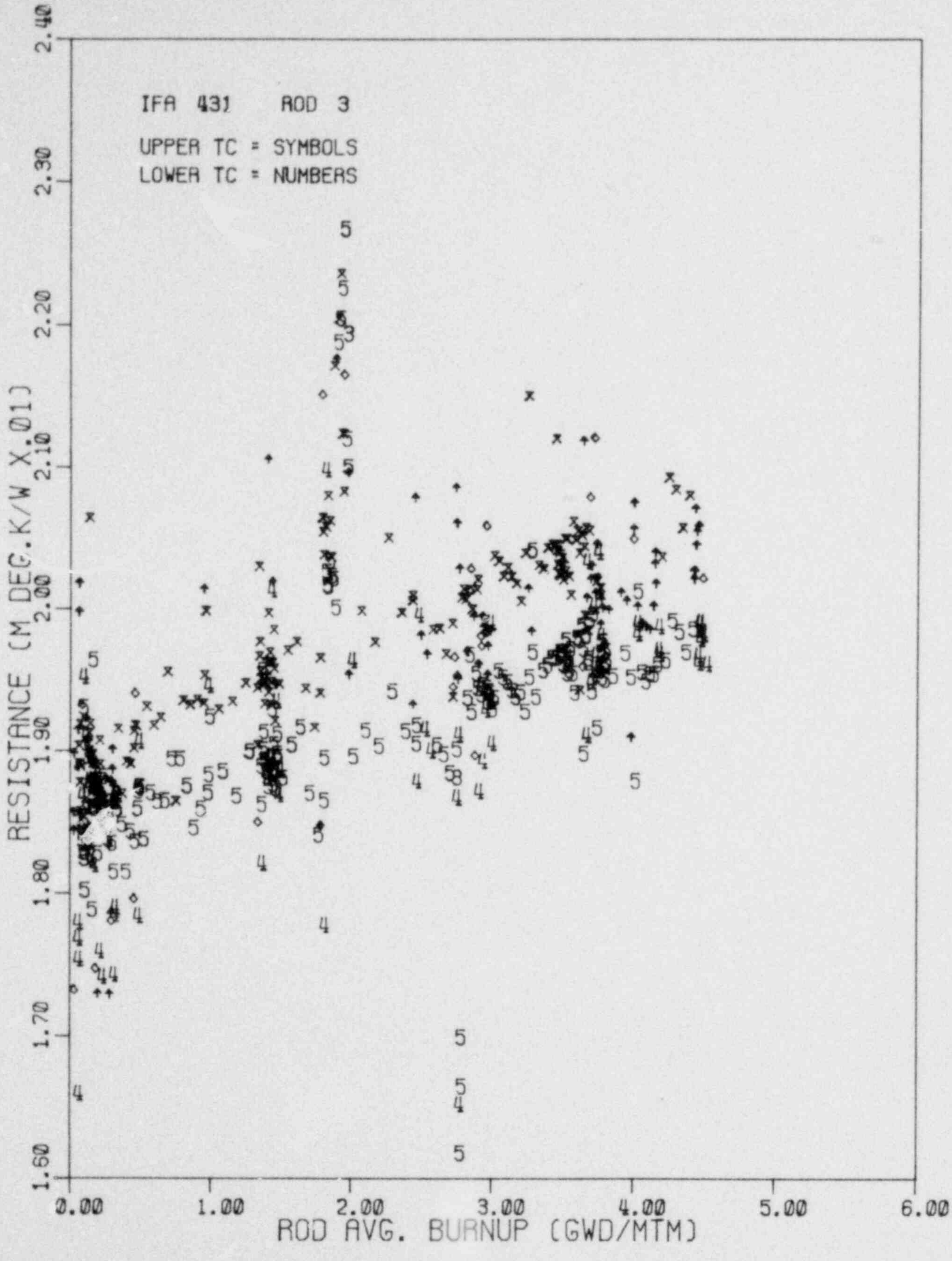

FIGURE B.5. Resistance History for Rod 3 of IFA-431

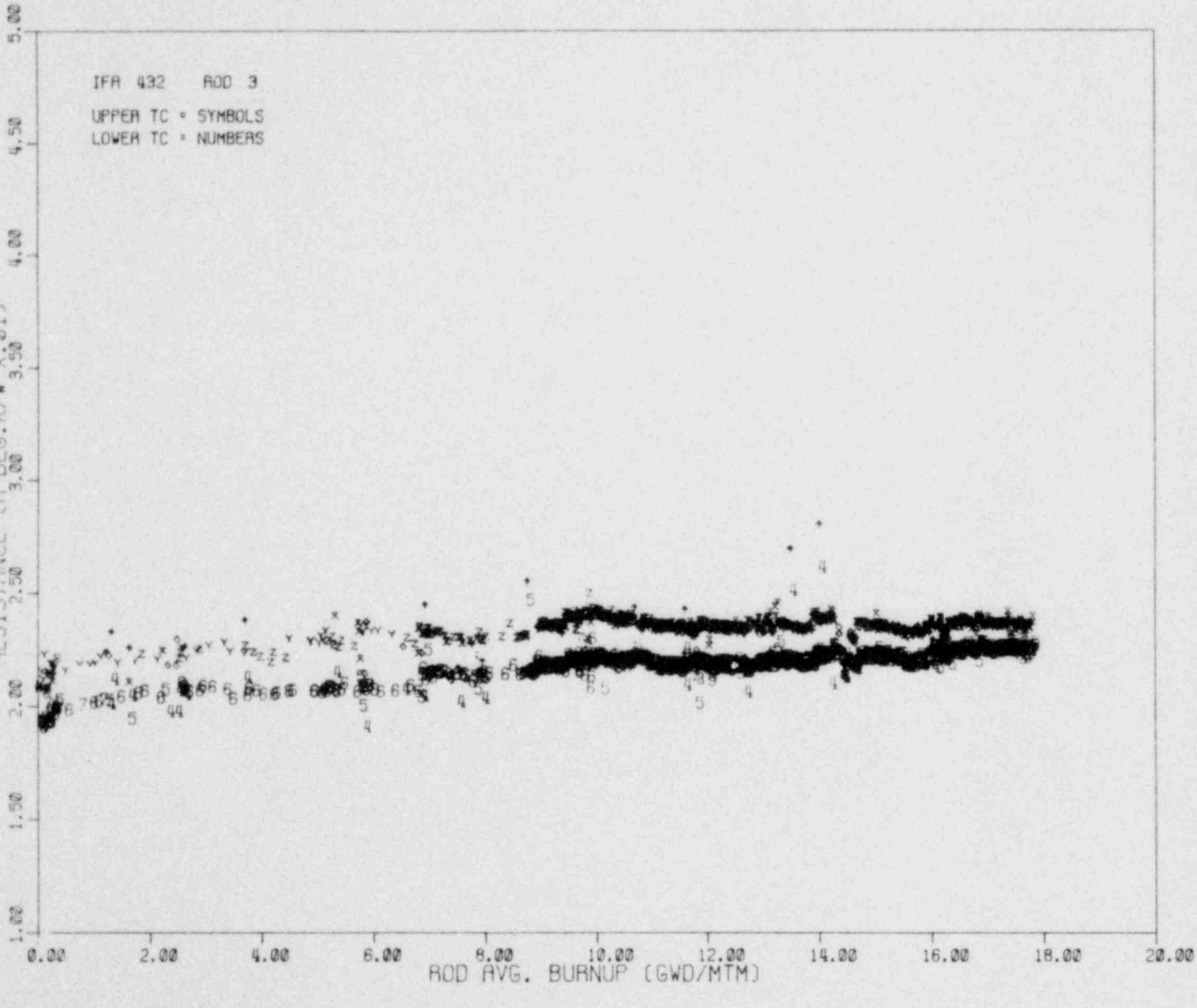

FIGURE B.6. Resistance History for Rod 3 of IFA-432

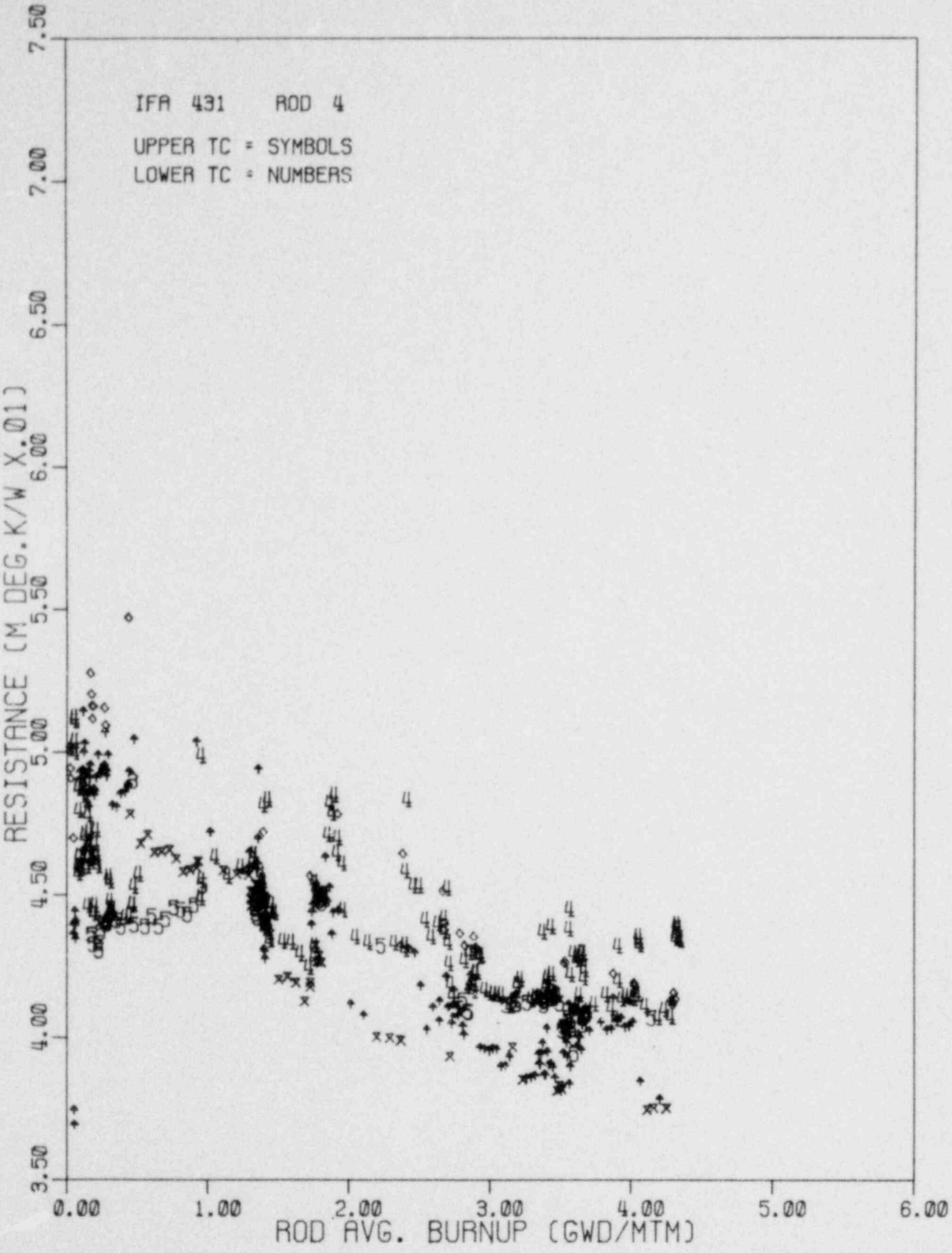

FIGURE B.7. Resistance History for Rod 4 of IFA-431

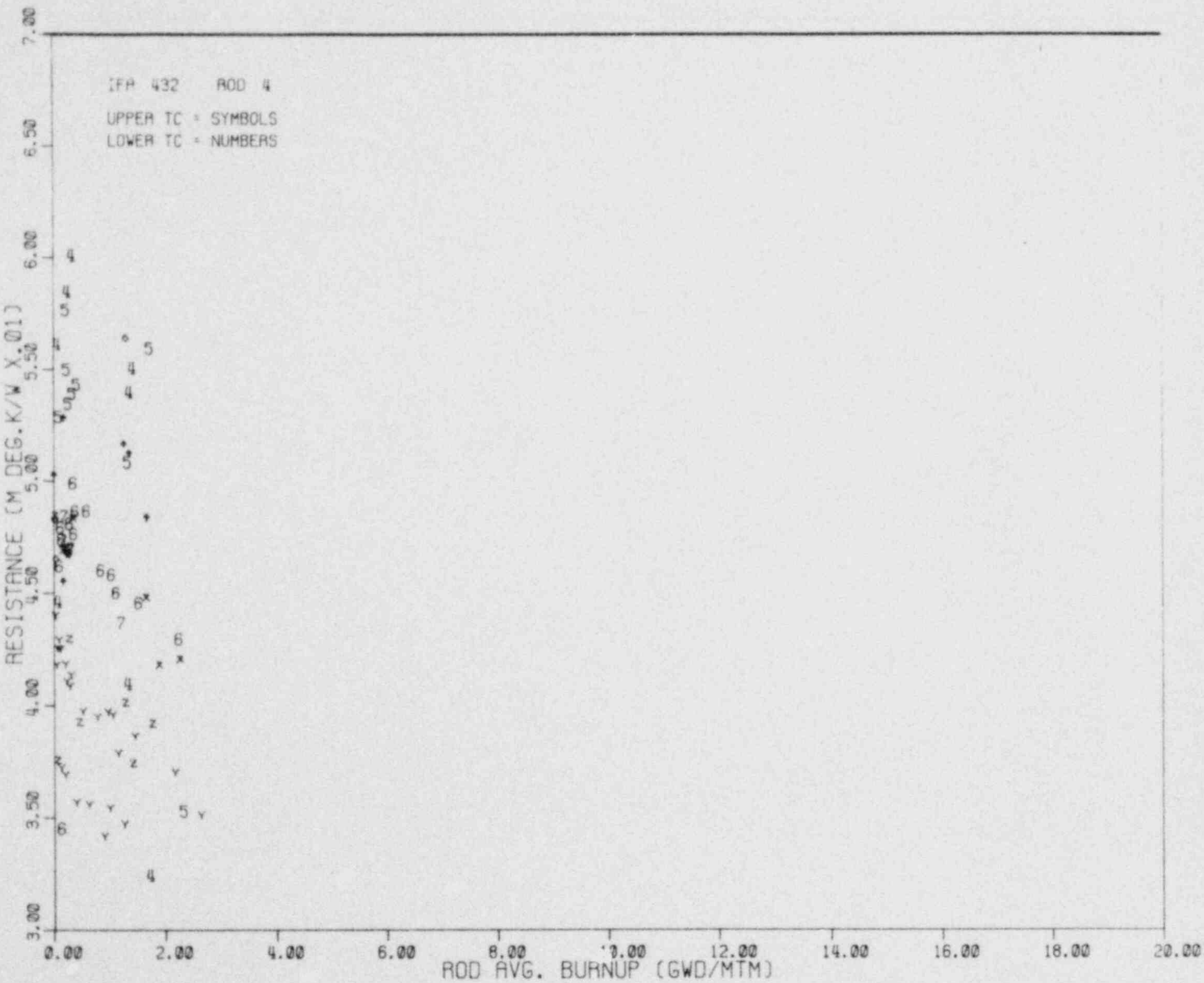

FIGURE B.8. Resistance History for Rod 4 of IFA-432

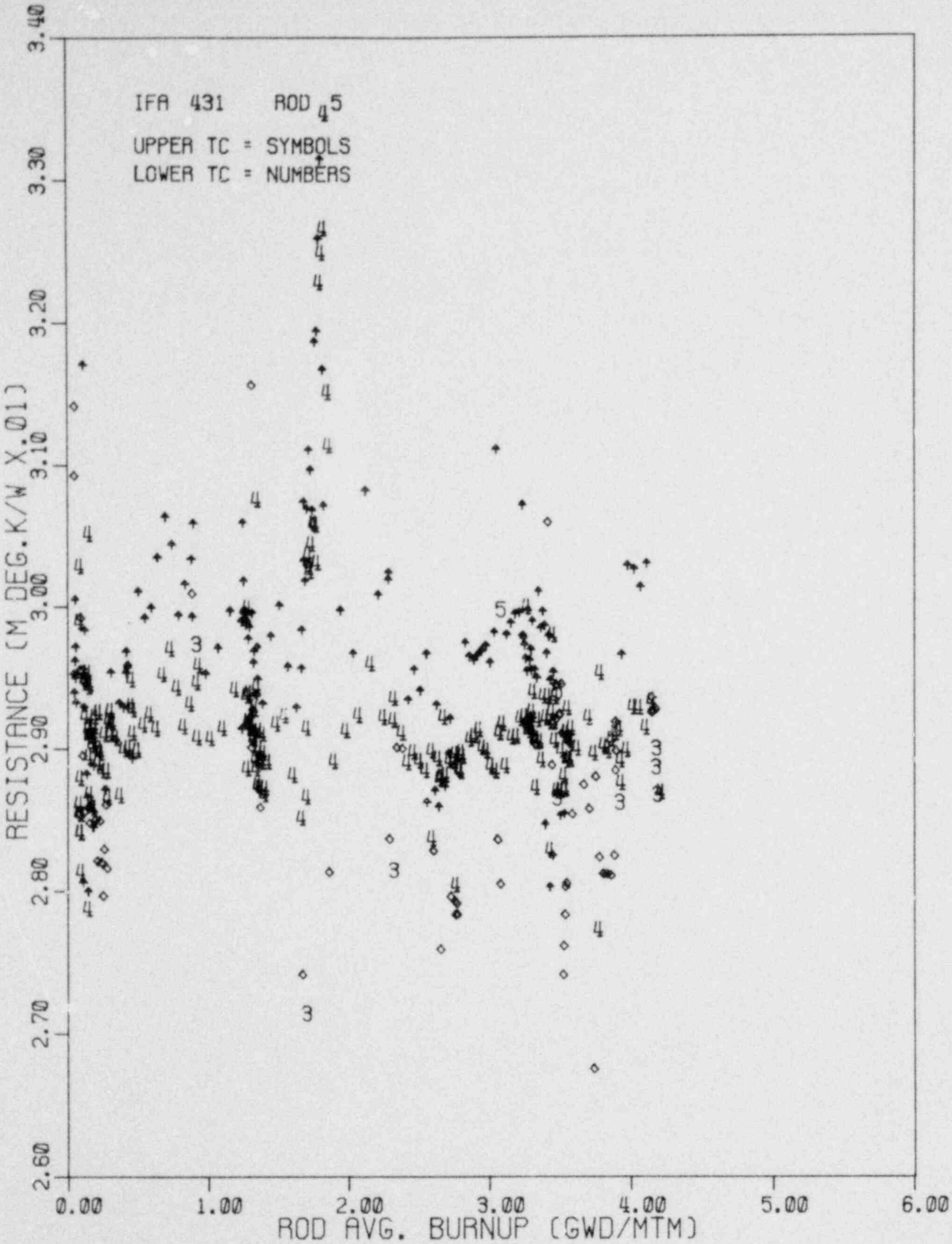

FIGURE B.9. Resistance History for Rod 5 of IFA-431

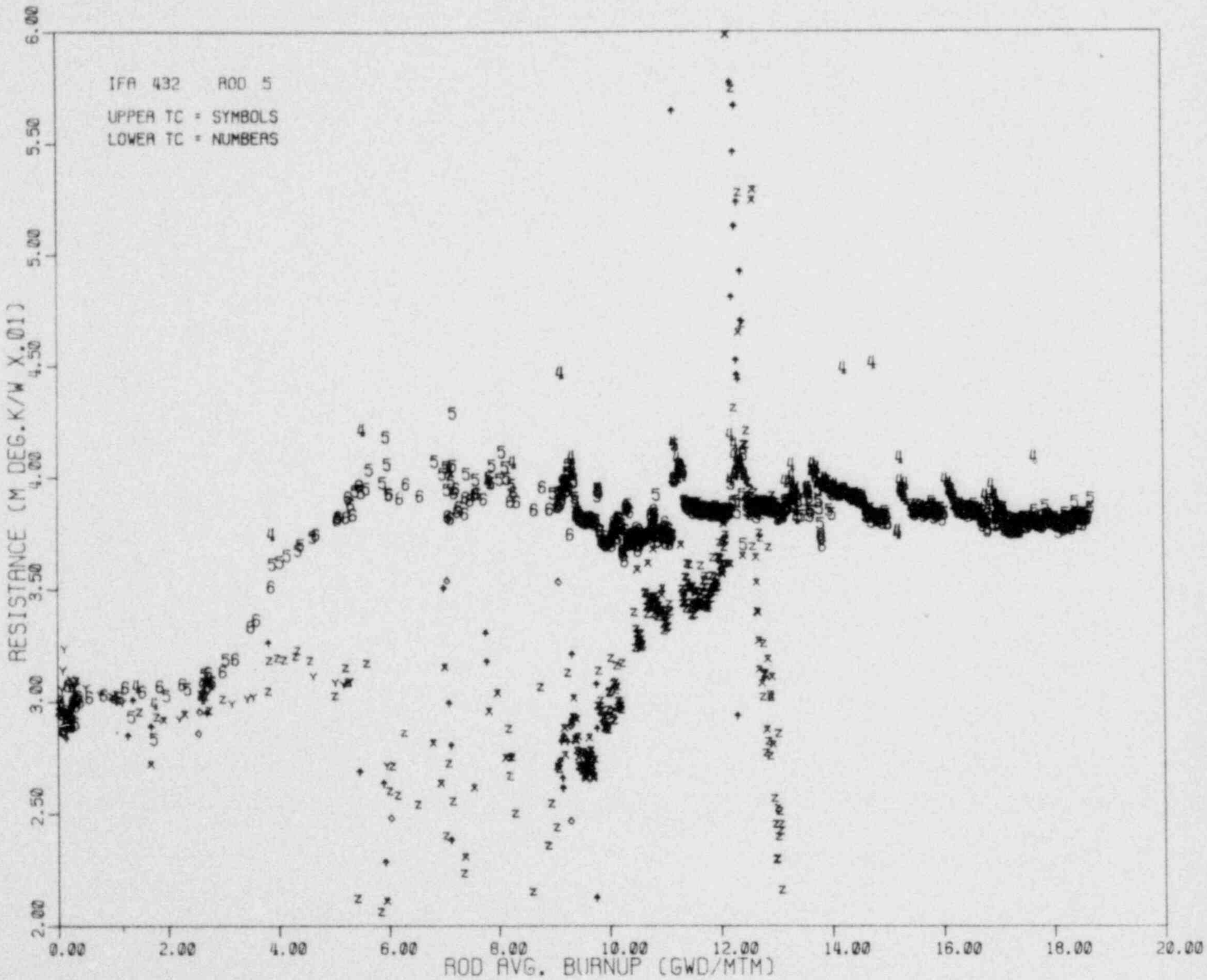

FIGURE B.10. Resistance History for Rod 5 of IFA-432

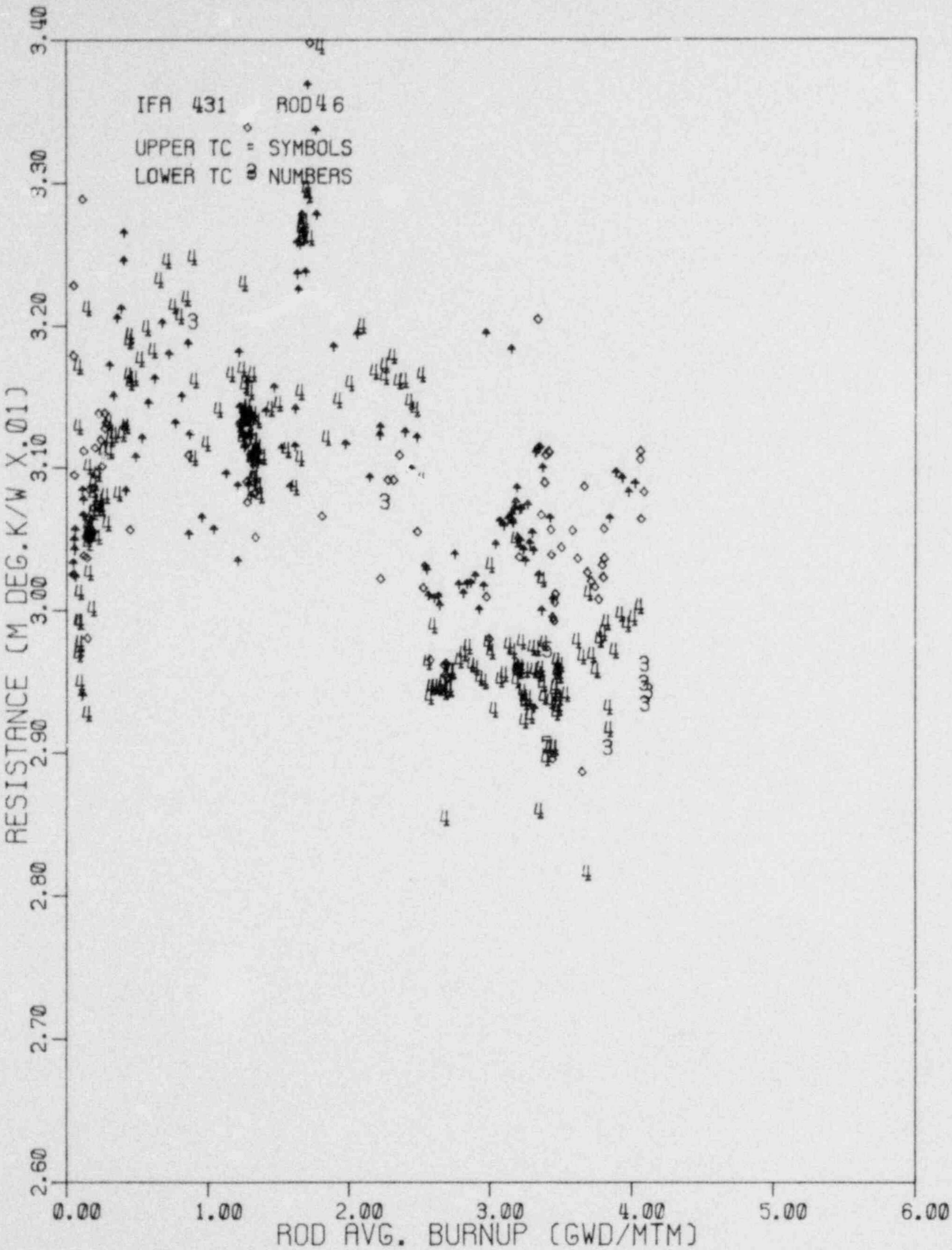

FIGURE B.11. Resistance History for Rod 6 of IFA-431

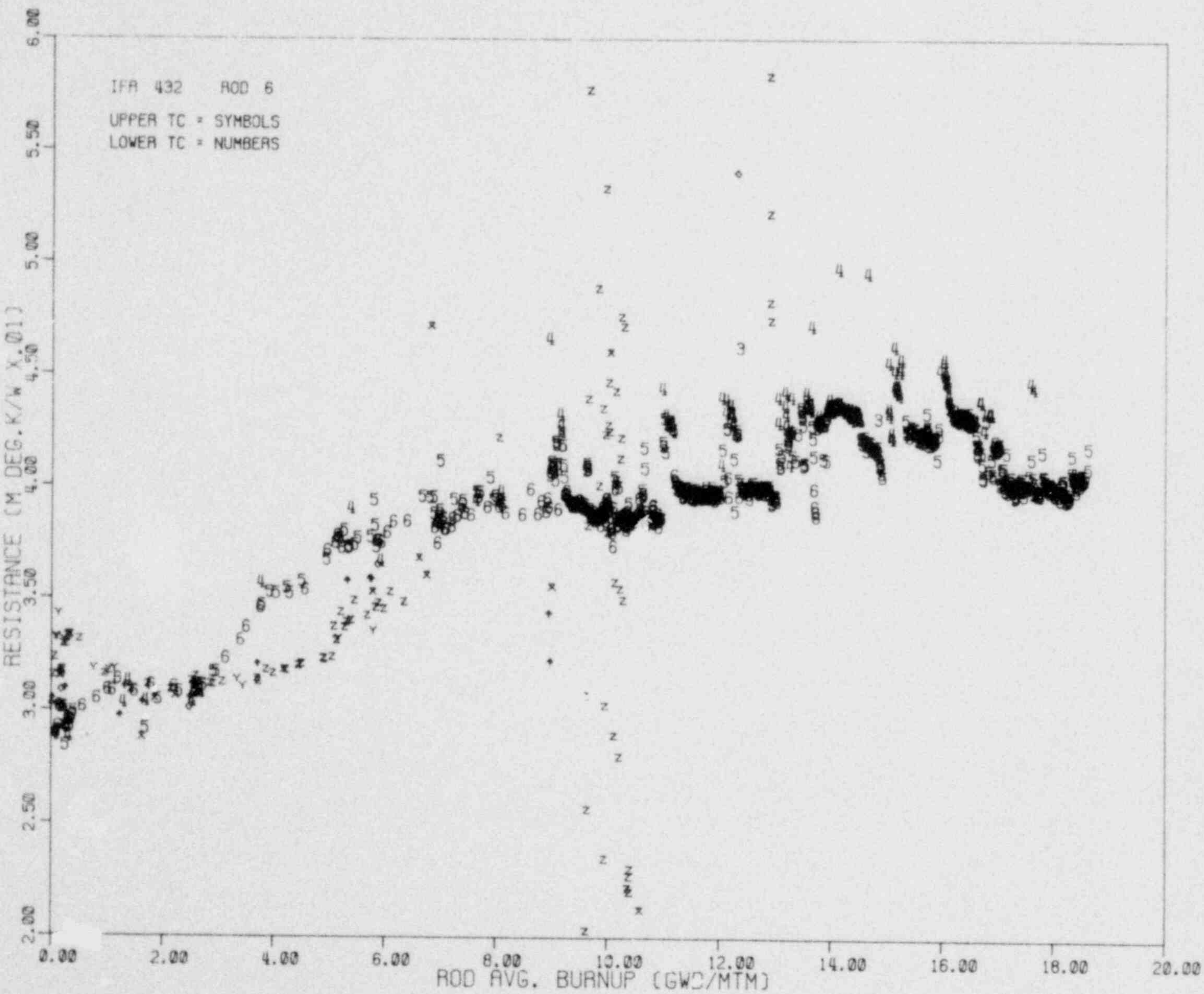

FIGURE B.12. Resistance History for Rod 6 of IFA-432

Comparing Figures A.2 (Appendix A) and B.1, it can be seen that the scatter of each band of data in Rod 1 IFA-431 is representative of the range of resistances to be expected at each thermocouple location over various power levels. Rod 1 is a typical BWR rod design. Note that the distance between each band of data is greater than the scatter within a band, and that the resistance at the lower themocouple location is greater than that at the upper thermocouple location. This implies that there was more pellet-cladding contact (PCI) at the upper end of the rod than at the lower. The rod seems to be slightly decoupled axially with respect to thermal data. The thermal behavior of the upper thermocouple region of the rod is apparently independent of the behavior at the lower thermocouple region.

This observation is based on the assumption that there exists adequate axial mixing of the fill gas within the rod, and is independent of the possibility of fission gas leaks through the thermocouple leads.[28] A lack of gas communication within the rods would have resulted in greater resistances at the upper thermocouple locations since this region ran at about 30% greater power than the lower ends of the rods. The local fission gas release would be higher in the higher temperature regions. All helium filled rods with open gaps (and fuel that performed as expected) experienced a greater increase in resistance at the lower thermocouple than at the upper.

Another question arises pertaining to any possible bias or error in the determination of local heat ratings. We believe these heat ratings have been properly quantified to reduce the uncertainty to approximately 5%.[29] These tests were designed to provide internal check points for this purpose in particular.[5] Analytical methods developed at PNL have shown the thermocouples to be operating properly.[30]

Figure B.2 shows the resistance history for Rod 1 of IFA-432. This rod exhibits a behavior similar to Rod 1 of IFA-431, except that the separation between bands of data becomes discernible at a greater burnup. A magnification of BOL data from this plot reveals that the resistance trends reverse direction more often than expected. The two bands of data begin complete separation at approximately 6 GWd/MTM and the same trend develops as in Rod 1 IFA-431, indicating that fuel-cladding contact is greater at the upper portion of the rod than at the lower. Notice that for the lower thermocouple the pattern of numbers on the plot indicate that resistance decreases with increasing power. This is the signature of a "gap-dominated" rod, where the "gap" is open and the fill gas has been degraded by fission product release. The upper thermocouple for Rod 1 of IFA-432 failed at approximately 8.5 GWd/MTM rod average burnup.

The large gap design Rod 2 of IFA-431 (Figure B.3) experienced a trend similar to Rod 1. Note that the separation of the data bands is greater for the larger gap rod. Rod 2 of IFA-432 is shown in Figure B.4. The upper portion of this rod contained an ultrasonic thermometer which failed at startup, consequently yielding no useful data. The lower themocouple resistance curve reflects the fission gas release from this large design gap, higher temperature rod. Gap dominated resistances are seen to develop with increasing burnup.

Figure B.5 shows the results for Rod 3 of IFA-431. In this case, the fuel and cladding were in firm contact very early in life due to the small initial cold gap. The state of the gap was the same at both upper and lower thermocouple locations. Since for a closed gap (fuel dominated resistance) the resistance rises with power, the resistance at the higher power upper thermocouple is greater than that at the lower. However, both bands of data rise slightly with burnup, reflecting fission gas release. Figure B.6 shows the small gap Rod 3 of IFA-432, which exhibits behavior very similar to Rod 3 of IFA-431, where the whole fuel column was in contact with the cladding from BOL.

Figure B.7 shows the history of Rod 4 of IFA-431, which was backfilled with xenon.[11] In this case, fission gas release cannot degrade the fill gas thermal conductivity. The decrease in resistance with burnup is a clear indication of increasing fuel-cladding contact. Gap domination of the total resistance is evident, and was expected for a fill gas of such low conductivity. Rod 4 of IFA-432 is shown in Figure B.8 and exhibits behavior similar to Rod 4 of IFA-431. Because of the high fuel temperatures experienced by this rod, the thermocouples failed relatively early in life, and the rod was removed from the assembly at the end of the first reactor testing cycle. It was replaced with a non-instrumented rod of Rod 1 design.

Rod 5 of IFA-431 is shown in Figure B.9. This rod contained fuel pellets that were 92% TD and stable with respect to in-reactor densification (Table 1). However, a review of pre-irradiation characterization data[5] has shown that this fuel was susceptable to thermally induced microcracking. This microcracking caused the fuel to expand and contact the cladding early in life, producing a fuel dominated total resistance. This is evident from the rise in resistance with power seen for this rod.

Rod 5 of IFA-432 is shown in Figure B.10. Its fuel was manufactured from the same material as Rod 5 of IFA-431. Although the resolution of Figure B.10 is not enough to demonstrate it, microcracking probably also occurred here,[5] and the total resistance was fuel-dominated at BOL. However, fission gas release caused the resistance at the lower thermocouple to become gap dominated after about 8 GWd/MTM. The upper thermocouple in this rod failed at approximately 5.2 GWd/MTM.

The history of Rod 6 of IFA-431 is shown in Figure B.11. This rod contained 92% TD fuel that was unstable with respect to in-reactor densification. Post-irradiation examination (PIE)[24] performed on this rod at Harwell, UK, shows that this fuel did indeed densify. However, there was also a larger than expected amount of fuel-cladding contact. This can be seen in Figure B.11 as a generally decreasing resistance that becomes increasingly fuel dominated with burnup. Rod 6 of IFA-432 was also fuel dominated at BOL.

Figure B.12 shows the resistance history for Rod 6 of IFA-432. The upper thermocouple of this rod failed at about 6.8 GWd/MTM. Although this rod had the same fuel as Rod 6 of IFA-431, a gap dominated resistance has developed with increasing burnup, indicating that PCI was not as extensive. Also, more fission gases were released due to the higher burnup and temperature.

It is evident from the foregoing discussion that a variety of results may be obtained from dimensionally similar rods. Rods with lower density fuel, densifying fuel or large initial free volume (gap) may exhibit more randomness than do the standard design BWR rods. These figures show in general that the rate of gap closure (increasing solid conductance) is faster than the rate of fission gas release for the first few GWd/MTM. Subsequently the rates reverse relative magnitudes and the total resistance tends to increase with burnup. The total free volume (initial gap size) affects the fuel temperatures, and thus apparently influences when this rate reversal occurs. Two consistencies are to be noted in this data. The first is the sharp rise in resistance at beginning of life, which is accompanied by cladding elongations that are greater than for subsequent cycles (see Figures B.13, B.14 and B.15 and Reference 4). The second is the tendency for the resistance to be greater for the lower power region than for the higher power region for rods of typical BWR design.

OBSERVATIONS FROM IFA-513

Resistance versus power plots for Rod 1 of IFA-513 are shown in Figures B.16 through B.19. The sections of the curves below about 10 kW/m should be disregarded. Although the powers have been corrected for asymmetries in the flux profile (radial tilt and axial shape) and for the response lag of the vanadium neutron detectors, there is evidently an effect at low powers due to some unknown factor. This effect has not been accounted for in these plots.

A slight rise in resistance magnitude and slope develops between ramps 1 and 2 for Rod 1. The increase in slope is an indication that the rod resistance has become more fuel dominated. The difference in magnitude between the lower and upper resistances at the same power level is apparently due to some path dependency, i.e., rate of thermal expansion or cracking rate.

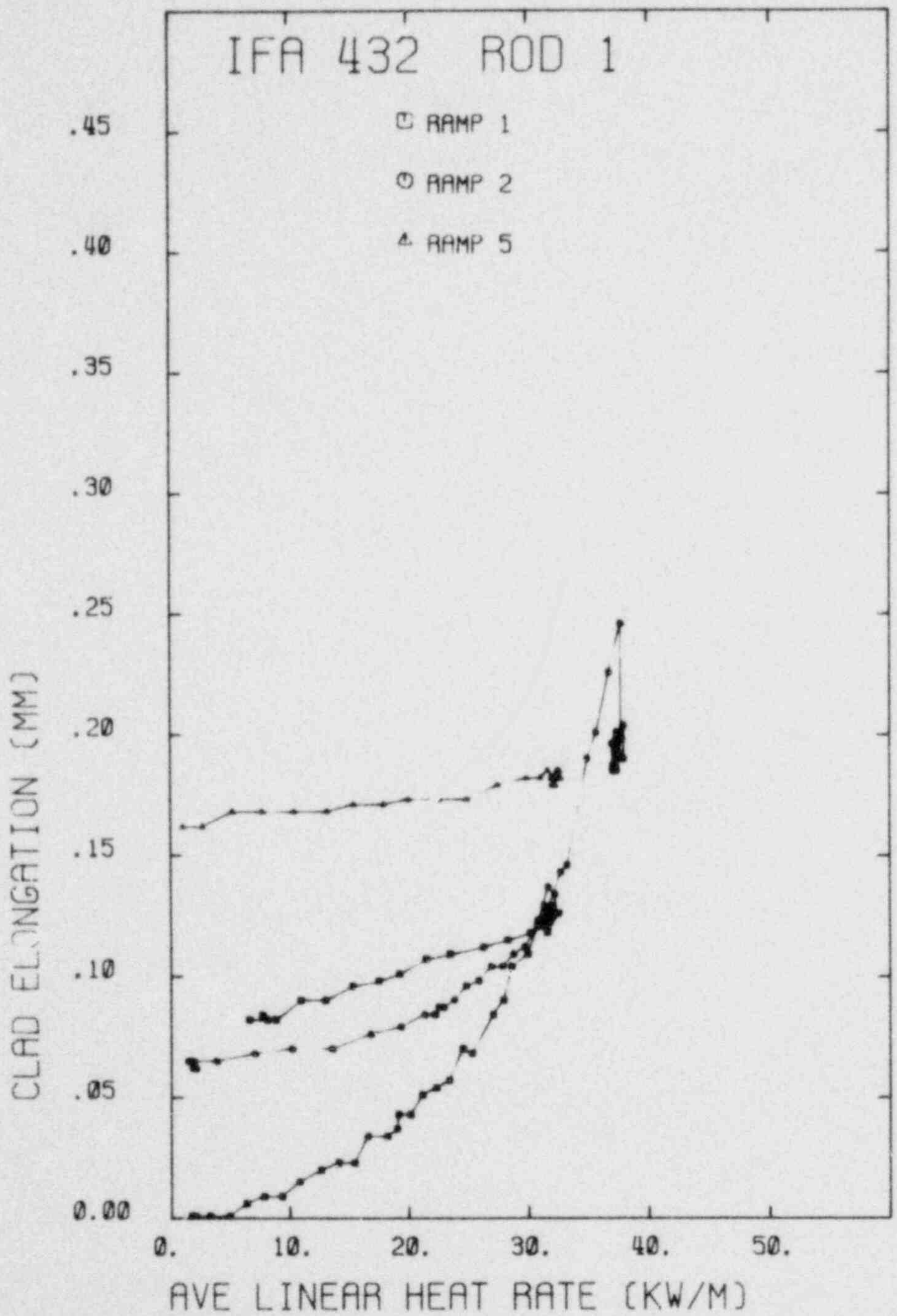

FIGURE B.13. Cladding Elongation for Rod 1 IFA-432

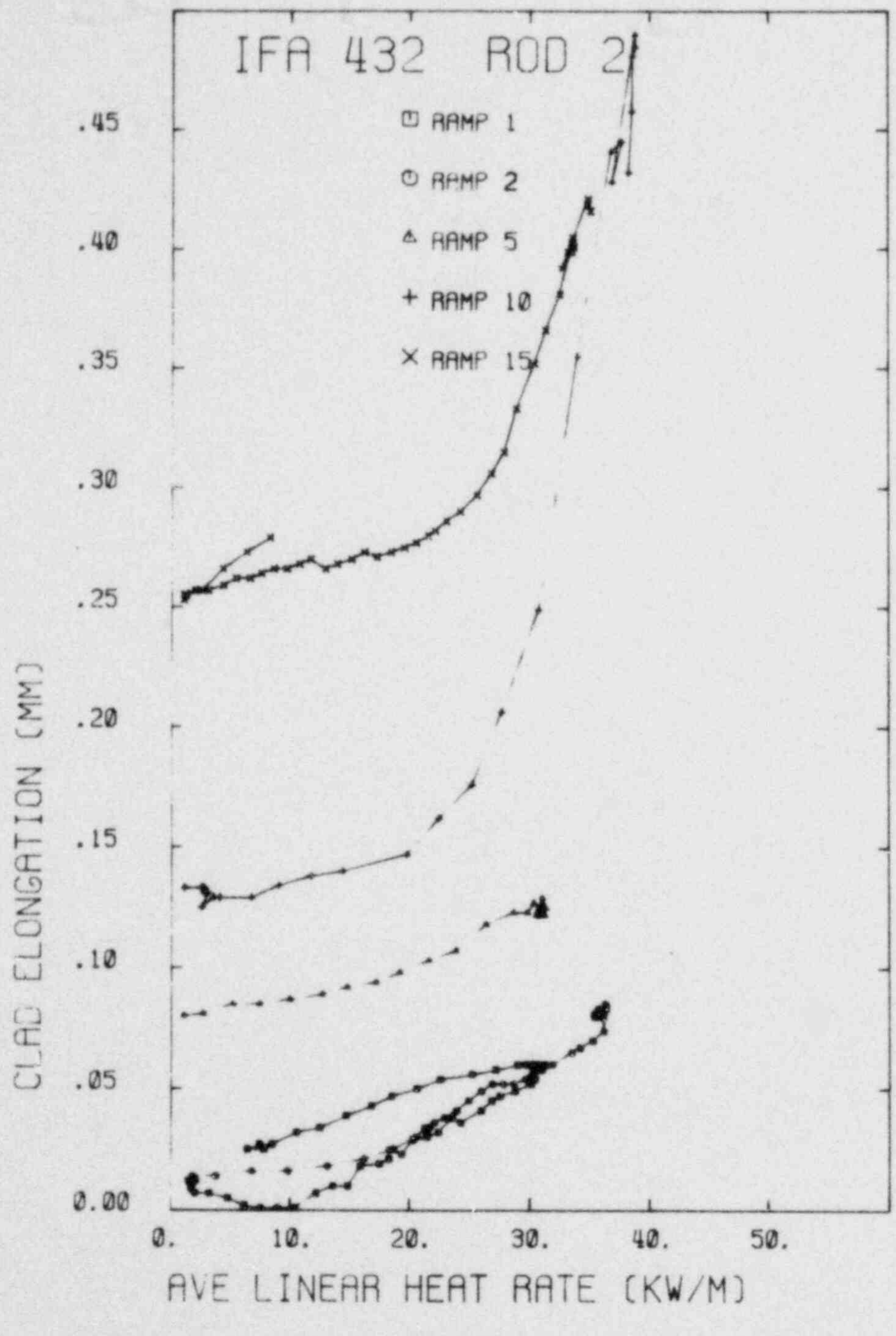

FIGURE B.14. Cladding Elongation for Rod 2 IFA-432

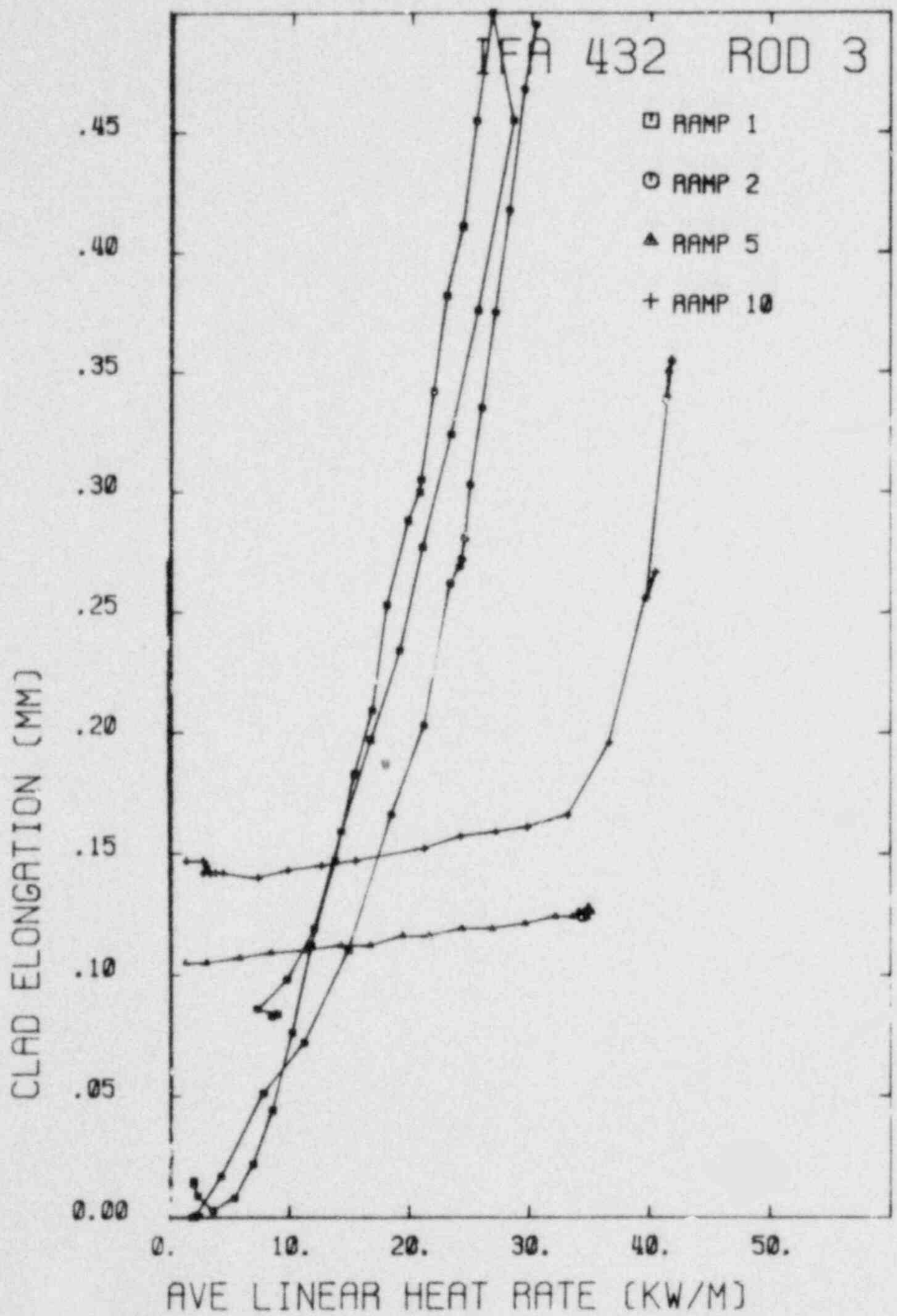

FIGURE B.15. Cladding Elongation for Rod 3 IFA-432

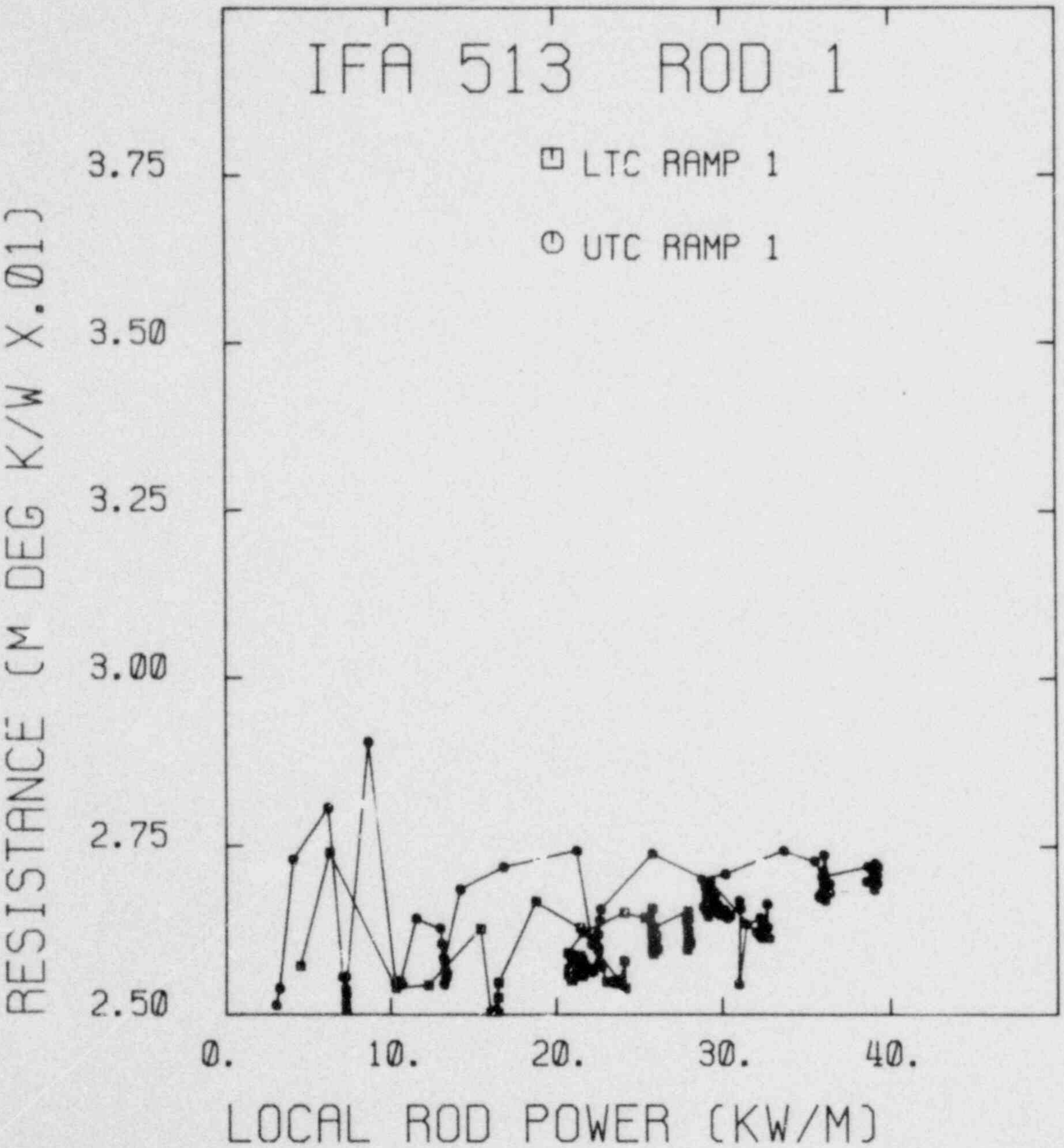

FIGURE B.16. Resistance for Rod 1 IFA-513 - Ramp 1

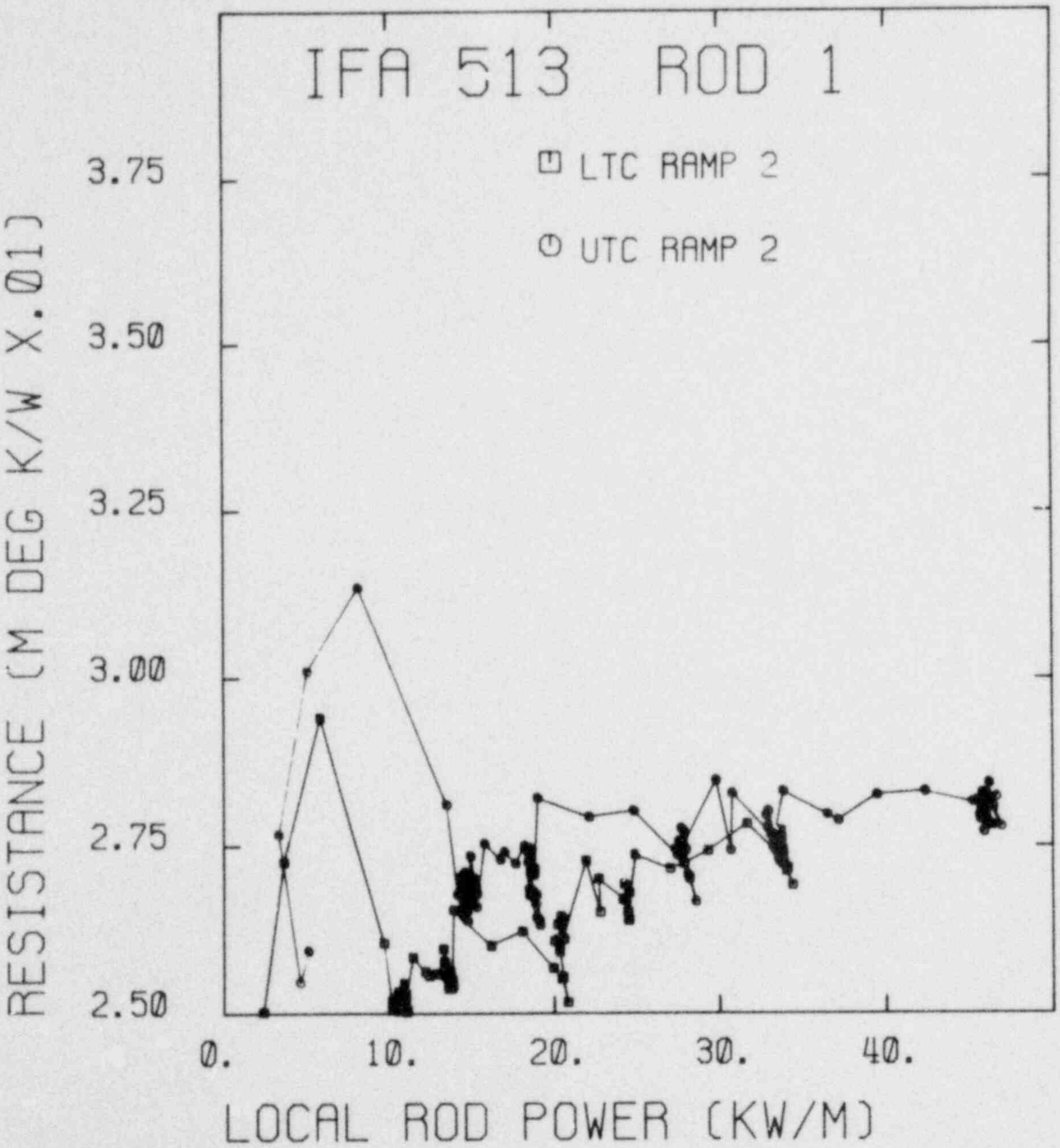

FIGURE B.17. Resistance for Rod 1 IFA-513 - Ramp 2

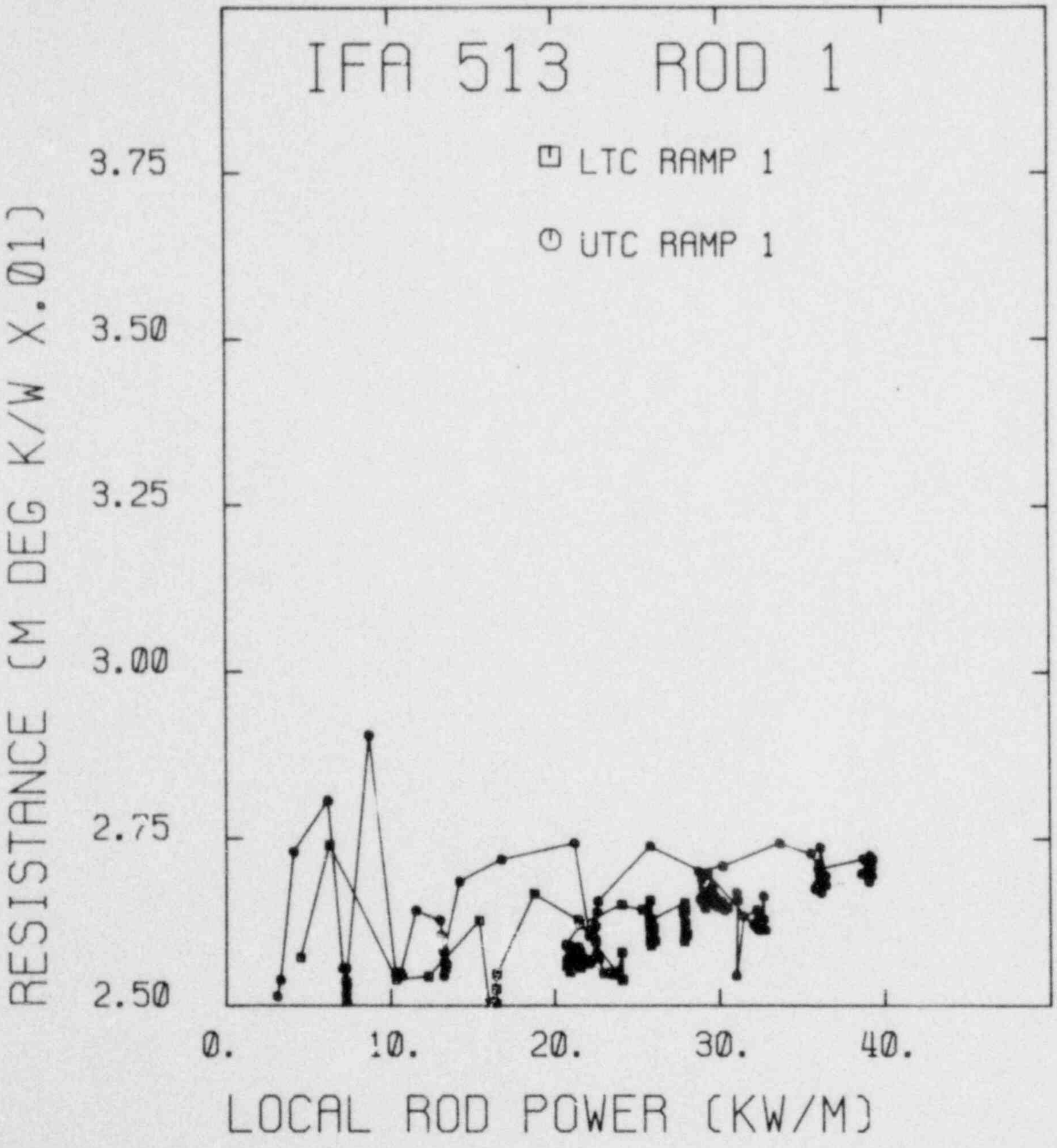

FIGURE B.16. Resistance for Rod 1 IFA-513 - Ramp 1

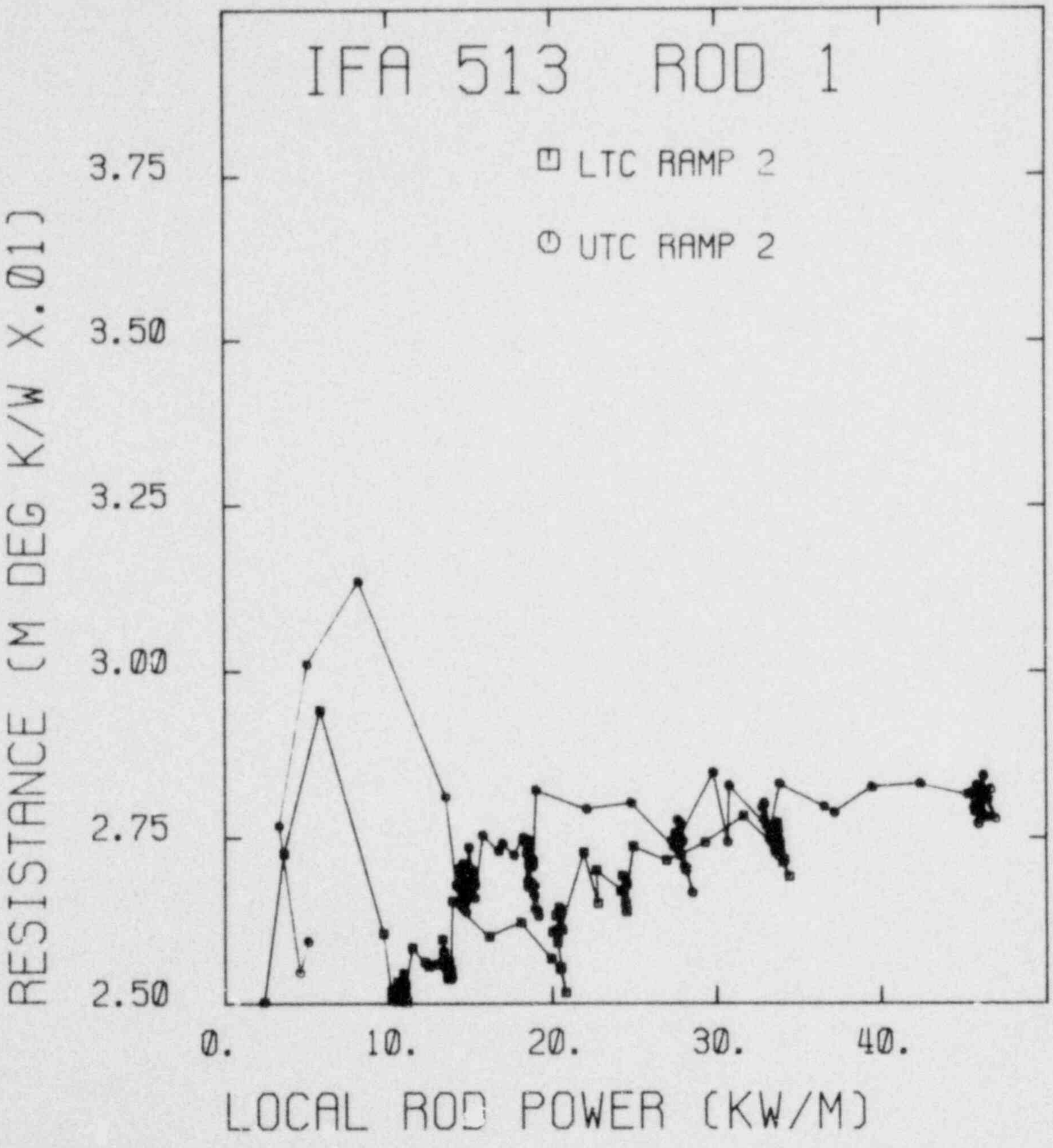

FIGURE B.17. Resistance for Rod 1 IFA-513 - Ramp 2

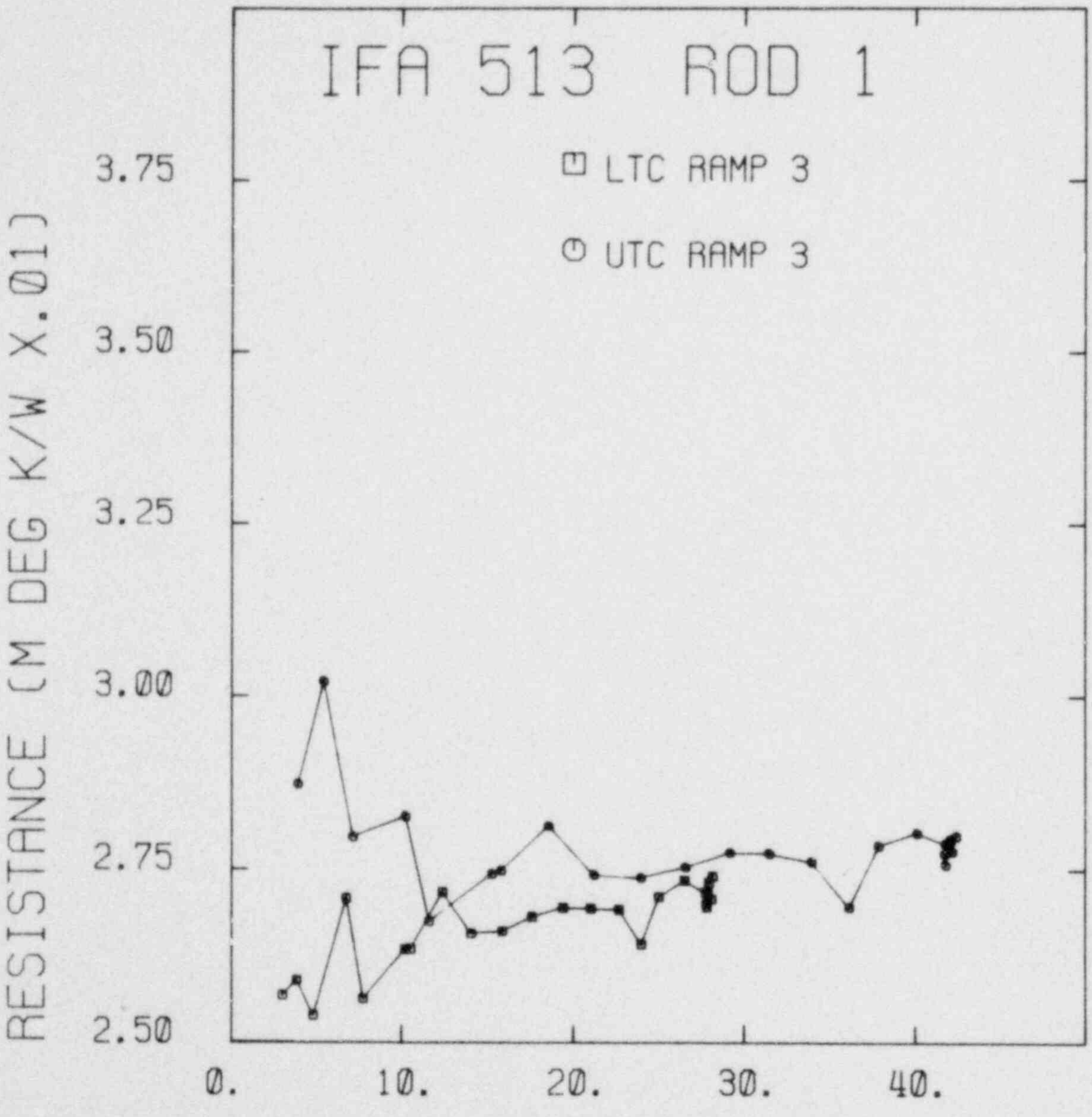

FIGURE B.18. Resistance for Rod 1 IFA-513 - Ramp 3

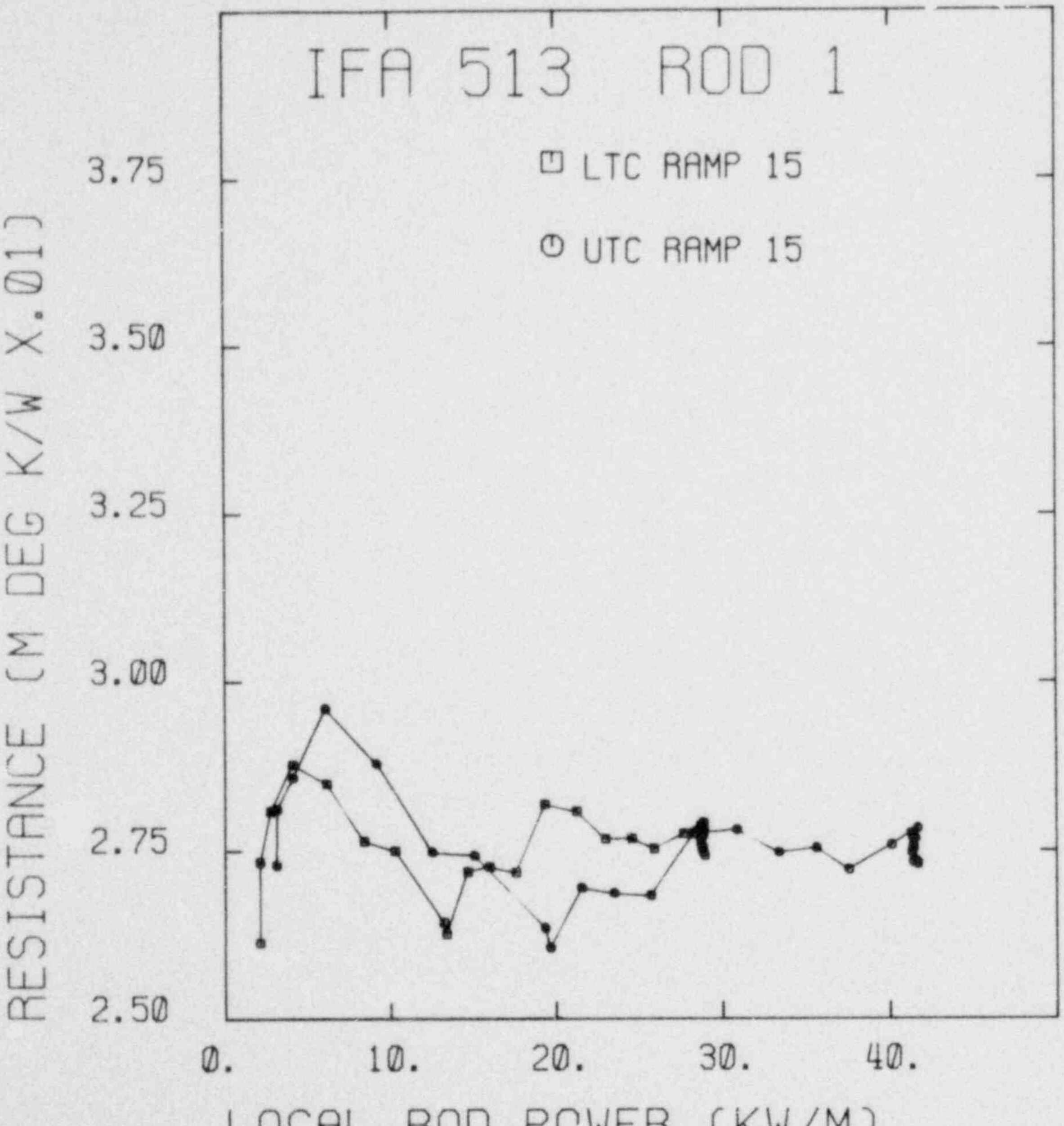

FIGURE B.19. Resistance for Rod 1 IFA-513 - Ramp 15

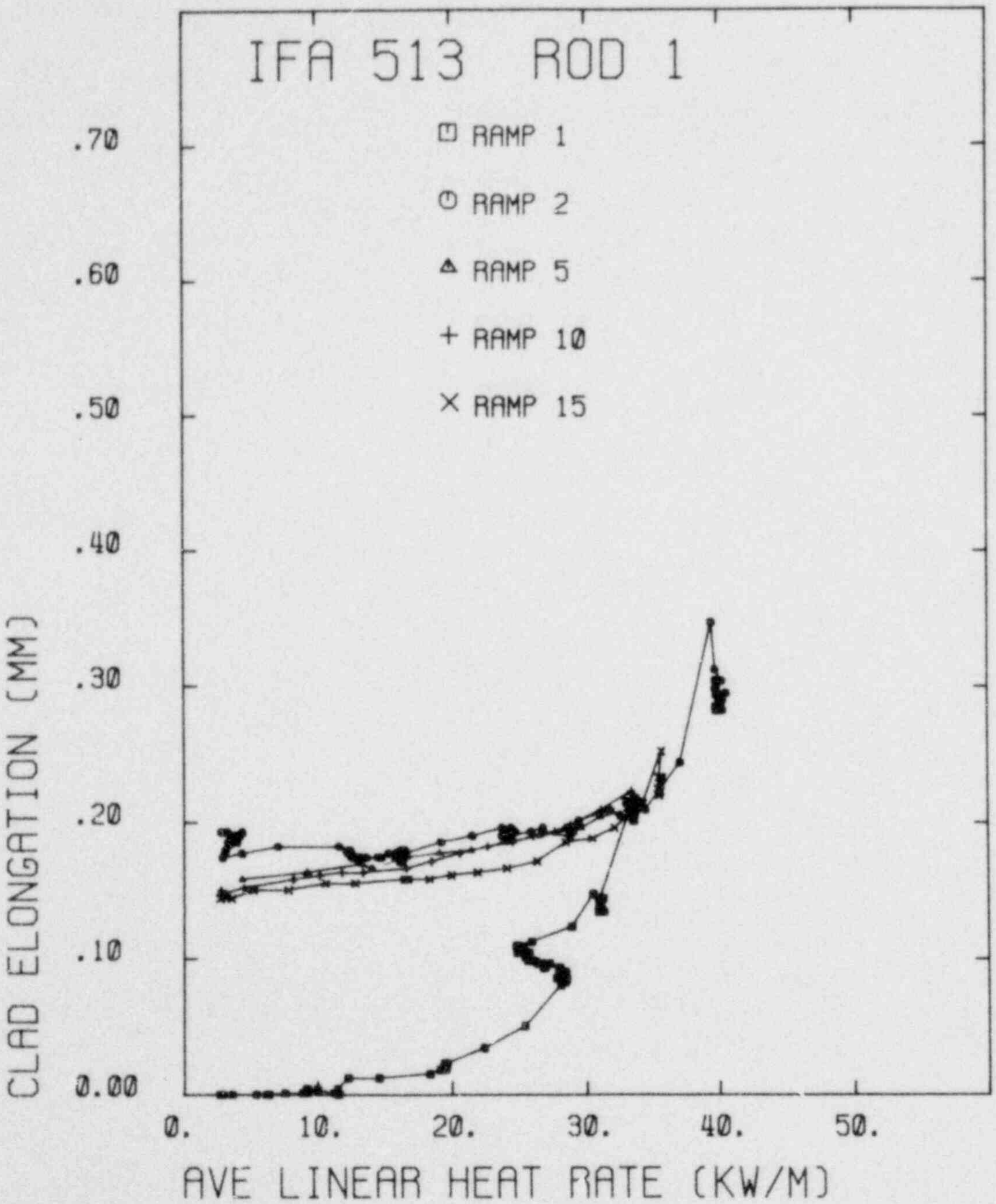

FIGURE B.20. Cladding Elongation for Rod 1 IFA-513

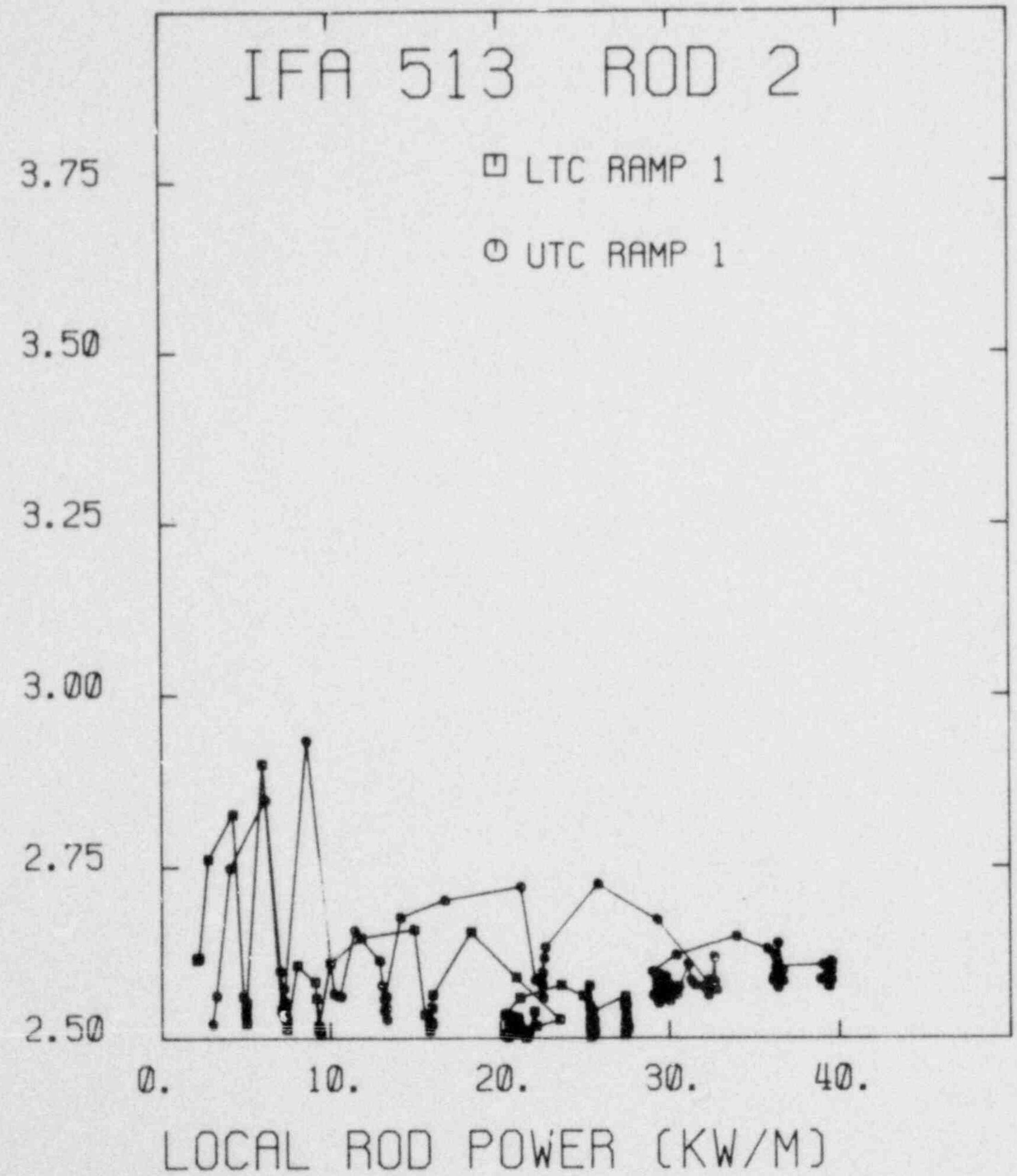

FIGURE B.21. Resistance for Rod 2 IFA-513 - Ramp 1

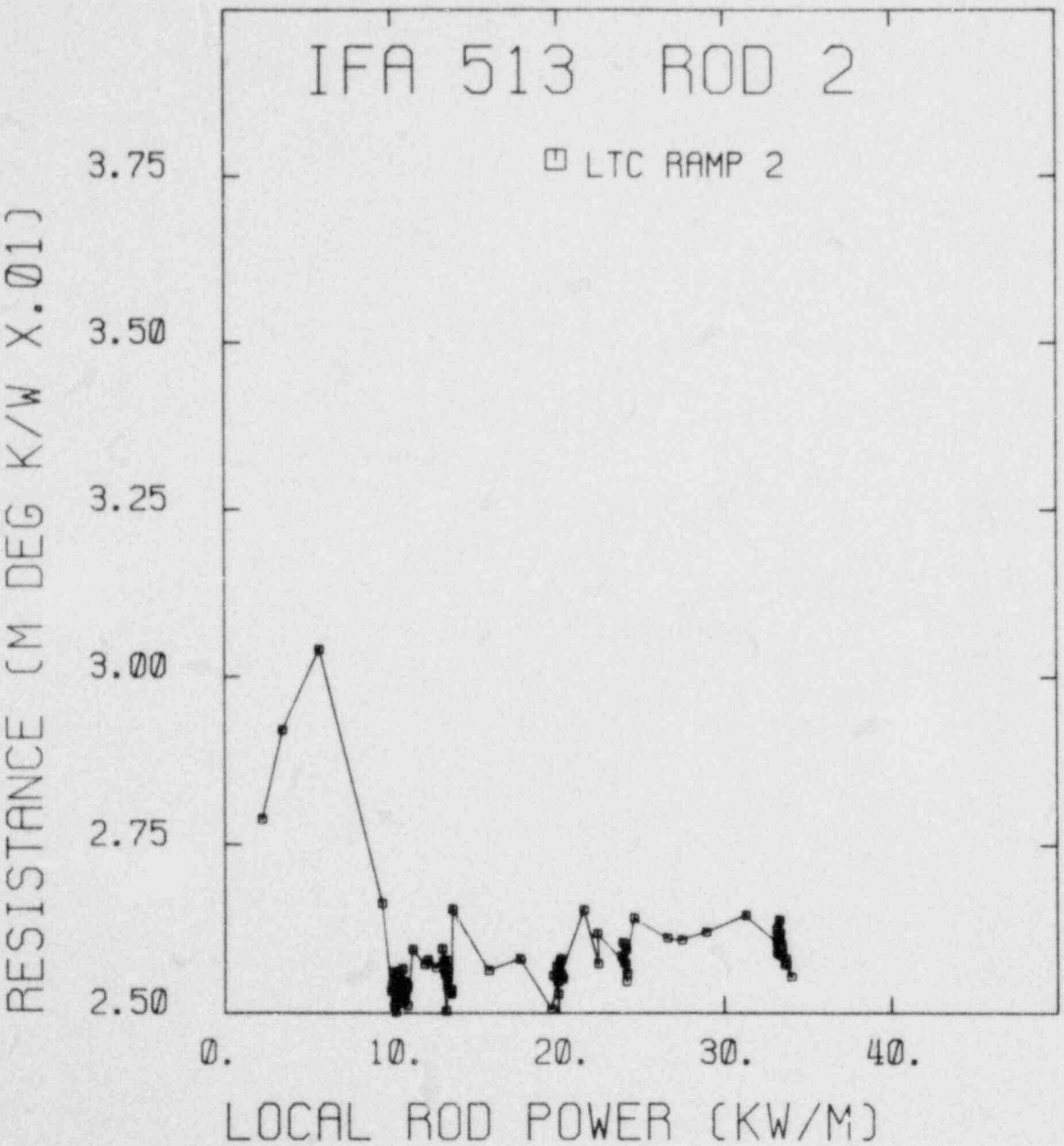

FIGURE B.22. Resistance for Rod 2 IFA-513 - Ramp 2

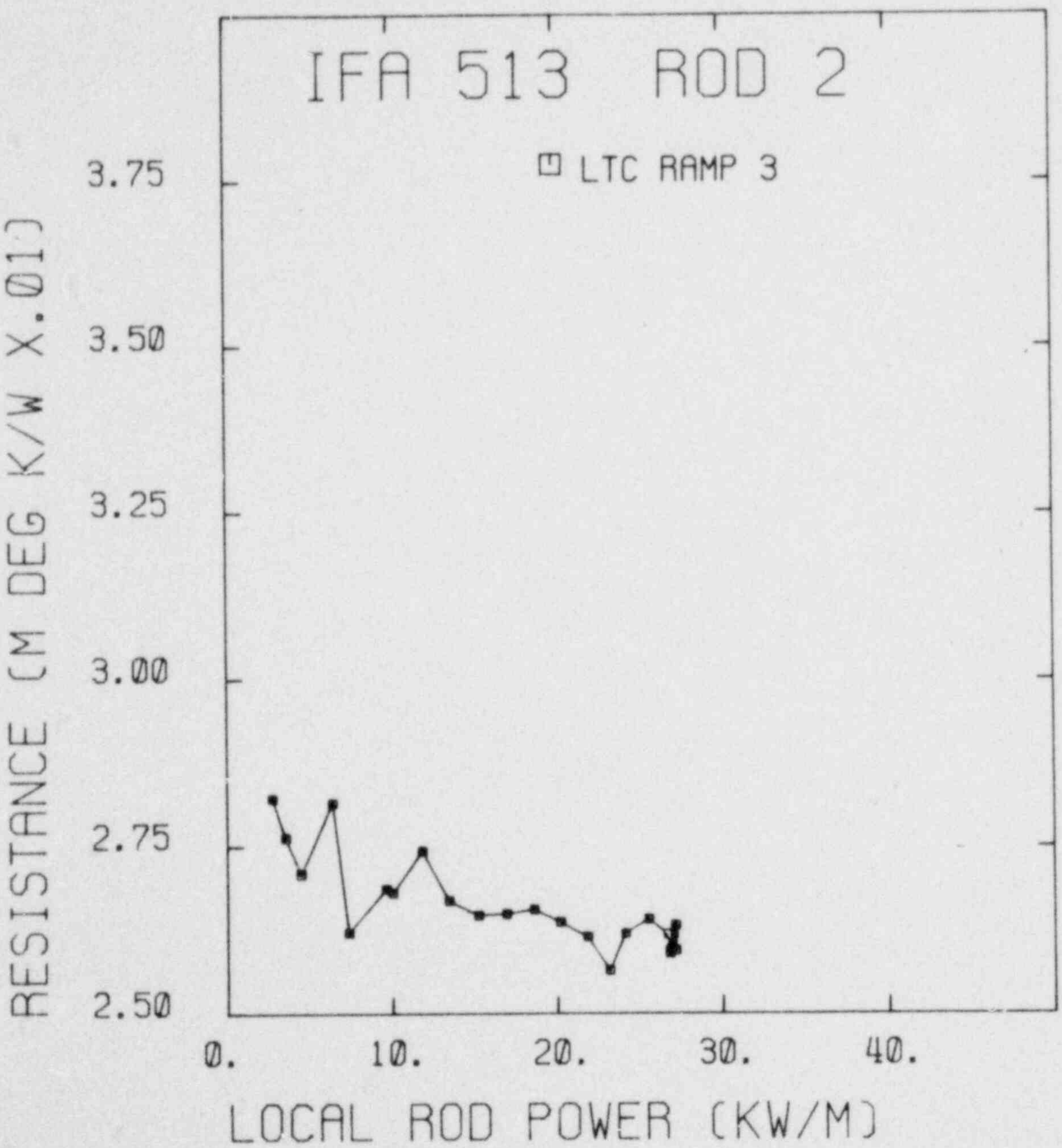

FIGURE B.23 Resistance for Rod 2 IFA-513 - Ramp 3

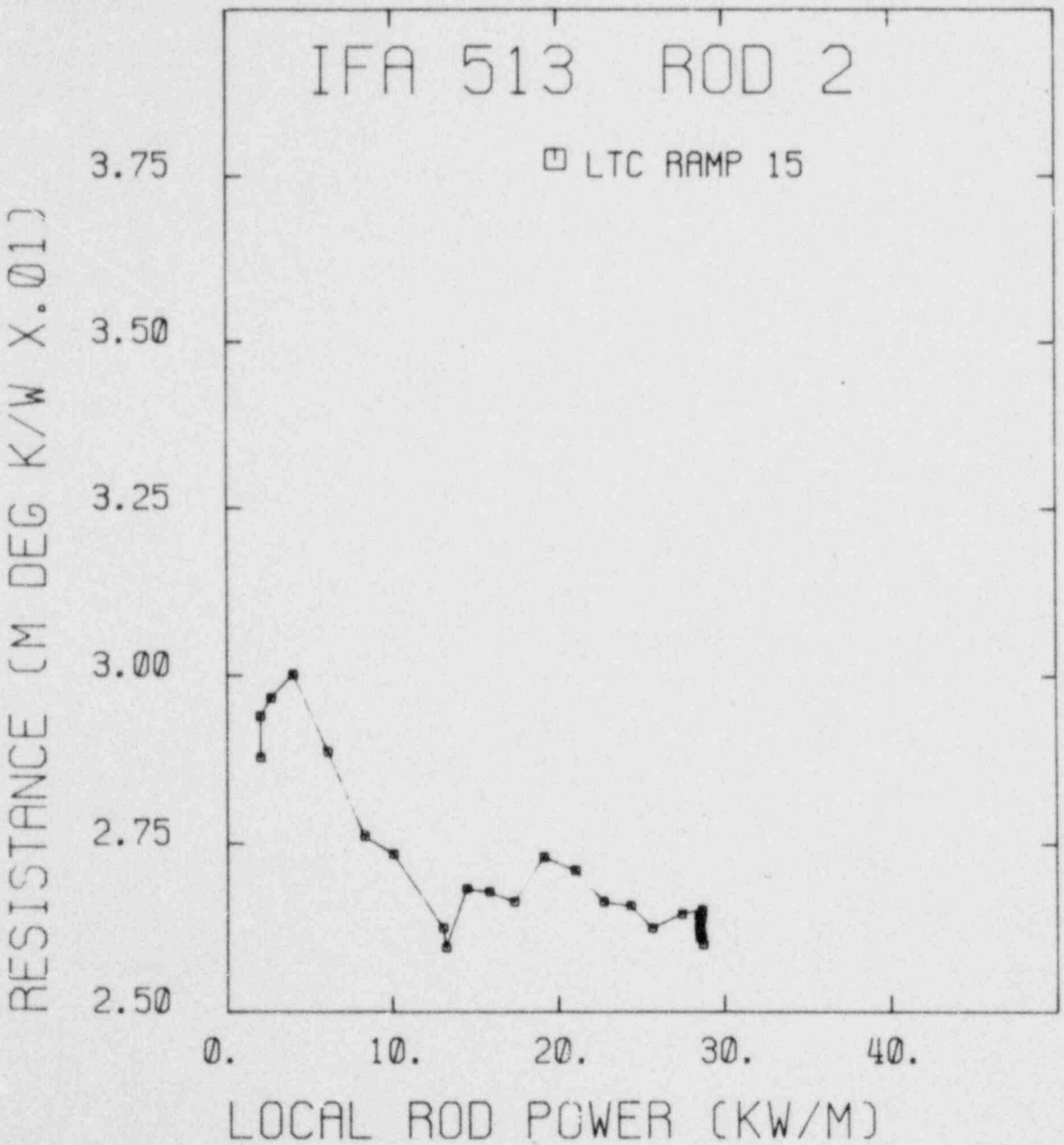

FIGURE B.24. Resistance for Rod 2 IFA-513 - Ramp 15

The cladding elongation sensor history for Rod 2 of IFA-513 is shown in Figure B.25. The characteristics of these curves are almost replicates of those for Rod 1. Also note that the power level to initiate PCI has increased from ramp 1 to ramp 2. It would appear that the fuel has become less rigid, i.e., that the effective elastic modulus has decreased. As in Rod 1, there is also a slight decrease in the permanent offset at zero power with increasing ramp number. This is an indication that the rod is undergoing a relaxation process of some type.

Resistance versus power plots and cladding elongation response for Rod 3 of IFA-513 are shown in Figures B.26 through B.30. This rod's response is very similar to Rod 2, except that the magnitude of cladding elongation response is slightly less. Comparison of cladding elongation responses between Rods 1 and 3 reveals a close resemblance that reflects the identical rod design (see Table 1).

Rod 4 of IFA-513 was backfilled with 8% xenon, 92% helium in order to reduce the gas thermal conductivity to 75% of that for pure helium. Accordingly, the resistance versus power plots (Figures B.31 through B.34) reflect this design parameter's influence. The upper thermocouple location has greater resistance than the lower at the same power level. This once again illustrates that the rod may be relatively decoupled thermally in the axial direction. The previously mentioned rate of thermal expansion or rate of fuel cracking may also contribute to this result.

Successive ramps show the resistances becoming increasingly fuel dominated due to fuel relocation. In this case, the resistances of the two thermocouple locations seem to be approaching a common behavior pattern. Unfortunately, the cladding elongation sensor for this rod has apparently failed, as shown in Figure B.35.

Rod 5 of IFA-513 was identical in design to Rod 1. Its response was also nearly identical, as shown in Figures B.36 through B.40. This is an example of the repeatability of rods of common design.

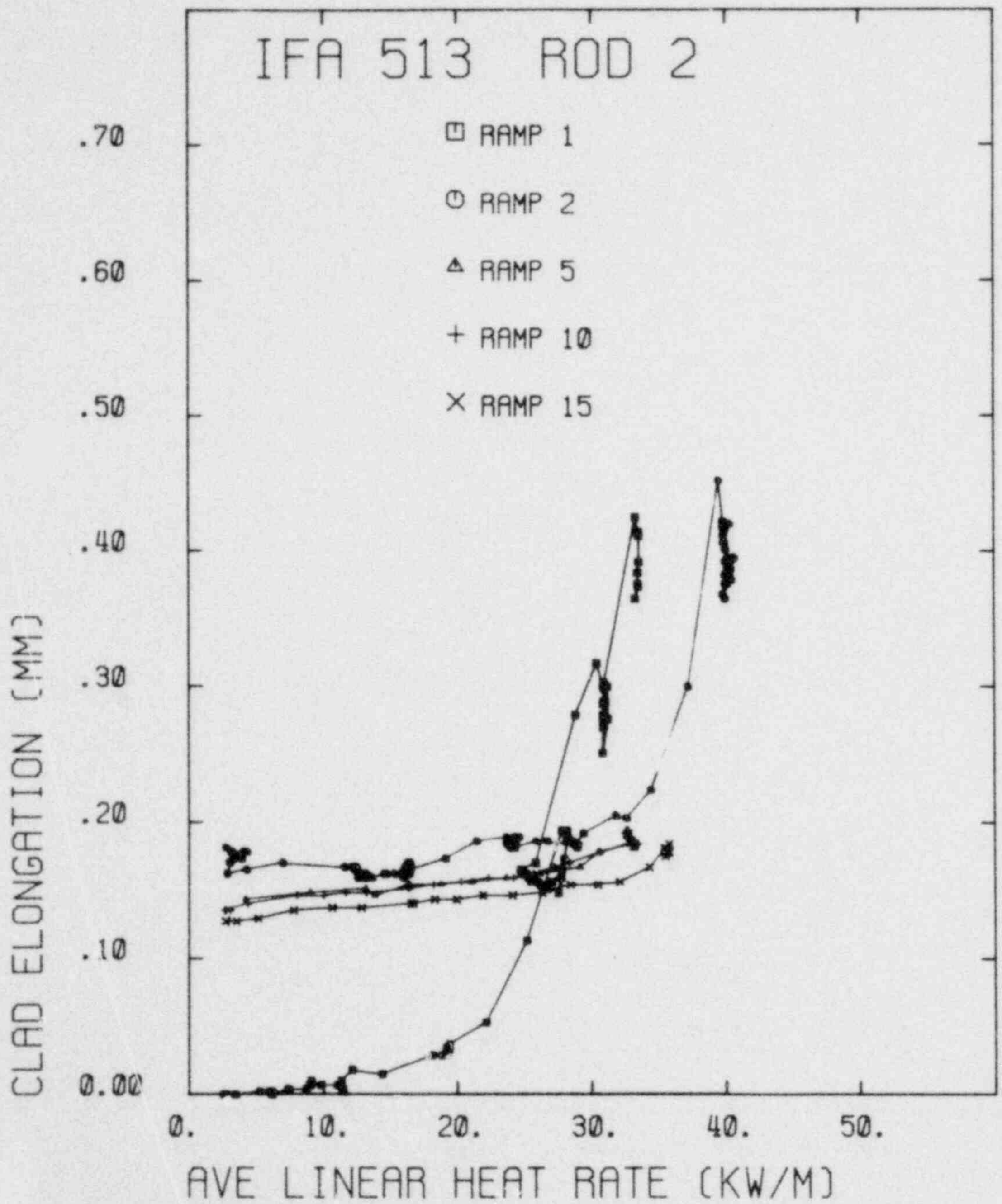

FIGURE B.25. Cladding Elongation for Rod 2 IFA-513

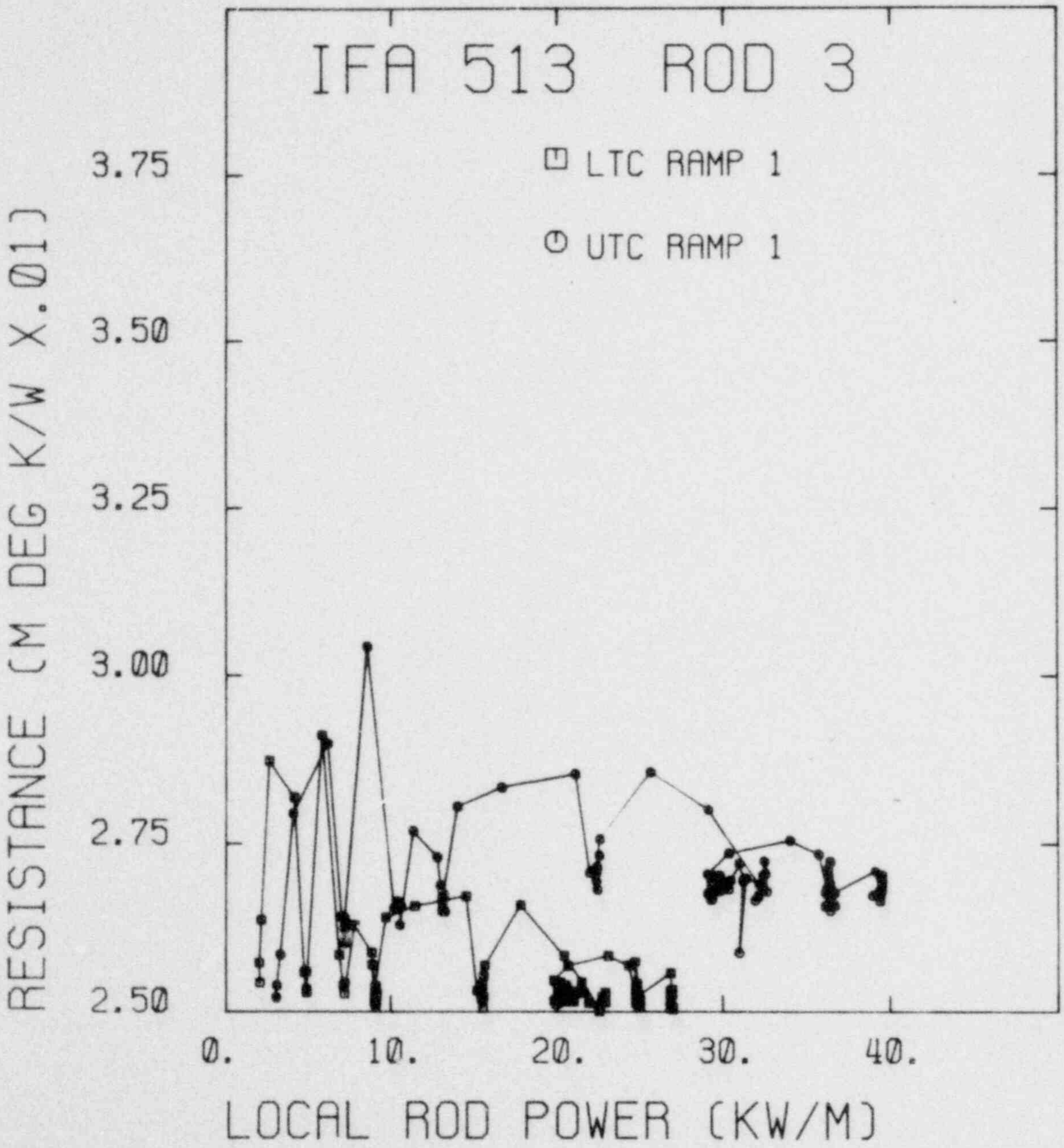

FIGURE B.26. Resistance for Rod 3 IFA-513 - Ramp 1

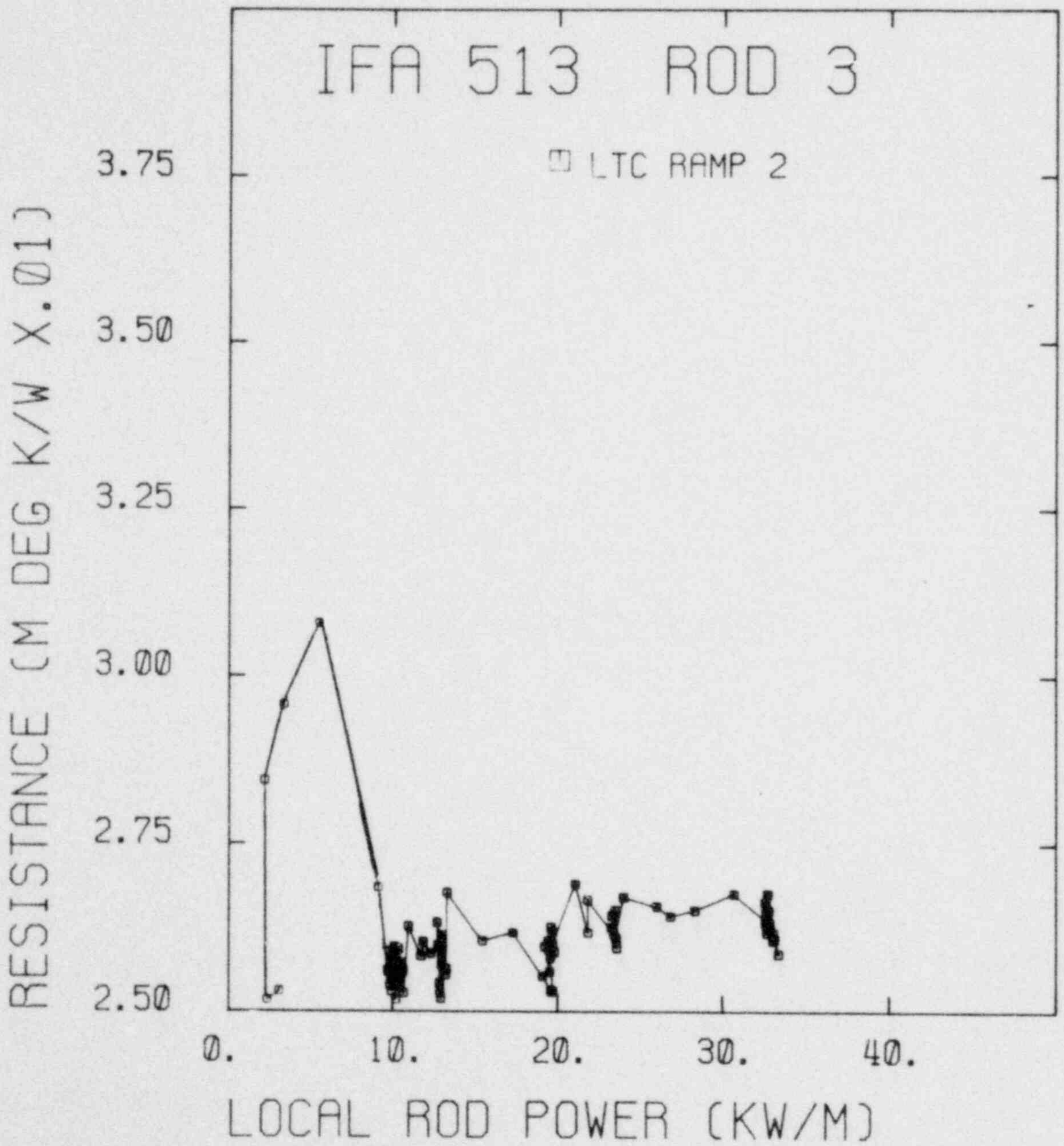

FIGURE B.27. Resistance for Rod 3 IFA-513 - Ramp 2

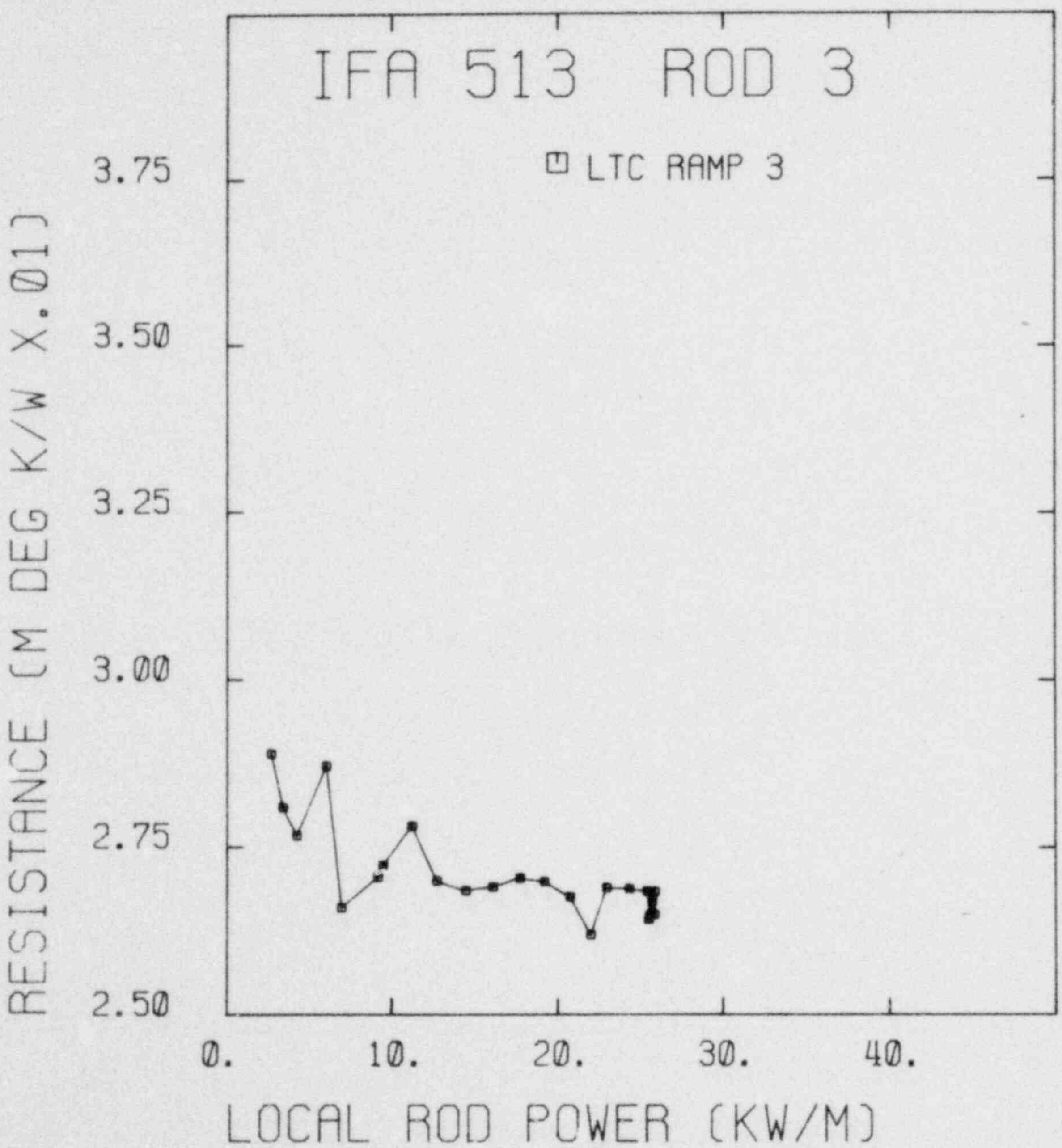

FIGURE B.28. Resistance for Rod 3 IFA-513 - Ramp 3

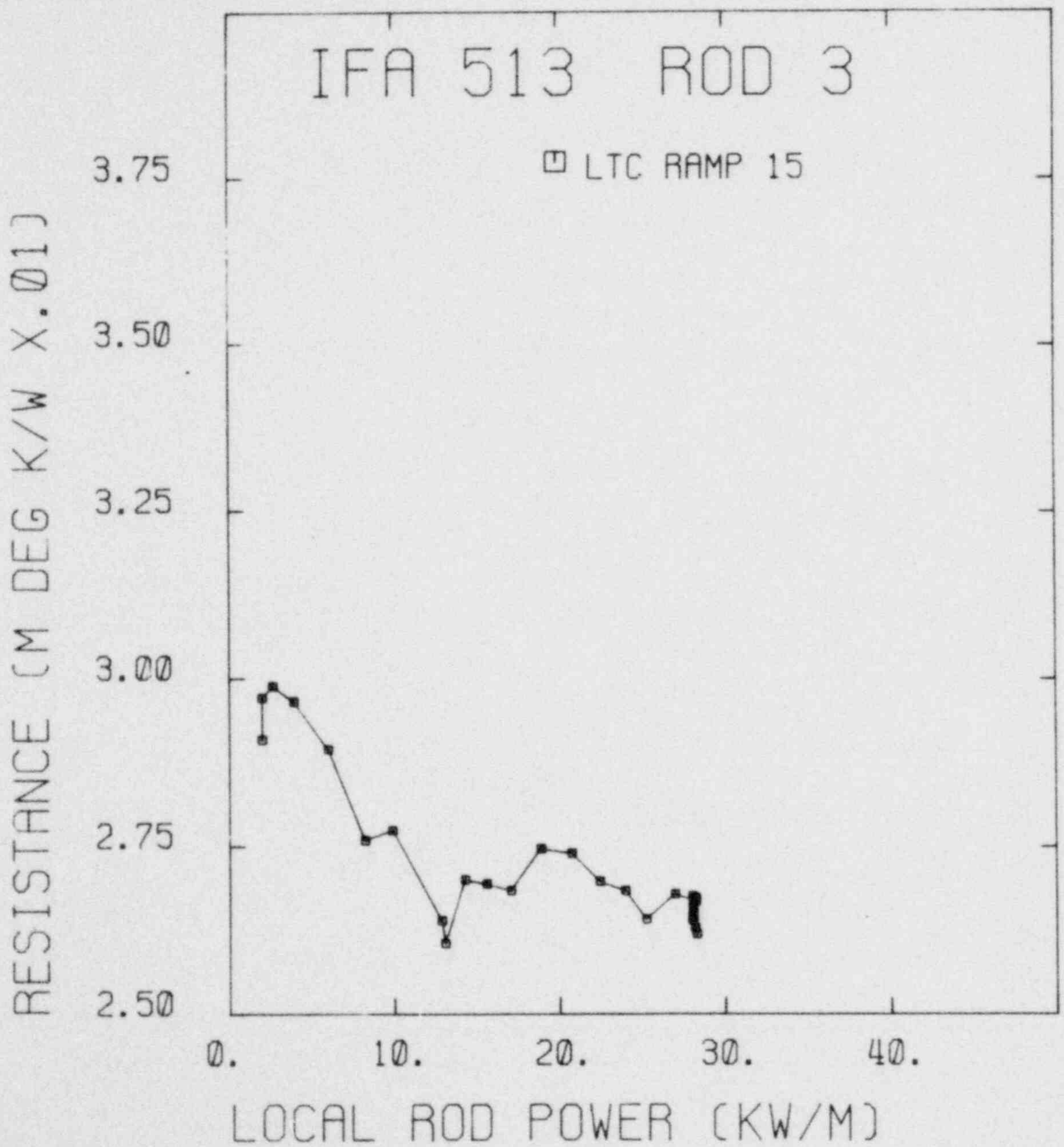

FIGURE B.29. Resistance for Rod 3 IFA-513 - Ramp 15

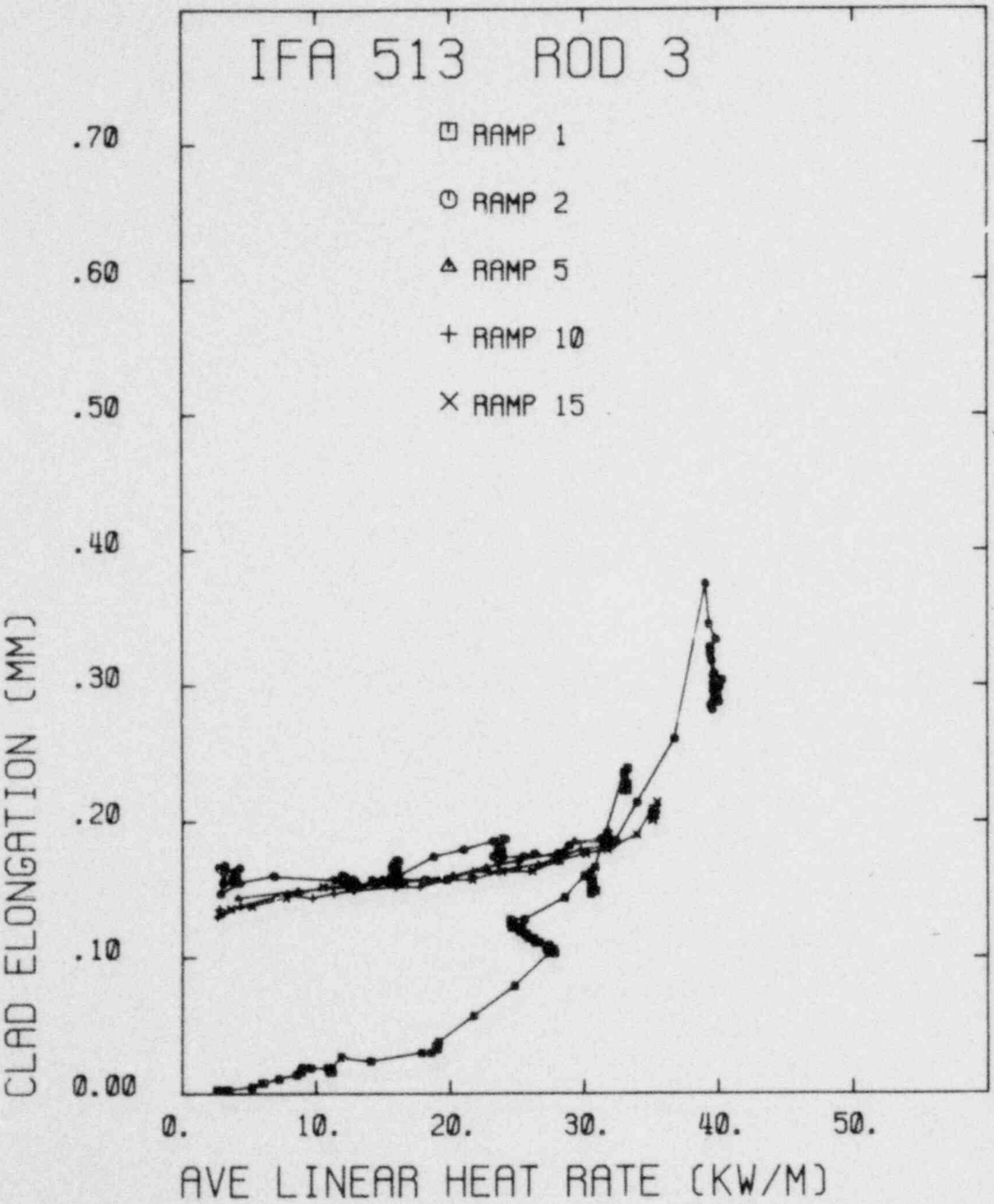

FIGURE B.30. Cladding Elongation for Rod 3 IFA-513

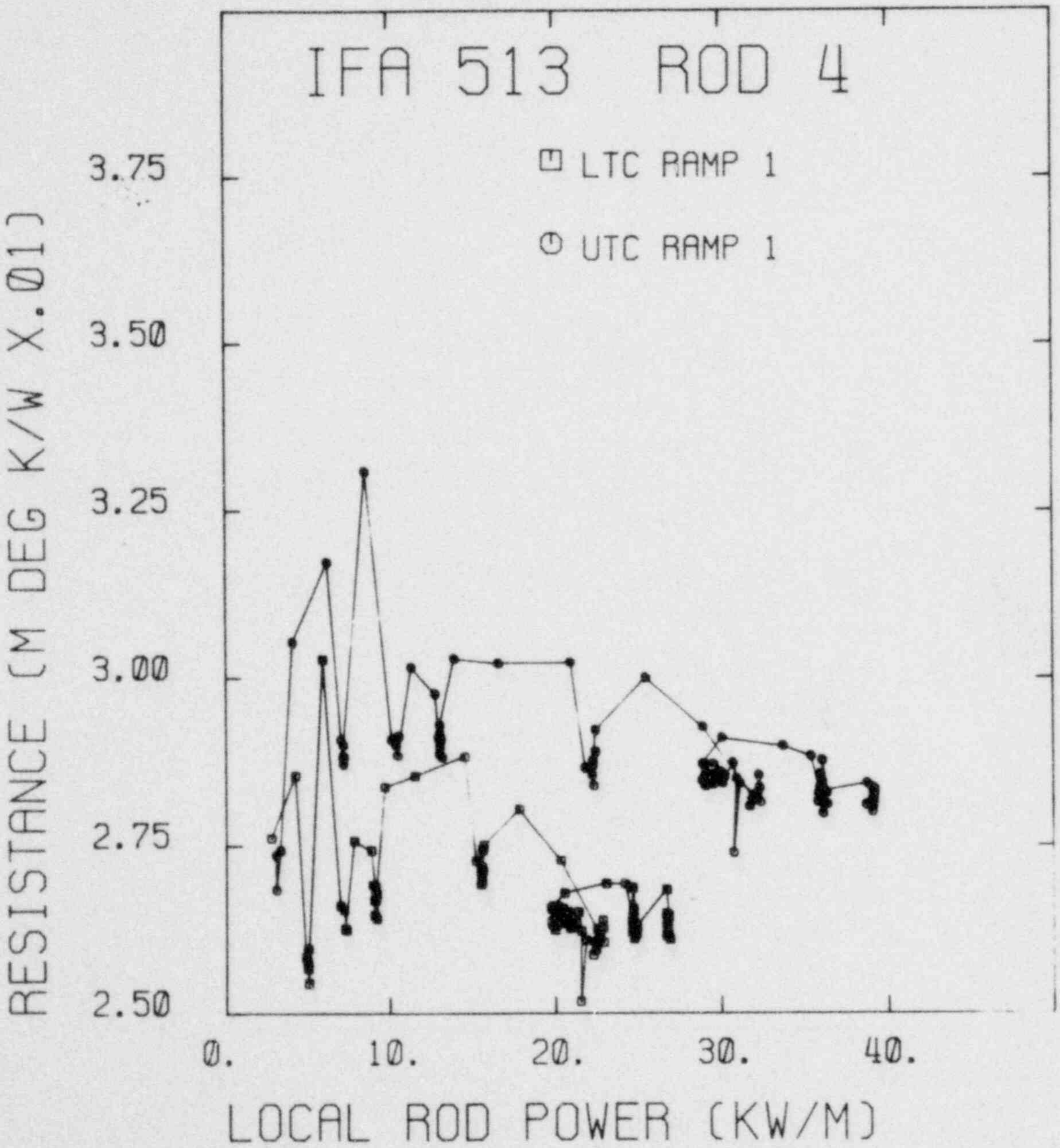

FIGURE B.31. Resistance for Rod 4 IFA-513 - Ramp 1

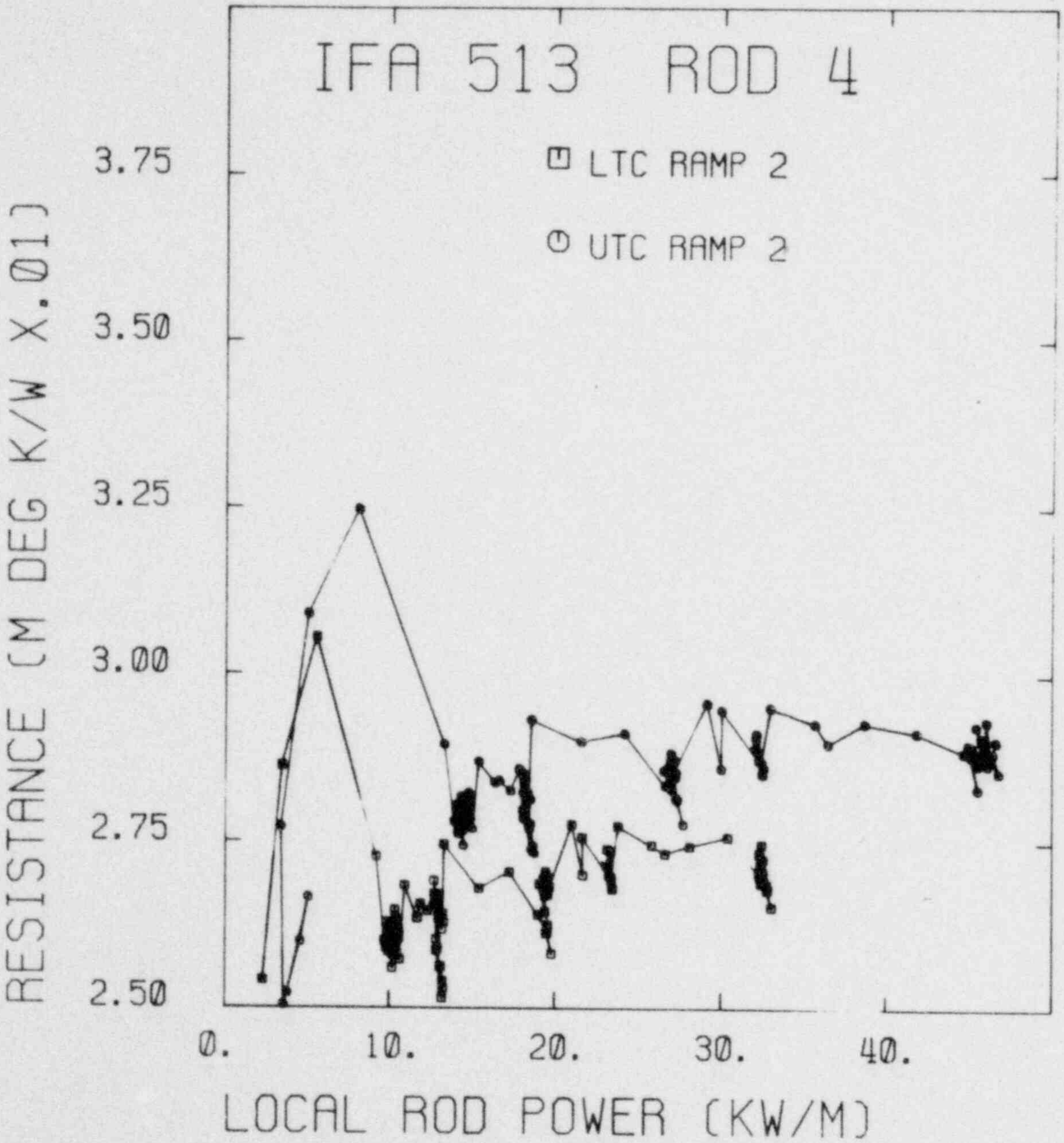

FIGURE B.32. Resistance for Rod 4 IFA-513 - Ramp 2

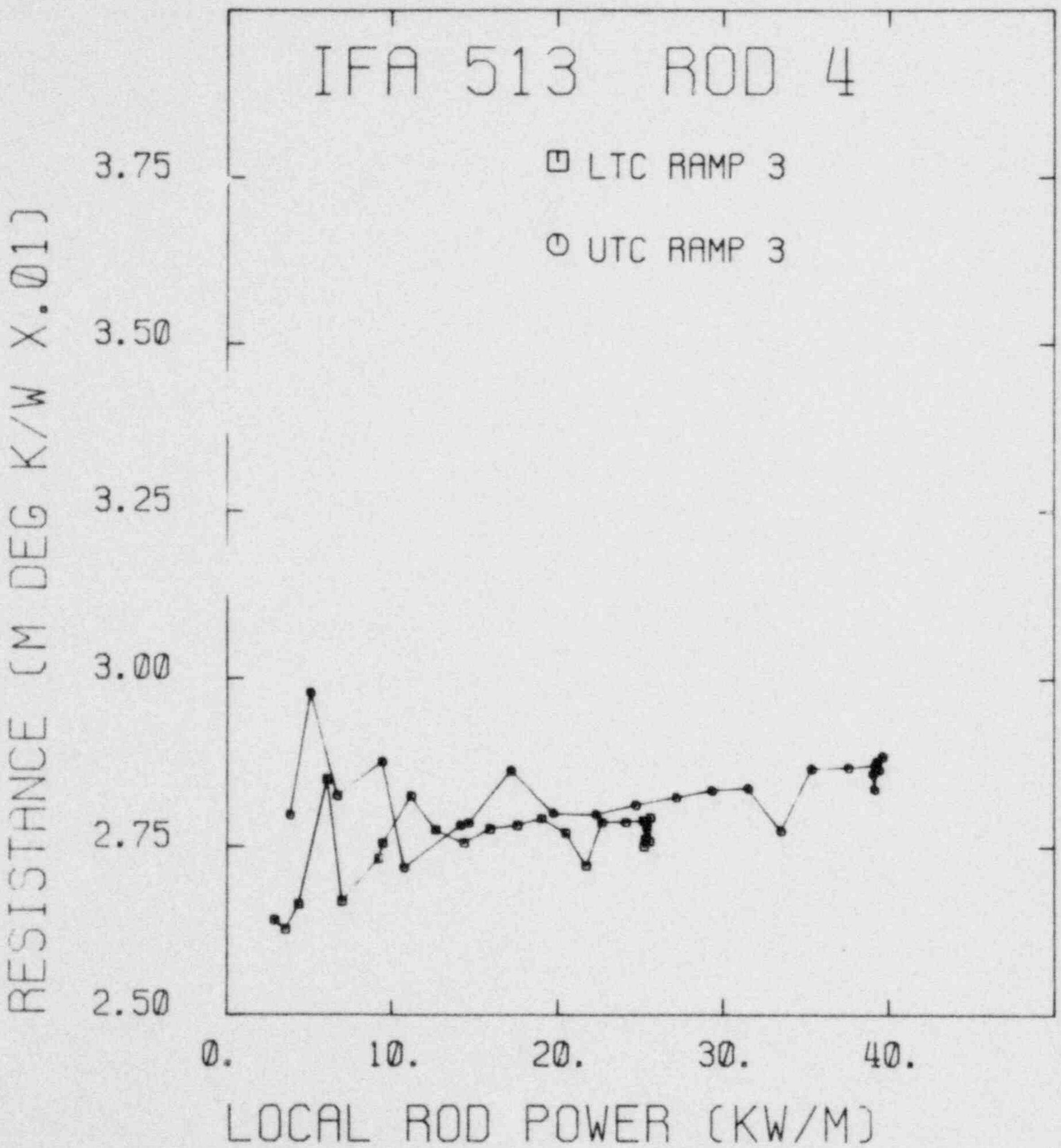

FIGURE B.33. Resistance for Rod 4 IFA-513 - Ramp 3

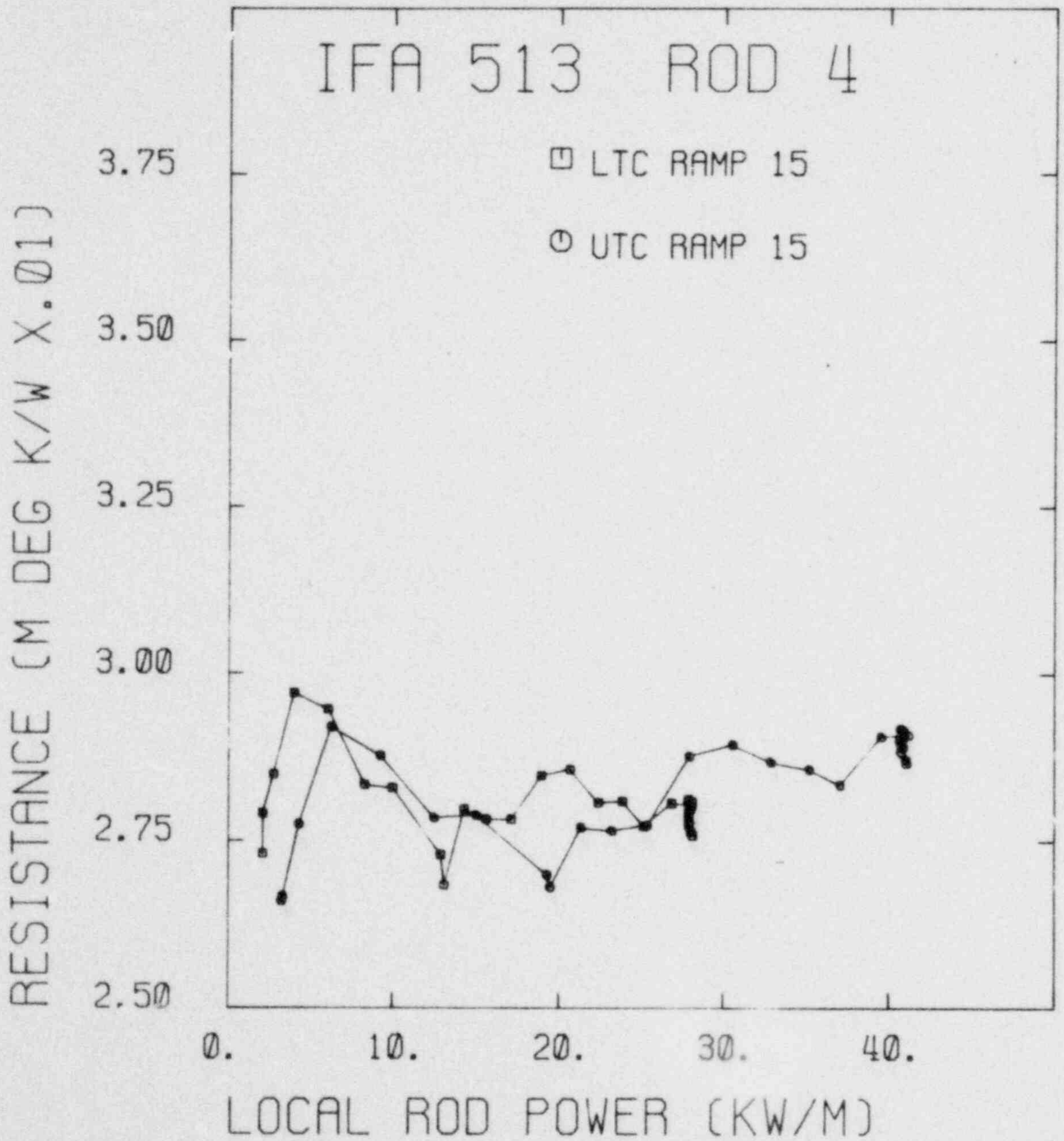

FIGURE B.34. Resistance for Rod 4 IFA-513 - Ramp 15

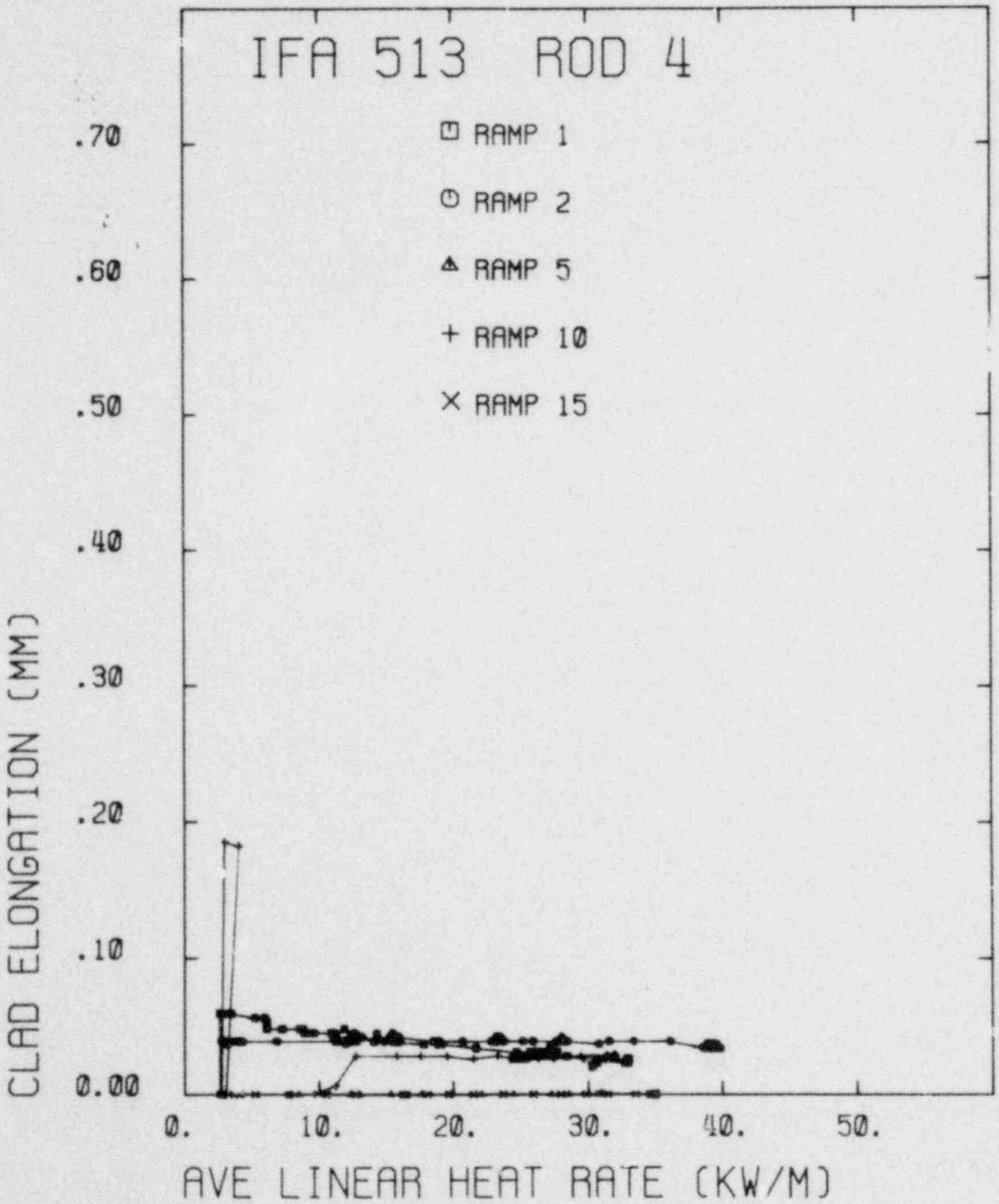

FIGURE B.35. Cladding Elongation for Rod 4 IFA-513

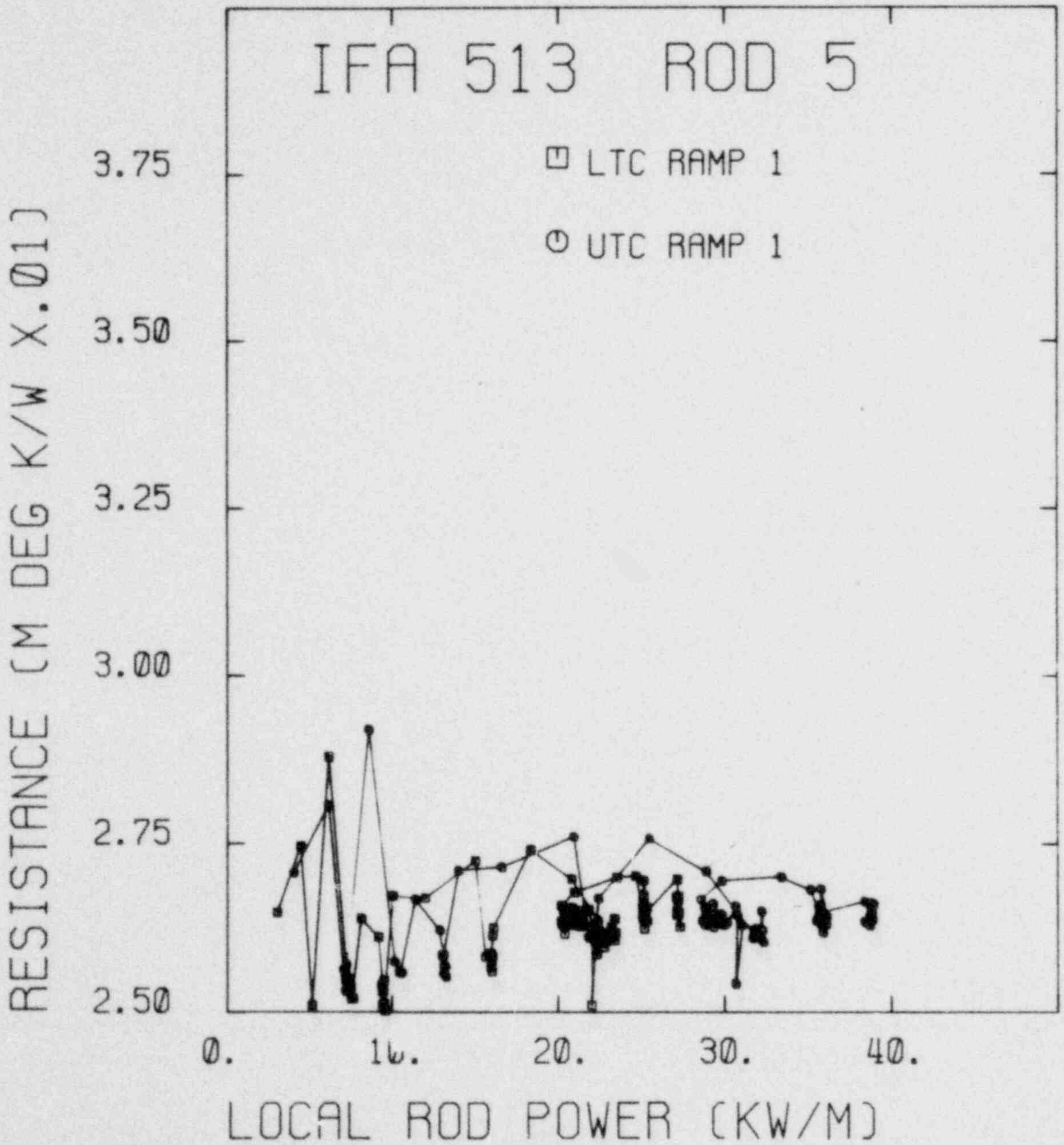

FIGURE B.36. Resistance for Rod 5 IFA-513 - Ramp 1

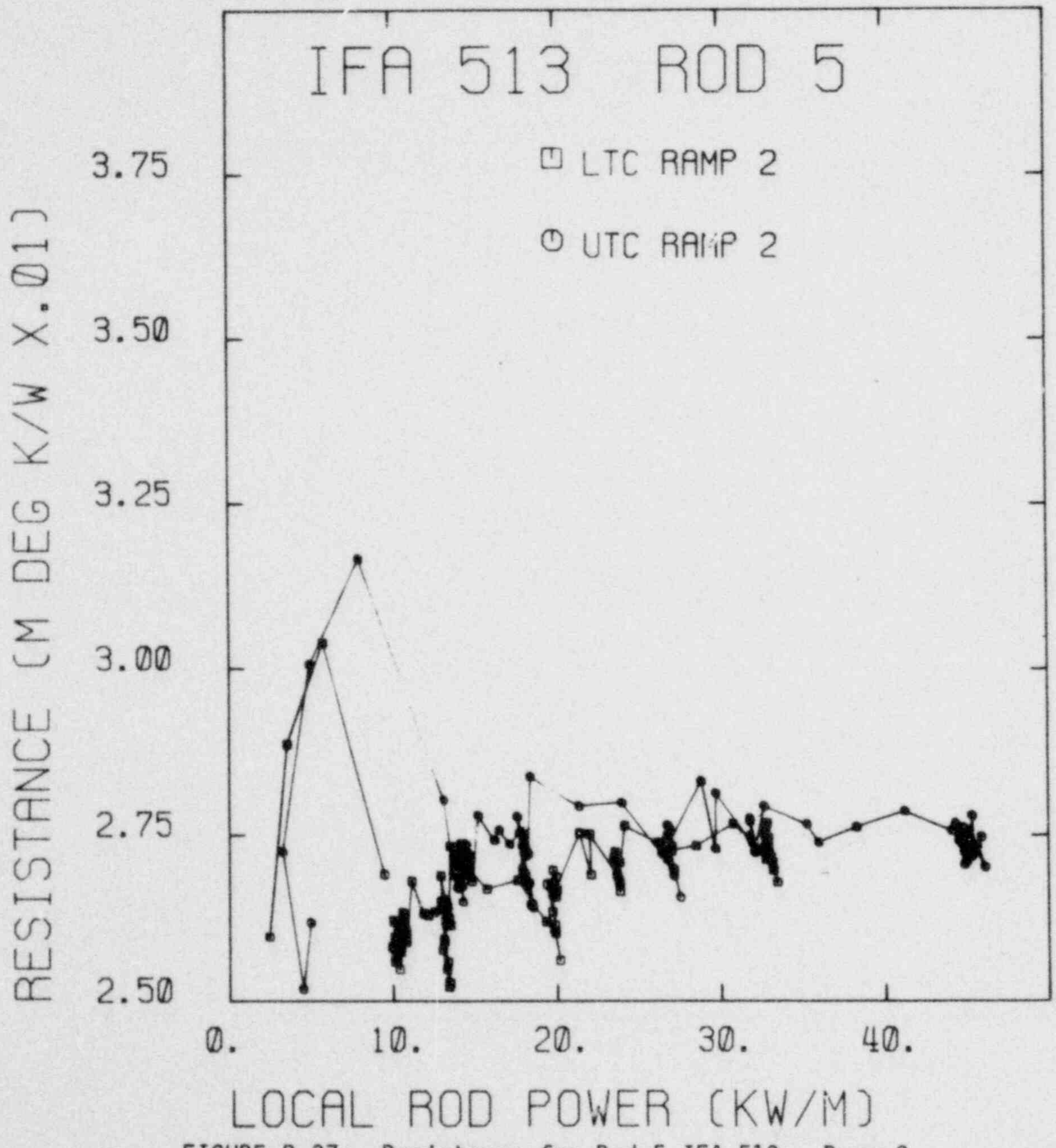

FIGURE B.37. Resistance for Rod 5 IFA-513 - Ramp 2

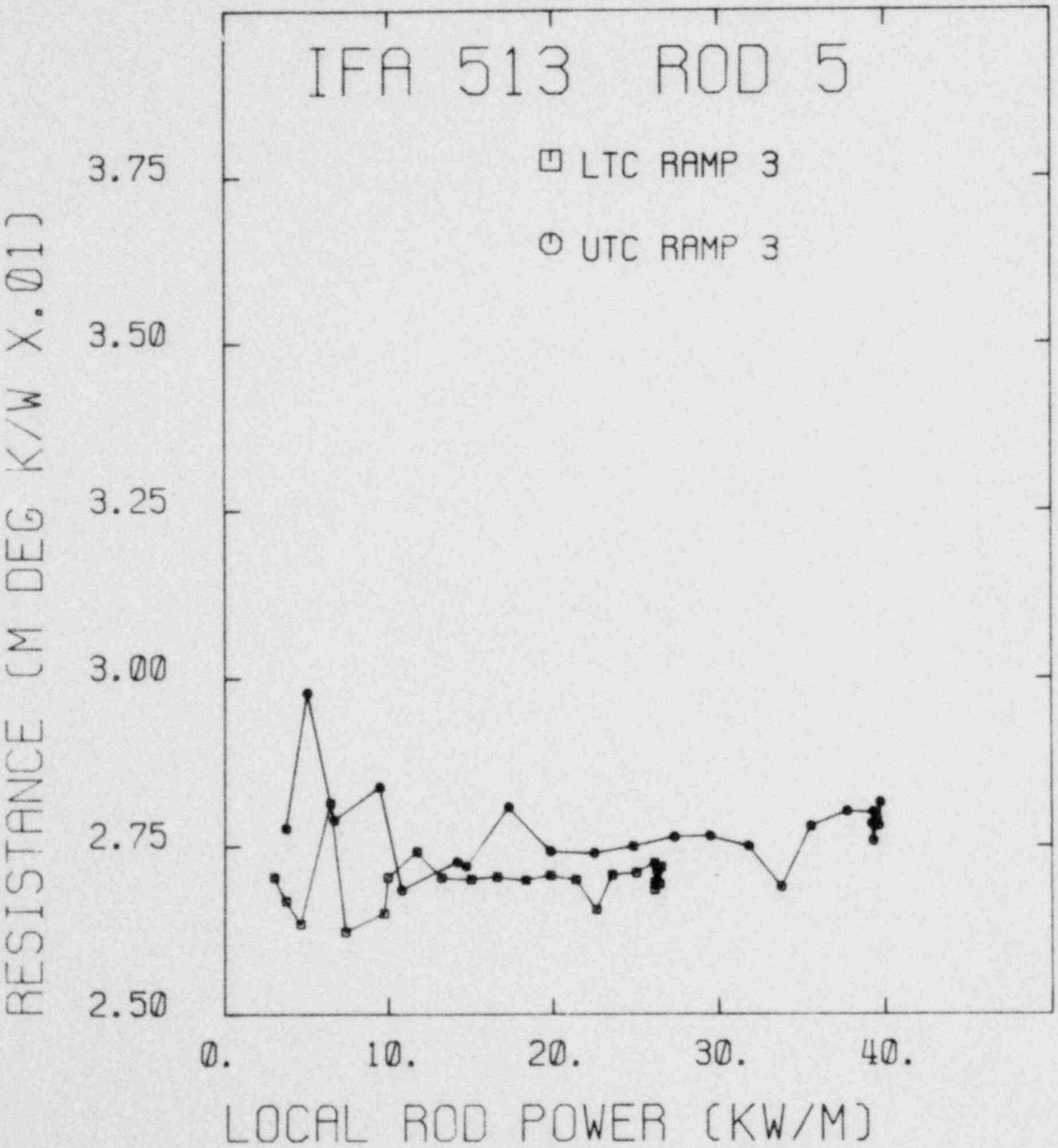

FIGURE B.38. Resistance for Rod 5 IFA-513 - Ramp 3

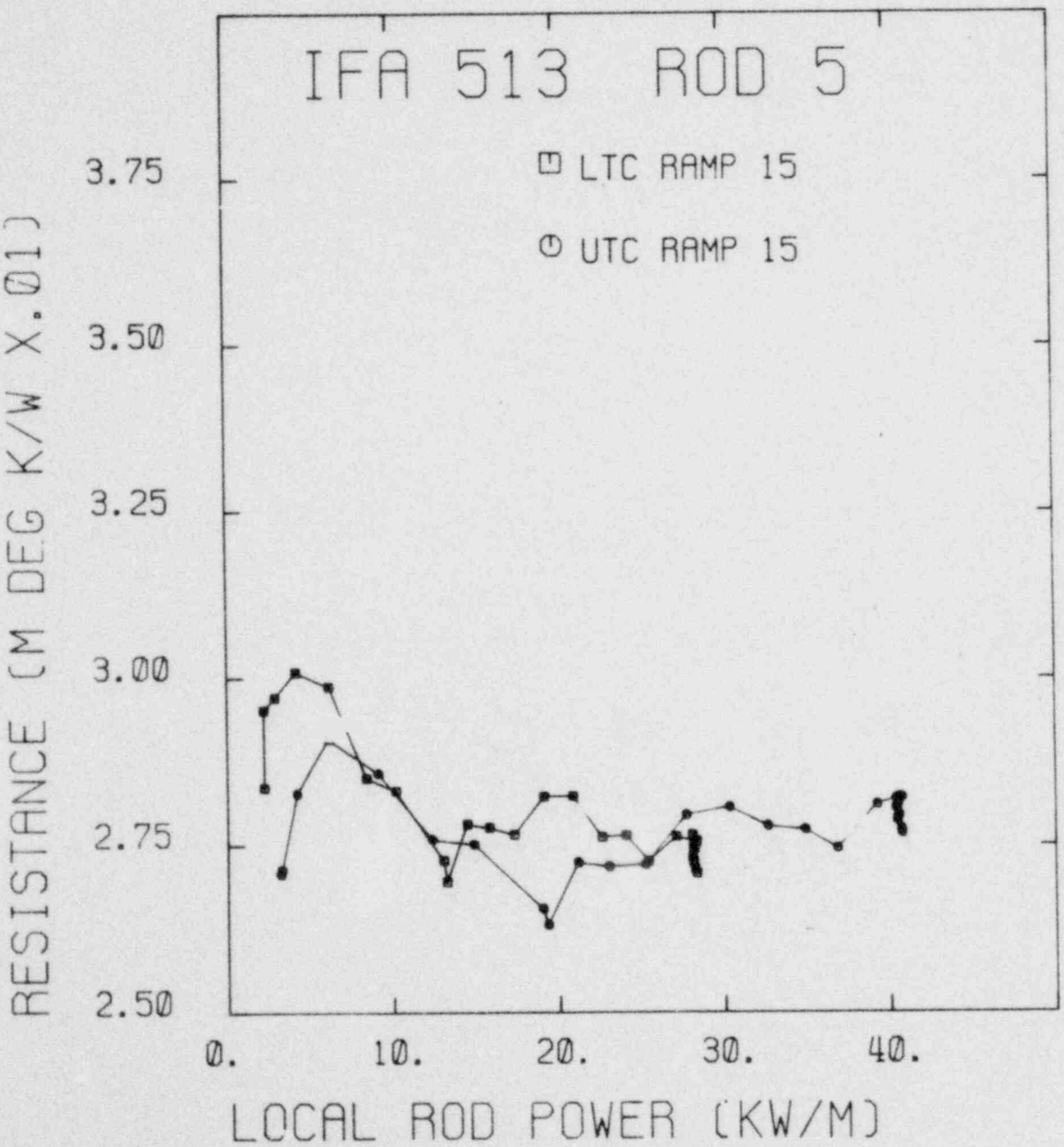

FIGURE B.39. Resistance for Rod 5 IFA-513 - Ramp 15

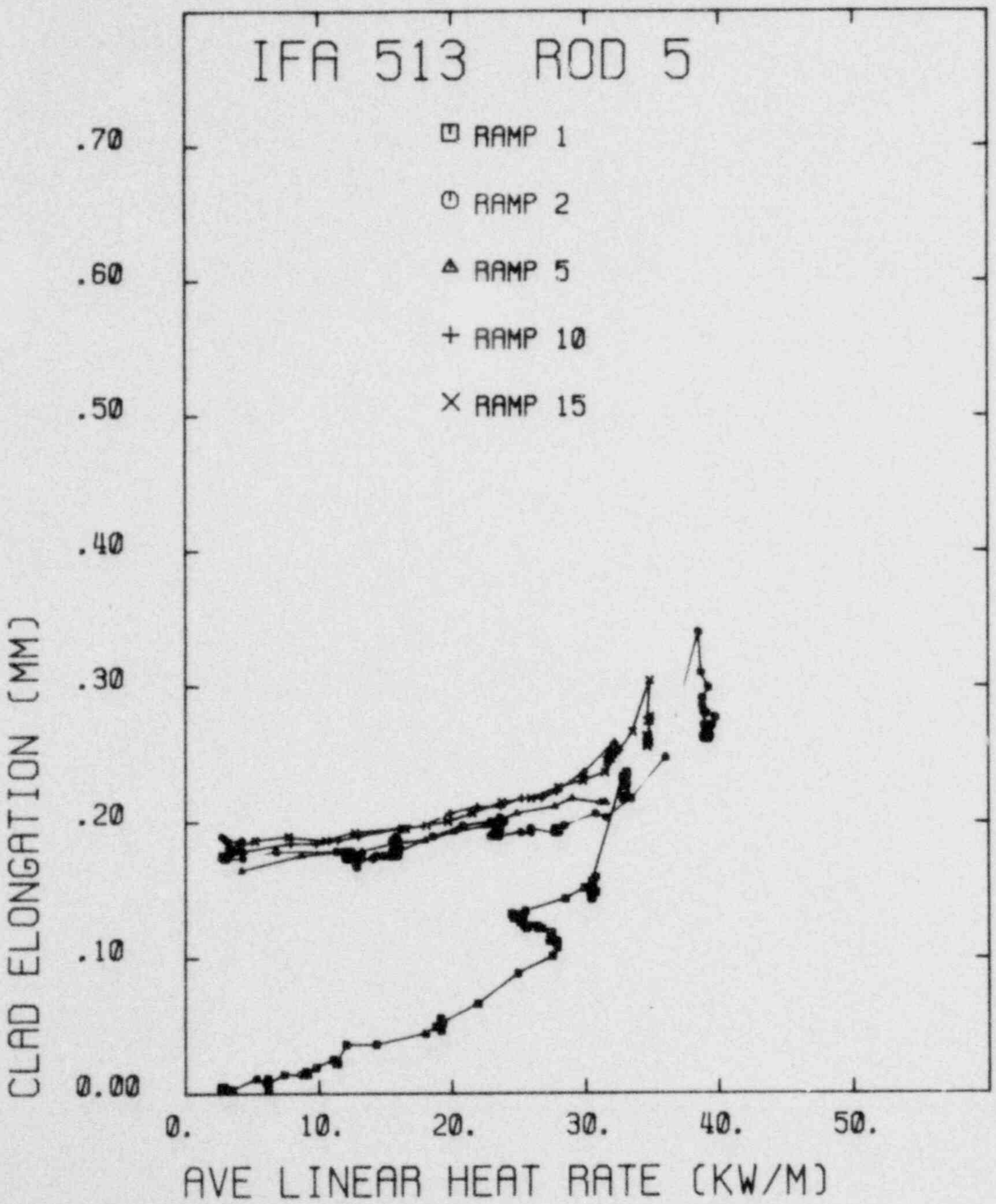

FIGURE B.40. Cladding Elongation for Rod 5 IFA-513

Figures B.41 through B.45 show the resistance and cladding elongations for Rod 6 of IFA-513. This rod was backfilled with 23% xenon and 77% helium to simulate a gas conductivity reduction to 50% of that for pure helium. The resulting gap-dominated resistance for the first ramp to power is shown in Figure B.41. In this case, the upper and lower thermocouple regions exhibit resistances of very similar magnitude at the same power. The higher temperatures cause more fuel thermal expansion than in the helium filled rods, and the internal voidage of the fuel rod has been consumed to a greater extent than in the helium filled rods. This is true at both thermocouple locations, and the plots indicate that the thermal effect of fuel cracking may damp out at higher powers. Thus the integral to melt maintains a reasonable value. Successive rises to power cause the cracked fuel to produce more solid contact with the cladding, and the resistance slope characteristics exhibit progressively less effects due the initial gas conductivity reduction.

The cladding elongation curves for this rod exhibit behavior similar to the other rods, except that they are slightly higher due to the increased temperature level.

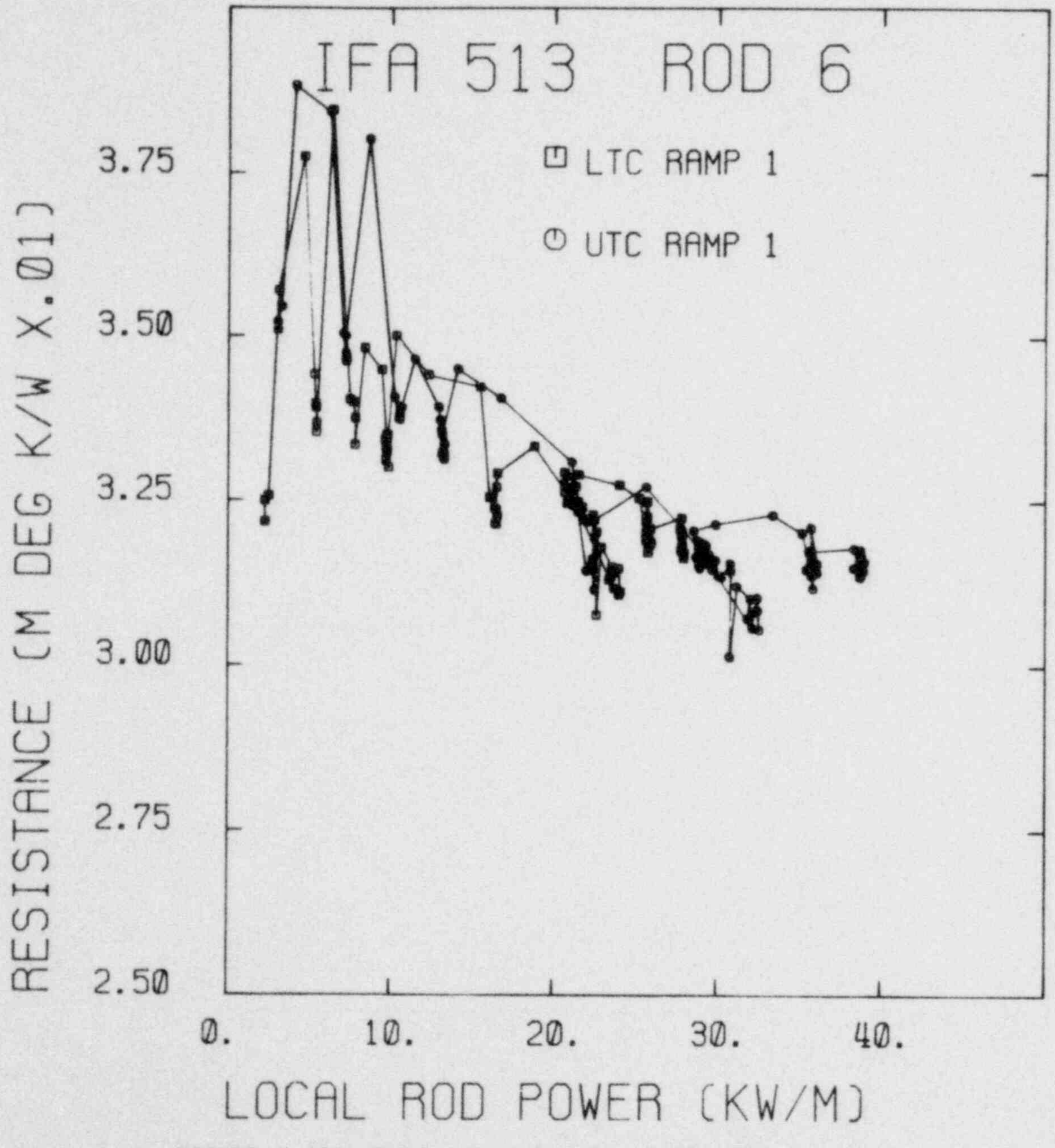

FIGURE B.41. Resistance for Rod 6 IFA-513 - Ramp 1

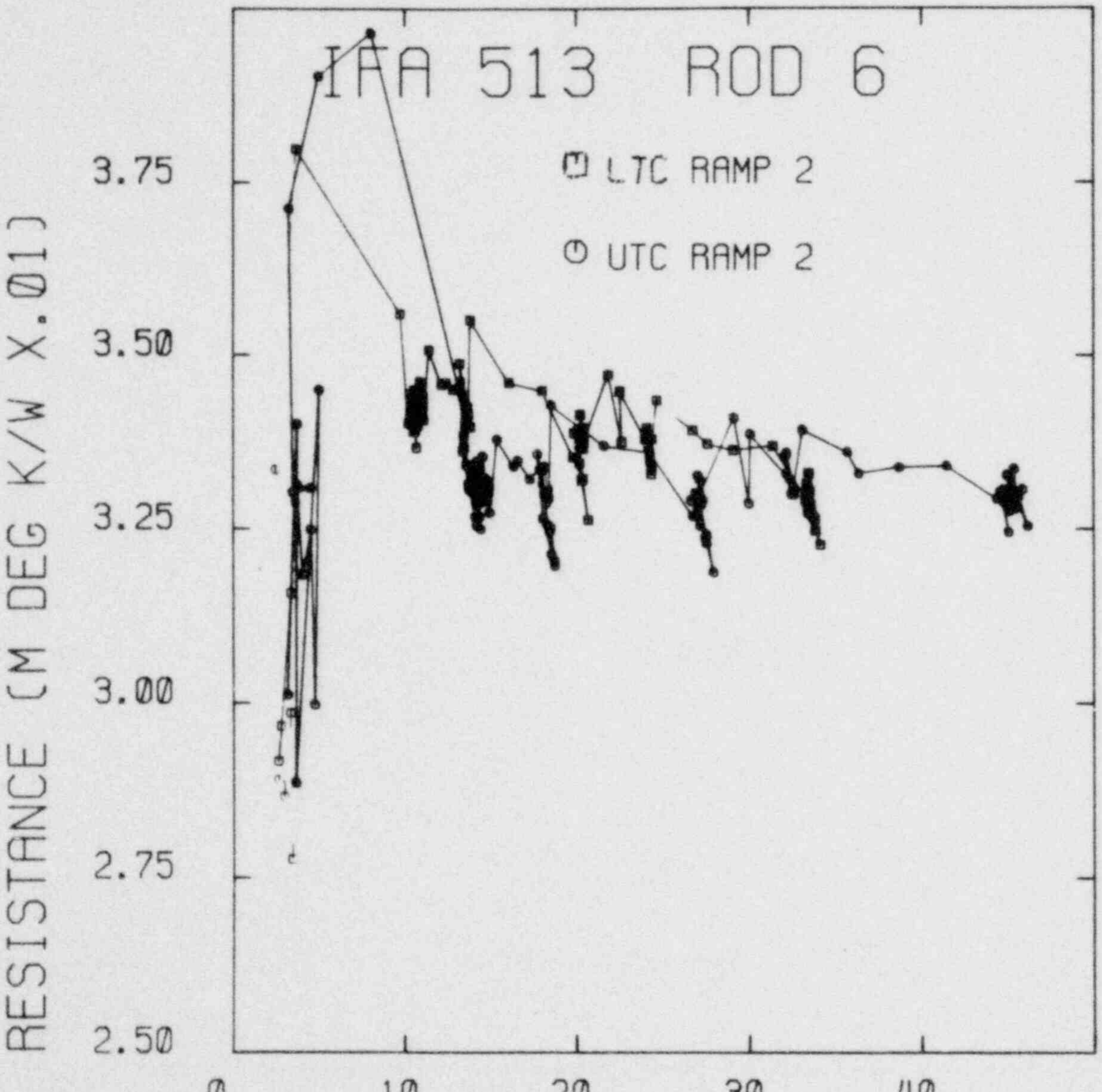

FIGURE B.42. Resistance for Rod 6 IFA-513 - Ramp 2

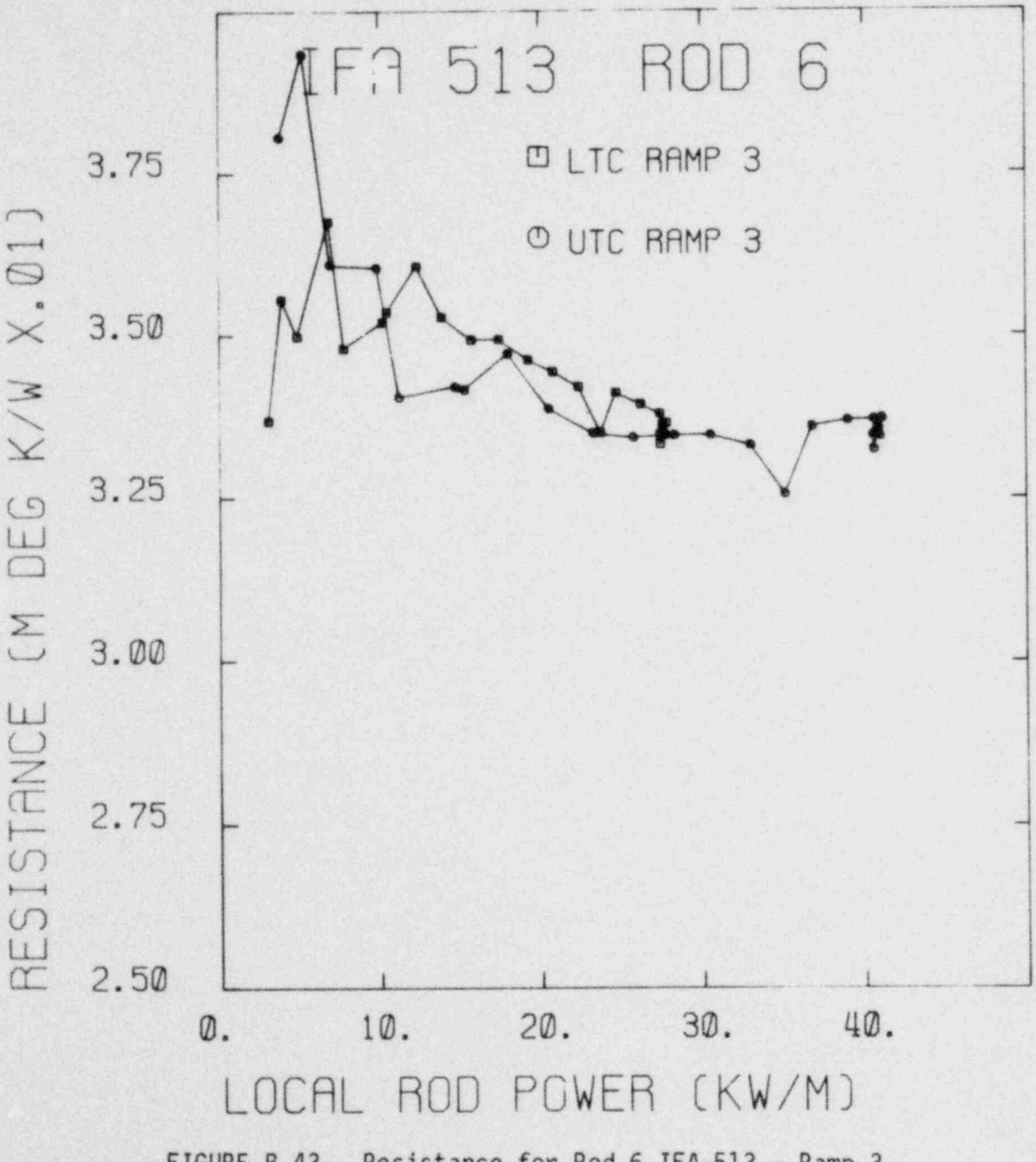

FIGURE B.43. Resistance for Rod 6 IFA-513 - Ramp 3

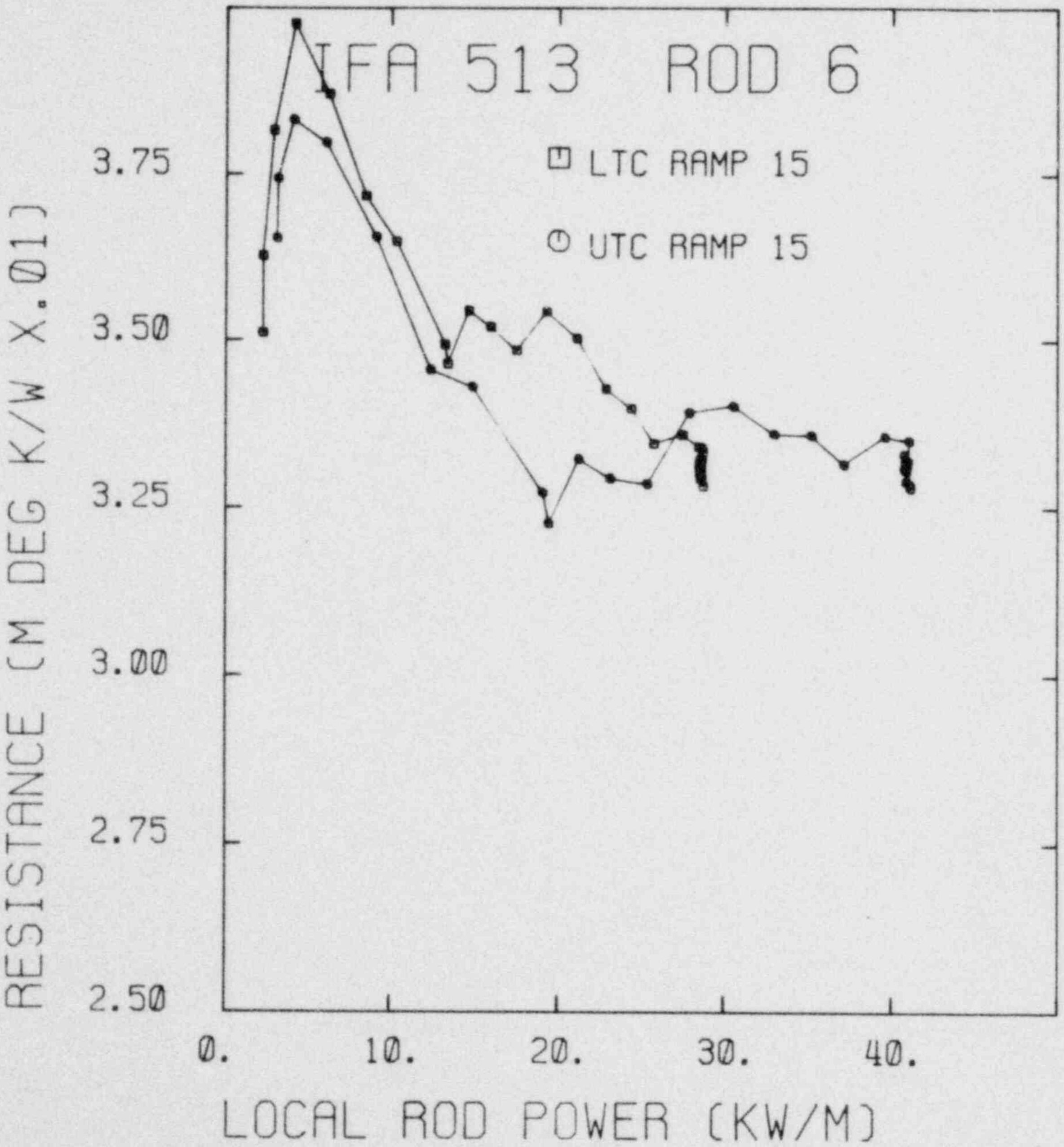

<u>FIGURE B.44</u>. Resistance for Rod 6 IFA-513 - Ramp 15

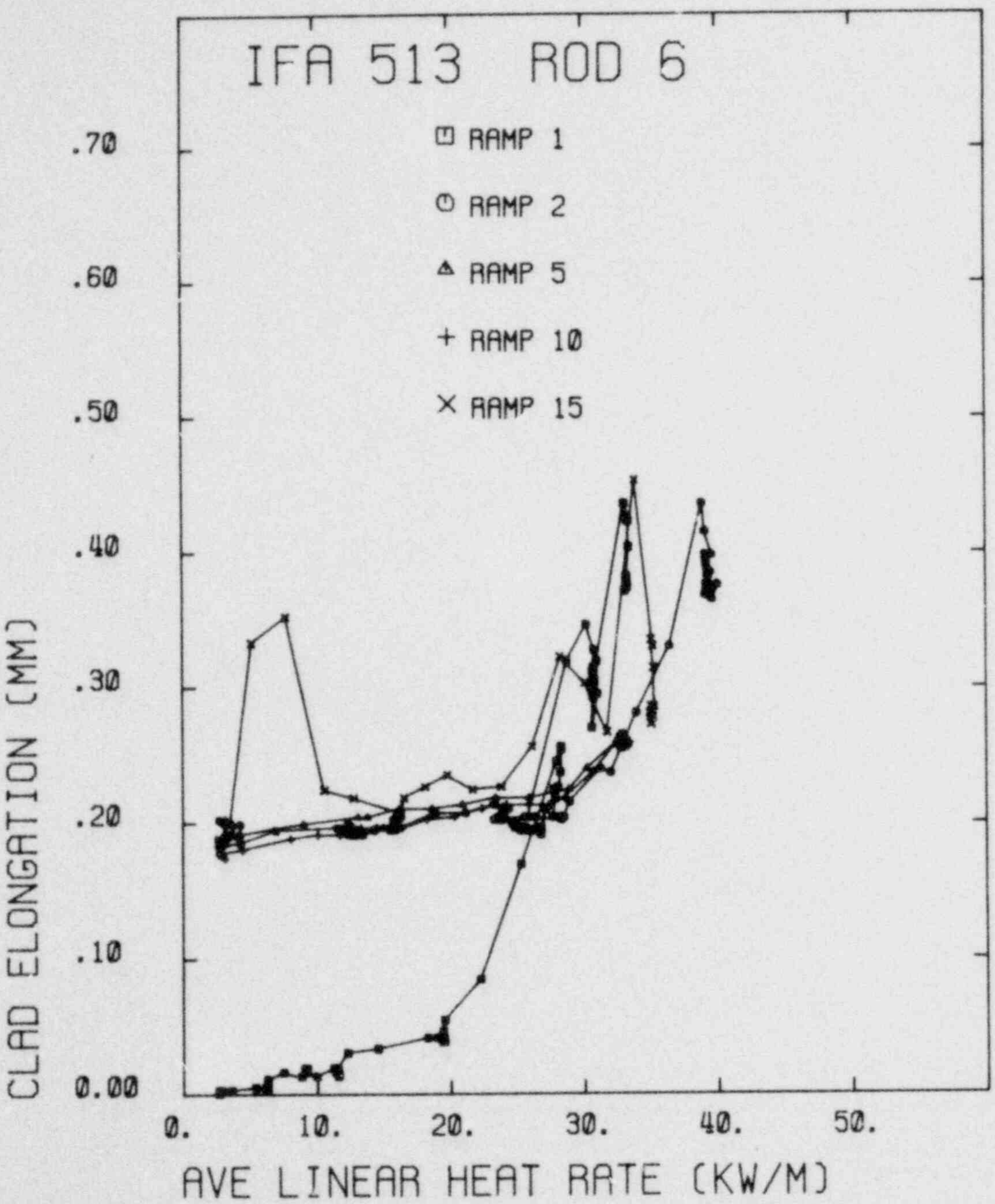

FIGURE B.45. Cladding Elongation for Rod 6 IFA-513

DISTRIBUTION

No. of Copies

OFFSITE

A. A. Churm
DOE Patent Division
9300 S. Cass Avenue
Argonne, IL 60439

375 Nuclear Regulatory Commission
Division of Technical Information and Document Control
7920 Norfolk Avenue
Bethesda, MD 20014

2 DOE Technical Information Center

4 W. V. Johnston
Chief, Fuel Behavior Research Branch
Division of Reactor Safety Research
U.S. Nuclear Regulatory Commission
Washington, D.C. 20555

No. of Copies

ONSITE

40 Pacific Northwest Laboratory

W. J. Bailey
J. O. Barner
E. R. Bradley
M. E. Cunningham
C. W. Dotson
M. D. Freshley
R. L. Goodman
R. J. Guenther
C. R. Hann
K. A. Hsieh
D. D. Lanning
R. K. Marshall
C. L. Mohr
C. Nealley
F. E. Panisko
P. J. Pankaskie
W. N. Rausch
R. E. Schreiber
P. E. Williford (15)
Technical Information (5)
Publishing Coordination Fe(2)